ENHANCED FINNED-TUBE CONDENSER DESIGN AND OPTIMIZATION

A Dissertation
Presented to
The Academic Faculty

By

Susan White Stewart

In Partial Fulfillment
of the Requirements for the Degree
Doctor of Philosophy in Mechanical Engineering

Georgia Institute of Technology
November 2003

ENHANCED FINNED-TUBE CONDENSER DESIGN AND OPTIMIZATION

Approved by:

Sam V. Shelton, Chairman

Comas Haynes

Yogendra Joshi

Amyn Teja

William Wepfer

Date Approved: November 24, 2003

ACKNOWLEDGMENTS

First and foremost, I would like to express the utmost gratitude to the select individuals who made my graduate education at Georgia Tech successful. All have shown continued support, encouragement, and advice throughout my graduate studies, most importantly my advisor Dr. Shelton. Dr. Shelton has inspired me to approach mechanical engineering and our work together with a sense of practicality, patience, and a desire to achieve results that will have an impact. Not only has he supplied me with his wealth of knowledge and experience, but he has also invested his personal time and energy into my graduate education. He has been a wonderful advisor and mentor.

Initially, one of the toughest decisions I've had to make was choosing which graduate school to attend after Penn State. Thankfully, Dr. Wepfer made Georgia Tech emerge as the clear choice. I am thankful for his guidance, support, and enthusiastic energy for Georgia Tech and me as a student in Mechanical Engineering.

I am very thankful to the rest of my thesis reading committee as well: Dr. Joshi for his technical input and guidance, which have served to make my dissertation more complete and accurate, Dr. Haynes for his encouragement and attention to detail in reviewing my thesis, and Dr. Teja for his comments, time, and perspective.

Several of my colleagues have also been sources of encouragement and support. I specifically want to thank Tracie Zoeller for her motivation, positive attitude, and advice over the last few years. I have learned so much from her and she has helped me strive to

always do my best. Also my predecessor, and now more of a mentor, Laura Schaefer has given me so much invaluable advice especially as I have finished up over the last year. I really appreciate the time she put into to responding to all of my questions. I also wish to acknowledge all of my current and former office mates and friends, Creed, Laura C., Benay, Peter K., Peter J., Brent, Jen, Kristinn, Matt, and many others. I really appreciate the friendships I have formed while at Georgia Tech.

I also wish to thank my husband Drew for being extremely supportive of my endeavors and for helping me to always keep things in perspective. Our parents and siblings have always been there for both Drew and I as well. We are so fortunate to have such a loving and supportive family. Thank you for everything.

TABLE OF CONTENTS

LIST OF TABLES

LIST OF FIGURES

NOMENCLATURE

Symbols

a	Ratio of X_l/D_o
a_{st}	Kays & London coefficient
A	Area
A_{ci}	Cross sectional area inside tube (evaporator)
A_1	Friedel correlation parameter
A_2	Friedel correlation parameter
A_{fr}	Frontal area of condenser (Width x Height)
A_{fin}	Surface area of the fins
A_o	Total heat transfer area on the air side ($A_{fin}+A_t$)
A_r	Heat transfer area on the refrigerant side ($\pi D_i L_{tot}$)
AR	Aspect ratio
A_s	Surface area
A_t	Surface area of the tubes
b	Ratio of X_l/D_o
B	Vertical hexagon length (X_l if $X_l<X_t/2$, or $X_t/2$)
$B(e^+)$	Graphical Dipprey & Sabersky parameter
B_{θ°	Bend coefficient
Bo	Bejan parameter

b_{st}	Kays & London power coefficient
C	Condenser material cost
circ	Number of parallel refrigerant flow circuits
C_r	Ratio of heat capacities (C_{min}/C_{max})
c_p	Specific heat at constant pressure
c_v	Specific heat at constant volume
C_{com}	Compressor experimental factor
COP	Coefficient of Performance
COP_{seas}	Average COP over a cooling season
C_z	Average row correction factor
C_{nHG}	Hiller & Glicksman constants (n=1,2,3)
D	Diameter
D_c	Collar diameter (D_o+2t_{fin})
D_h	Hydraulic Diameter ($4A_{min}D_{depc}/A_o$)
$D_{h.W}$	Hydraulic diameter for Wang 1999b ($4A_{min}/L$)
D_i	Inside tube diameter
D_{depc}	Depth of the condenser in the direction of air flow (rows x X_l)
$\left(\frac{dp}{dz}\right)$	Total pressure drop (frictional + momentum) per length
$\left(\frac{dp}{dz}\right)_f$	Frictional pressure drop per length
$\left(\frac{dp}{dz}\right)_g$	Gravitational pressure drop per length

$\left(\frac{dp}{dz}\right)_m$	Momentum pressure drop per length
e+	Roughness Reynolds number
E_{cav}	Cavallini correlation parameter
E_O	Eötvos number
E_{std}	Friction power expended per unit surface area ($W\Delta p/\rho A$, W/m^2)
Eu	Euler number
f	Darcy friction factor
f'	Fanning friction factor
f_r	Sand grain roughened friction factor
F_{cav}	Cavallini correlation parameter
F_P	Fin pitch [1/mm]
Fr	Froude number ($G^2/gD_i\rho_{TP}$)
fr_i	Fraction of total temperature bin hours
F_S	Fin spacing ($1/F_P$) [mm]
g	Acceleration of gravity
g_{cs}	Units conversion constant (32.17 $lb_f/(lb_m\text{-}ft/s^2)$)
$\bar{g}\left(e^+\right)$	Graphical Dipprey & Sabersky parameter
G	Mass velocity
G_{max}	Mass velocity through minimum air flow area
G_W	Transition flow rate
H	Diagonal hexagon length $\left(\frac{1}{2}\sqrt{\left(\frac{X_t}{2}\right)^2 + X_l^2}\right)$

h_{fg}	Latent heat
h_n	enthalpy at state n (n=1, 2, 2s, 2a, 2b, 3, 4, 4a)
h_{TP}	Two phase local heat transfer coefficient
$h_{TP,an,JG=2.5}$	Two phase local heat transfer coefficient for annular flow at J_G=2.5
$h_{TP,slug}$	Two phase local heat transfer coefficient for slug flow
$h_{TP,strat}$	Two phase local heat transfer coefficient for stratified flow
h_{std}	Convective heat transfer coefficient at standard conditions
$h_{TP,trans}$	Two phase local heat transfer coefficient for transition flow
$\bar{h}_a$	Air-side average convective heat transfer coefficient
$\bar{h}_r$	Refrigerant-side average convective heat transfer coefficient
$\bar{h}_{r,SP}$	Single phase refrigerant-side convective heat transfer coeffcient
JF	Heuristic augmentation figure of merit
j	Colburn j-factor ($StPr^{2/3}$)
j_4	j-factor for 4 row coil
j_z	j-factor for fewer than 4 rows (z = number of rows)
J_G	Dimensionless vapor mass velocity
JP	McQuiston & Parker parameter
k	Thermal conductivity
k_1	Staggered array geometry factor
k_{b,θ^o}	Two phase flow bend drop pressure coefficient for θ^o
k_f	Roughness constant
K	ESDU ε-NTU parameter

L	Length of tube
L_h	Louver height
L_p	Louver pitch
m_{es}	Extended surface parameter $\left(\frac{2\bar{h}_a}{k_a t_{fin}}\right)^{1/2}$
$\dot{m}$	Mass flow rate
n_B	Blasius coefficient
NTU	Number of transfer units
Nu	Nusselt number
P	Pressure
ΔP	Pressure drop
P_{hex}	Perimeter of hexagon
PD	Piston Displacement
PF	Cavallini penalty factor
Pr	Prandtl Number (ν/α)
P_r	Pressure ratio ($P_{sat,cond}/P_{sat,evap}$)
q	Heat transfer per unit mass
q'	Heat transfer rate per unit length
$\dot{Q}$	Heat transfer rate
q_{cst}, r_{cst}, s_{cst}, t_{cst}, u_{cst}	Rich power series parameters
r	Radius
r_b	Tube centerline radius

r_r	Relative radius
r_t	Outside tube radius
R	Radius of a circular fin
R_b	Bend recovery length
R_e	Equivalent circular fin radius
Re	Reynolds number
$\mathrm{Re_{Dc}}$	Reynolds number based on collar diameter
$\mathrm{Re_{Di}}$	Reynolds number based on inside tube diameter
$\mathrm{Re_{Do}}$	Reynolds number based on outside tube diameter
Re_l	Reynolds number based on longitudinal tube spacing, X_l
rows	Number of rows
P_{hex}	Perimeter of Hexagon
S	Entropy
SEER	Seasonal Energy Efficiency Rating
$\dot{S}_{gen}$	Entropy generation
$\dot{S}'_{gen}$	Entropy generation per unit length
$\dot{S}_{\Delta P}$	Irreversibility due to pressure drop
$\dot{S}_{\Delta T}$	Irreversibility due to heat transfer
St	Stanton Number (Nu/RePr)
T	Temperature
T^+	Dimensionless temperature
ΔT	Difference between wall temperature and bulk fluid temperature

ΔT_{SC}	Degrees of sub-cool exiting sondenser
ΔT_{SH}	Degrees of superheat entering condenser
$\bar{T}_s$	Entropic average temperature
t_{fin}	Fin thickness
tpr	Tubes per row
tprc	Tubes per row in a circuit
u_τ	Shear velocity
UA	Overall heat transfer coefficient * heat transfer area
V_{ac}	Velocity of air over condenser
v	Specific volume
$\mathbf{v}$	Design vertex
w	Work per unit mass
$\dot{W}$	Power
W_c	Width of condenser
We	Weber number ($G^2 D_i/\rho_G \sigma_L$)
x	Quality
$\mathbf{x}$	Design parameter
X_{diag}	Diagonal spacing between tubes
X_l	Longitudinal tube spacing
X_t	Transverse tube spacing
X_{tt}	Martinelli parameter
y	Equivalent length of tube bend

z	Number of tube rows
z_n	Geometry parameters of hexagon (n=1,2,3,4)

Greek characters

α_L	Cavallini heat transfer coefficient parameter for liquid
α_{LO}	Cavallini heat transfer coefficient parameter for liquid only
β	H/B (Fin efficiency calculations)
β_r	Ratio of total heat transfer area one side of heat exchanger to total volume of heat exchanger ($4\sigma/D_h$, m^2/m^3)
δ	Film thickness
δ^+	Dimensionless film thickness
ε	Heat exchanger effectiveness
ε_{pr}	Pipe roughness for drawn copper tubes
ε_r	Roughness
ε_v	Void fraction
$\varepsilon_{v,z}$	Zivi void fraction
ϕ	Fin efficiency parameter
ϕ_m	Modified fin efficiency parameter
Φ	Irreversibility distribution ratio
Φ^2_{LO}	Two-phase multiplier for liquid only
$\Phi^2_{b,LO}$	Two-phase multiplier for tube bend
μ	Dynamic viscosity
η	Efficiency

η_f	Fin temperature effectiveness, dimensionless
η_{fin}	Fin efficiency
η_o	Overall surface temperature effectiveness $(1-(1-\eta_f)A_{fin}/A_o)$, dimensionless
$\eta_{s,a}$	Air-side surface efficiency
γ	Ratio of specific heats, c_p/c_v for R410A
γ_c	Coefficient of contraction
Γ^2_b	Physical property coefficient for tube bend
θ	Angle of vapor-liquid interface
ν	kinematic viscosity
ρ	Density
ρ_c	Coefficient of reflection
σ	Minimum free flow area / frontal area
σ_L	Surface tension of the liquid phase
σ_c	Coefficient of shrinkage
ψ	β/r_t
τ	Shear stress
χ_c	Coefficient of expansion

Subscripts

a	Actual state
ac	Condenser air-side
ac1	Condenser air-side inlet conditions

ac2	Condenser air-side exit conditions
ae	Evaporator air-side
ae1	Evaporator air-side inlet conditions
ae2	Evaporator air-side exit conditions
air	Air
amb	Ambient conditions
amb,c	Ambient conditions in the condenser
amb,e	Ambient conditions in evaporator
ave	Average
b	Tube bend
c	Condenser
c,i	Cold inlet
com	Compressor
cond	Condenser
cor	Corrected
e	Equivalent circular
e	Exit
eff	Effective
evap	Evaporator
f	Saturated liquid state
fan	Fan
fin	Fin
g	Saturated vapor state

G	Gas phase
h,i	Hot inlet
H	High temperature reservoir
house	House
i	Inlet
k	Iteration
L	Liquid phase
L	Low temperature reservoir (Chapter V)
lat	Latent (heat)
LO	Liquid only
m	Mean
max	Maximum
min	Minimum
o	Total
opt	Optimum
r	Refrigerant
R	Reference case
S	Ideal state
s	Surface
sat	Saturated
sc	Sub-cooled
seas	Average over a cooling season
sens	Sensible (heat)

sh	Superheated
S	Straight
SP	Single phase
space	Properties of cooled space
std	Standard conditions
t	Tube
tubes	Bare tubes
tot	Total
TP	Two-phase
valve	Valve
vol	Volumetric
x	Free choosable parameter
1	State 1, entrance to compressor
2	State 2, entrance to condenser
2a	State 2a, saturated vapor state in condenser
2b	State 2b, saturated liquid state in condenser
2s	State 2s, isentropic state 2 (s_1=s_{2s})
22a	Value for superheated region of condenser
2a2b	Value for saturated region of condenser
2b3	Value for sub-cooled region of condenser
23	Total condenser
3	State 3, entrance to expansion valve
4	State 4, entrance to evaporator

4a	State 4a, saturated vapor state in evaporator
44a	Value for saturated region of evaporator
4a1	Value for superheated region of evaporator

SUMMARY

Finned-tube heat exchangers are widely used in space conditioning systems, as well as any other applications requiring heat exchange between liquids and gases. Their most widespread use is in residential air conditioning systems. Residential systems dictate peak demand on the U.S. national grid, which occurs on hot summer afternoons, and thereby sets the expensive infrastructure requirement of the nation's power plant and electrical distribution system. In addition to peak demand, residential air conditioners are major energy users that dominate residential electrical costs and environmental impact.

The only significant opportunity for electrical power use reduction of residential air conditioners is in technology improvement of the finned-tube heat exchangers, i.e., condenser and evaporator coils. With the oncoming redesign of these systems in the next five years to comply with the regulatory elimination of R-22 used in residential air conditioners today, improvement in the design technology of these systems is timely.

The design of finned-tube condenser coils, (heat exchangers), requires the selection of 14 design parameters by the designer, including the air flow velocity and fan power. The refrigerant side flow and condensation heat transfer characteristics inside the tubes depends mostly on the tube diameter design parameter and has been thoroughly studied. However, the air side flow around the tube bundle and through the fin gaps is a much more complex process and depends on over a dozen design parameters. Therefore, optimization of the air side design is a very complex problem and has not been addressed

in a comprehensive manner to lead the air conditioner system designer to an optimum condenser design.

This study creates a comprehensive and detailed model of the condenser coupled to a rigorous model of the rest of the air conditioning system. The resulting mathematical model consists of a set of highly non-linear transcendental mathematical equations numbering over 1800. Solution of this set of equations predicts the detailed component performance and the system efficiency, (COP), as a function of the 14 condenser design parameter inputs.

An optimization search methodology is then utilized with consistent and appropriate constraints to search the design space for the set of 14 design parameters which produces the maximum figure of merit, i.e., COP. It is first shown that increased air frontal area and decreased tube diameter increases efficiency for a fixed cost condenser coil, as well as thinner fins always being better until structural integrity becomes an issue. As expected, zero sub-cool is also shown to be optimal. Packaging constraints are then imposed on the design to limit the coil frontal area and aspect ratio.

Plain fins and augmented fins, (louvered), are compared. The results show that adding augmentation to an optimum plain fin coil design can decrease system efficiency. However, if the augmented fin coil design parameters are re-optimized, significant benefit can result from fin heat transfer augmentation for the same coil costs.

Results show that increasing the heat exchanger cost constraint improves system performance up to a point and then the system performance starts to decline. This is due to the frontal area constraint imposed by packaging considerations causing the coil to

increase in depth until the increased flow resistance outweighs the increase in air side surface area.

Other conclusions are that tube spacing is important and the optimum spacing is at the limit of the experimental data available, and thereby at the limit of applicability of the experimental correlations. There is therefore a need for additional finned tube experimental data beyond the bounds of that available to determine if the coil design can be further improved.

Additionally, to decrease the complexity of the model and computation time, an isolated condenser model was also developed. Comparisons are made between designs optimized via the system model (maximizing COP) versus optima from the isolated model (minimizing condenser entropy generation). It was shown that designs very close in performance to those found from the system-based optimization can be obtained from the isolated model with a significant decrease in computation time, if appropriate constraints are considered.

An air conditioner condenser finned tube coil design optimization methodology is derived and shown to lead to improved residential air conditioner efficiency at fixed equipment cost. This optimization is impractical by systematic experimental testing and iteration of tens of thousands condenser coils in an air conditioner system. This methodology and results can be used in the redesign of residential systems for the new mandated environmentally friendly refrigerants and to meet increasing regulatory minimum system efficiencies.

CHAPTER I

INTRODUCTION

I-A: Motivation

Residential heat pump and air-conditioning systems used today run on a basic vapor compression refrigeration cycle. The working fluid used in these cycles is commonly a synthetic refrigerant. Up until 1995, Chlorofluorocarbons (CFC's) were used extensively as refrigerants, but they were phased out of use due to their high Ozone Depletion Potential (ODP). Now Hyrdochloroflourocarbons (HCFC's), such as R-22, dominate the residential air-conditioning market. Because R-22 is not entirely harmless, even though it is environmentally friendlier than CFC's, the US Environmental Protection Agency (EPA) has published regulations prohibiting the production of R-22 after 2010 except for servicing equipment produced prior to 2010, while after 2020 the production of R-22 will be completely banned (EPA, 2001).

The Hydroflourocarbon (HFC) refrigerant 410-a (R-410a) is a strong candidate to replace R-22 as the working fluid in residential space conditioning systems due to its zero ODP and many favorable performance characteristics such as good cycle efficiency, non-flammability, and high working pressures. Because R-410a has higher working pressures and vapor densities than R-22, current A/C system designs are not appropriate. However,

there is limited public information about the optimization of air-conditioning systems using R-410a.

Recent environmental discussions have also focused on reducing emissions of CO_2. While at present the United States has not complied with the Kyoto Agreement, reducing CO_2 emissions is still a pressing issue. By using higher efficiency energy systems, energy usage can be decreased, reducing power plant output, which in turn reduces CO_2 emissions. In a warm climate, such as the southern US, residential air-conditioners consume the largest percentage of a household's total energy. Additionally, since they are only run when the outside temperatures are high, a peak electrical demand occurs only on hot days, which means that utilities must invest in an electric power generation and distribution infrastructure to meet the air-conditioner peak demand (Wenzel et. al 1997). These factors, along with public awareness, have created pressure for the efficiency of space conditioning equipment to improve. Therefore, due to the need for a replacement refrigerant for R-22, a significant effort should be placed on making the new refrigerant A/C System designs required over the next decade as energy efficient as possible, to help reduce the electrical demand of A/C systems.

The heat exchanger components, the condenser and evaporator, have the most potential for improvement in the design optimization of air-conditioning systems. The condenser has many variables that can be manipulated to design for maximum efficiency. The evaporator, however, has dehumidification constraints (as well as the added complication of wet coils) that limit its design flexibility for improved efficiency relative to the condenser. Therefore the condenser component is the focus of the current study.

Figure 1-1 shows typical outdoor condensing units for residential air-conditioning systems.

Figure 1-1: Typical Outdoor Air-Conditioning System Condensing Unit

The most common type of heat exchanger used as residential air-conditioning system condenser coils is of the plate fin-and-tube variety. These heat exchangers consist of mechanically or hydraulically expanded round tubes in a block of parallel continuous fins as shown in Figure 1-2. The analysis and modeling of these heat exchangers is far from trivial, having complex airflow patterns on the airside as well as complex refrigerant side circuitry operating through superheated, saturated and subcooled flow regimes. Most previous studies of these heat exchangers have focused solely on the refrigerant side aspects, while in the current study both the air-side and refrigerant side are considered, with more focus upon the air-side conditions.

Additionally, there are more than a dozen design parameters that are required to define the heat exchanger. In optimizing the design of the component, all of these

parameters must be considered simultaneously with the added complexity that they are interrelated (as one is varied, it effects the optimum design of the others). There is a continual trade-off between increasing the heat transfer coefficient of the heat exchanger and increasing the frictional pressure drop on both the air-side and refrigerant side. Because of this, selection of an appropriate measure of fitness is extremely important. This is an area in which there is very little consistency between different authors and many figures of merit are used that hold no theoretical basis.

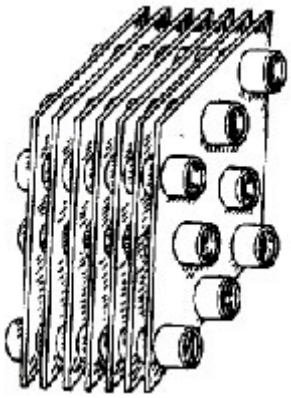

Figure 1-2: Finned-Tube Heat Exchanger

Additionally, enhanced surfaces are often employed to effectively improve the airside heat transfer performance of the fin-and-tube heat exchanger. One of the very popular enhanced surfaces is the interrupted fin. Again there is a trade-off in the adding of this enhancement of increased heat transfer performance and increased frictional pressure drop.

Therefore, this study's main goal is to create a practical design tool and methodology for designing high efficiency air-conditioning systems by optimizing the

finned-tube condenser component using R-410a as the working fluid with a focus on the air-side. Additionally, the appropriate figures of merit for optimization are explored as well as the effects of fin enhancements on the chosen figure of merit.

I-B: Air Conditioning Design Background

Approximately 80 percent of all U.S. homes now use air conditioning for summer comfort. The most typical residential air conditioner system sold is rated to supply 8.8 kW (30,000 Btu/hr) of cooling at an ambient temperature of 35ºC (95˚F), which is the standard temperature at which these systems are tested for cooling capacity. The efficiency rating of interest for these systems is averaged over the summer season. The minimum value for this seasonal efficiency rating is specified and regulated by the U.S. Department of Energy. All residential systems must have a minimum Seasonal Energy Efficiency Rating (SEER) of 10 Btu's of cooling output per Watt-hour of electricity used. This minimum allowed efficiency value is scheduled to be increased to 12 Btu/Watt-hour in 2006. Currently, most residential air conditioner manufacturers carry a product line including systems with a SEER of 10 (standard), 12 (high efficiency), and 14 (super efficiency). The SEER can be converted to a non-dimensional coefficient of performance, (COP = cooling output divided by electrical power input,) by dividing by a conversion factor of 3.412 Btu/Watt-hr.

When air conditioner system manufacturers design these systems, the issue of interest, i.e., figure of merit, is the system's manufacturing cost and its seasonal efficiency. Of course the design must be constrained to produce a fixed cooling output at 35ºC (95˚F). One of the primary components of focus for the designer is the condenser

coil, which is a finned tube heat exchanger in all conventional units. The designer has a figure of merit for the condenser of low cost and high system seasonal COP.

The condenser cost is directly related to the amount of copper and aluminum material in the condenser, which is discussed more fully in Chapter III. More dollars buys more heat transfer surface area, which produces a higher heat exchanger overall heat transfer conductance between the condensing refrigerant and the air, i.e., UA. There then exists a direct one-to-one relationship between the system efficiency and the condenser heat exchanger costs. High cost produces a higher COP, and lower cost produces a lower COP. Therefore, the designer either sets a desired COP and tries to minimize condenser costs as the figure-of-merit, or sets a desired condenser cost and tries to maximize the COP as the figure of merit. Either question will lead to the same optimum design.

In this study, the problem posed is to develop a condenser design that will optimize the COP for a fixed cost condenser. COP is the single figure of merit, and cost is constrained along with the cooling capacity at 35ºC (95˚F). Optimum designs will be studied for different condenser costs.

The condenser design requires specification of 12 to 14 design parameters. In this study, these design variables, such as tube spacing, will initially be constrained only by the limits of the data from which required empirical correlation equations were derived. As expected, some variables will optimize to their limits, which in some cases are zero or infinity. Since the purpose of the study is to arrive at practical designs, these design parameters will then be constrained to practical limits, and the remaining variables optimized to produce the maximum seasonal COP for a fixed cost condenser.

After developing the methodology, optimum design trends, and optimum designs for given condenser costs using COP as the figure of merit, entropy generation will be studied as an alternative figure of merit in place of system COP with the goal of minimizing modeling, analysis, and computation time.

I-C: Contributions of the Current Study

Wright (2000) developed a model of a residential air-conditioning system using R-410a as the working fluid. The model included a detailed simulation of the components of the air-conditioning system for various designs with the finned-tube condenser as the focus. Wright attempted to manually optimize some of the condenser parameters to maximize the systems' efficiency. Aspelund (2001) took Wright's model and implemented an optimization search scheme that allowed for eight of the parameters of the condenser's design to be optimized simultaneously with cost and/or frontal area constraints. The works of Wright & Aspelund form the starting point for the model developed in the current study.

Aspelund's resulting optimum design had a non-intuitive tube spacing. Because of this, one of the first steps of this study was to investigate the limits on the correlations used by Wright & Aspelund, as well as some alternative correlations, and modify the model relative to these limits as necessary.

Aspelund (2001) used the Simplex Search Method (Nelder & Mead 1965) to optimize the condenser design parameters. Since this method has a few drawbacks, such as being a continuous solver and it can get caught within local optima, alternative search

schemes were researched. The use of a genetic algorithm optimization scheme was investigated in detail as discussed in the next chapter.

Wright's model was based on a finned tube condenser with plain fins, however this is not the current industry standard. Most condenser fins have either waves or louvers in them for heat transfer augmentation. In recent years these techniques have been used to make heat exchangers smaller while achieving the same heat transfer rate. The heat transfer augmentation increases the heat transfer coefficient, but it is always coupled with an increase in frictional pressure drop. These two effects compete with each other making it difficult to quantify whether the enhancement technique has helped or hurt the system efficiency. To investigate whether heat transfer augmentation can increase efficiency, and gain an understanding of the enhancement effects, a simple case study was carried out comparing entropy generation due to heat transfer and friction for smooth vs. rough tubes. Then the developed model and optimization scheme was used to compare the system performance of optimized louvered vs. plain fins.

Since the competing effects of increased heat transfer and increased pressure drop make it difficult to determine the relative goodness of a design, the appropriate selection of a figure of merit is very important. There are many different figures of merit used by authors today, as discussed in Chapter II, and they all depend on what aspects of the system are being held constant throughout the analysis. As discussed above, the most appropriate figure of merit for an air-conditioning system is the system seasonal COP, coupled with a cost constraint. Additionally, the cooling capacity of the system should be held constant throughout the comparison, and has not always been constrained in other published studies.

Another figure of merit, which is directly related to the COP through fundamental relations (as shown in a later section), is entropy generation. In this case the inverse of the entropy generation is used as the figure of merit for determining the best design (also known as entropy generation minimization (EGM)). Again, care must be taken in setting constraints to make sure the design optimization is comparing "apples to apples".

The methods discussed above require modeling and analysis of the entire system. Another, more controversial, method is thermoeconomic isolation, which is defined as the ability to optimize independently each unit of a system and yet still arrive at the optimum for the system as a whole (Muñoz & von Spakovsky 2003). In this case, instead of analyzing a figure of merit based on the entire system performance, a figure of merit for the individual component that is being optimized (the condenser in the current study) is investigated. As discussed in detail in Chapter II, many authors have assumed that this technique holds true in the optimization of heat exchangers to simplify the complex nature of analytically integrating the component into the context of the overall system design. However, in many studies, the figures of merit used did not always prove to be true predictors of the effect on the overall system design. Since the model that has been developed provides for the unique opportunity of integrating the condenser design into the entire system, as well as studying it as an individual component (isolated from the rest of the cycle), this idea of thermoeconomic isolation was explored in this study, with comparisons made between the resulting designs found from optimizing the systems COP vs. minimizing the entropy generation in the isolated condenser component.

CHAPTER II

LITERATURE REVIEW

II-A: Heat Exchanger Modeling and Optimization

There are a large variety of heat exchangers available today, each useful for many different types of applications. In residential air conditioning systems, finned-tube heat exchangers are most commonly used. These heat exchangers consist of mechanically or hydraulically expanded round tubes in a block of parallel continuous fins as shown in Figure 1-2. Several authors have investigated these heat exchangers for simulation, design, and/or optimization purposes as described below.

II-A.1: Finned-Tube Heat Exchanger Models

Several authors, such as Vardhan and Dhar (1998), Bensafi et al. (1997) and Corberan & Melon (1998), have developed comprehensive simulation models of the individual finned-tube heat exchanger component with reasonable accuracy (~1%-30% error) compared to experimental data. Each of these models uses a nodal analysis approach and requires significant computation time to obtain performance results; therefore these models were not used for optimization purposes.

II-A.2: Heat Exchanger Models with Optimization Schemes

Jiang et al. (2002) also developed a simulation tool for design of finned-tube coils. While the model developed by Jiang et al. has not yet been experimentally validated, it seems to be able to account for several detailed aspects of the coil, such as complex circuitry, various flow configurations (counter-cross, parallel-cross) and non-uniform air distributions. In general there is a focus on the refrigerant side design rather than the air-side.

The model discretizes the tube into segments and solves the momentum and energy equations for each segment alternatively and repeatedly until convergence is obtained. The momentum equations were solved with the Newton-Raphson method, and the energy equations were solved with the successive substitution method.

In addition to the simulation tool, Jiang et al. mention an example optimization case using a genetic algorithm to optimize the number of rows, number of tubes per row, option of parallel-cross flow or counter cross flow, and tube diameter. The objective function was minimum total heat transfer area at a given heat load subject to maximum allowable pressure drops of the refrigerant flow and air flow. This optimization requires fairly detailed information (pressure drops) in order to perform the optimization. Additionally, the objective function is subjective. The optimization results in a more compact (smaller) heat exchanger for the price at whatever allowable pressure drops are specified. But it is not discussed how or why one would choose a particular pressure drop and nothing on the air side of the heat exchanger is optimized.

Tayal et al. (1999) also looked at searching for optimum individual heat exchanger components using a combinatorial (mixed discrete & continuous variable)

optimization scheme such as the genetic algorithm, using minimum heat transfer area as well as cost as objective functions in their optimization procedures. Tayal et al. conclude that genetic algorithms are equally effective as compared to simulated annealing in solving black-box optimization model problems. Their study focuses on shell-and-tube heat exchangers for process industries.

II-A.3: Finned-Tube Heat Exchanger Optimization in Refrigeration Cycles

Richardson et al. (2002) developed a program that simulates a vapor compression system. This program is then used to optimize the system level variables using gradient based and genetic optimization routines. Parameters included in this simulation program are: refrigerant charge, COP, weight, capacity, and cost. Optimization objective functions used were COP, capacity and system weight. This study did not optimize the design of the individual components; rather it used a collection of specific components and found the best combination of them for specified inputs. Additionally, the heat exchanger models used in this simulation program are simplistic, assuming infinite air flow rate and fixed properties at the inlet regime for refrigerant pressure drop calculations.

Wright (2000) developed a model in Engineering Equation Solver (EES) (Klein & Alvarado 2003) of an air-conditioning system using R-410a as the working fluid. The model included a detailed simulation of the components of the air-conditioning system for various designs, including the compressor, non-augmented finned-tube condenser, evaporator, and expansion valve. The condenser was the focus of Wright's model incorporating the best available simulations for the air-side and refrigerant-side pressure

drops and heat transfer coefficients based on R-410a as the working fluid. Wright was not able to perform a comprehensive design optimization search using this model due to computational time limitations resulting from a manual search scheme. Therefore, Aspelund (2001) added to Wright's study by implementing a design optimization search technique to optimize ten controllable, operational, and geometric design parameters of the condenser. Aspelund's results showed a 23% reduction in cost for a design that produced the same COP versus Wright's optimum design found through a manual search. The combination of Wright's model and Aspelund's optimization technique is the starting point for the current study.

II-B: Comparison of Optimization Techniques

Aspelund's (2001) original program used the downhill Simplex Search Method developed by Nelder and Mead (1965) to optimize the design parameters of the finned-tube condenser component. This method was chosen because it does not require the calculation of derivatives and it is very robust to convergence (Haupt & Haupt 1998). The downfalls of this method, however, are that it is a continuous solver and may be more likely to get stuck in local minima than some other methods. Because of these reasons, genetic algorithms were investigated as an alternative method for optimization. Genetic algorithms are a subset of evolutionary algorithms that model biological processes to optimize highly complex cost functions. A genetic algorithm allows a population composed of many individuals to evolve under specified selection rules to a state that maximizes the "fitness" (i.e. minimizes the cost function). The method was developed by John Holland (1975) over the course of the 1960's and 1970' and finally

popularized by one of his students', David Goldberg (1989), who was able to solve a difficult problem involving the control of gas-pipeline transmission for his dissertation (Haupt & Haupt 1998).

Some of the advantages of the genetic algorithm over the simplex method are that it can optimize with continuous or discrete parameters (combinatorial), both of which occur in finned-tube heat exchangers, it can jump out of a local minimum, and it provides a set of optimum designs, not just a single design, which may be of interest to manufacturers since some designs may be more adaptable to existing tooling. As with the Simplex method, genetic algorithms also do not require derivative information. Plus, in many situations genetic algorithms will achieve a solution quicker than using other optimization methods. However, the random aspect of the method, which gives it its advantages, is also a problem for its application to the current design optimization. The system of equations (1800+) used to calculate the fitness function cannot accommodate values too far away from the current guess value. A genetic algorithm will randomly "jump around" within the entire cost surface searching for the minimum cost function. This jumping around causes problems in the solution of the cost function. If the guess values of the variables in the equation solver are too far away from the solution, the solver will not converge. Since the Simplex method moves more slowly from one position on the cost surface to another, it is a much more appropriate optimization technique for the current study. Addressing some of the issues of the Simplex method compared to the genetic algorithm:

- All of the parameters are at first solved on a continuous basis, after which, the parameters that are in reality discrete values are searched around the upper and lower bounds of their continuous optimum value, while all of the remaining continuous values are re-optimized. This process is automated as a 2nd step to the optimization technique.

- No optimization technique (except for an exhaustive search) has proven to be able to find a global minimum/maximum. In the current optimization problem, from experience thus far, the Simplex method does not often get stuck in local optima. And when it does, it is quite obvious.

- As far as speed goes, the Simplex search is quite fast in its current application; therefore any increase in speed from using a genetic algorithm would not be very noticeable.

- For the purposes of this study, in making comparisons, a single design is required, rather than having a set of optimum designs.

II-C: Heat Exchanger Enhancement Techniques

To reduce the air-side thermal resistance of air-cooled heat exchangers, researchers have been studying the effects of fin surface enhancements for several decades (Cantaloube 1968, Gunter 1969, Wang 2000). The practice of adding surface enhancements to the fins of finned-tube heat exchangers has become widely used in

many products, notably residential space-conditioning finned-tube condenser heat exchangers of interest here.

Many different heat transfer enhancement techniques have been investigated over the last several decades. Techniques are categorized as passive or active. Passive techniques involve changes made to the surface or shape of the material (tubes or fins) or the use of fluid additives. Active techniques require external power such as electric or acoustic fields and surface vibration (Webb 1994). Only passive techniques are investigated in this study because they are commonly used in air cooled condenser designs. Most passive augmentation techniques involve creating more turbulent mixing. The use of interrupted fins is a very widely accepted method of increasing the heat transfer coefficient on the air-side of the condenser. The surface interruption renews the boundary layer, and hence reduces its average thickness. There are several different types of fin interruptions used such as waves, slits (offset strips), louvers and convex louvers (a combination of wavy and louver fin geometries). The louver fin, as shown in Figure 2-1 (where F_P is the fin pitch and $1/F_P$ is the fin spacing, L_h is the louver height, and L_p is the louver spacing), is the most popular interrupted surface owing to its relatively low cost in mass production (Wang et al. 1999c); therefore it is the focus of this study.

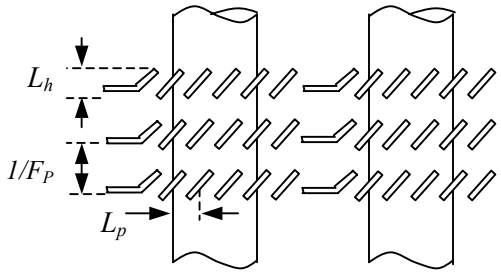

Figure 2-1: Louver Configuration, cross section view
Air flows from left to right.

Many empirical correlations have been developed to describe the heat transfer coefficient and friction factor for the air-side of the condenser for enhanced fin geometries (Wang et al 1999b, Wang et al 2001a, Wang & Chi 2000b, Du & Wang 2000, Chang et al 2000, Wang et al 1999c, Wang et al 1998, Kang & Webb 1998, Kim et al 1997). In Wang (2000), a very good summary of all of the different types of fin enhancements is given with correlations. The friction factor and heat transfer coefficient correlations used in this study for the louvered fin geometry with a round tube configuration are those recommended by Wang (2000) and developed by Wang (1999b).

Adding louvers to a finned tube condenser heat exchanger in an air conditioning system will reduce compressor power by increasing the refrigerant-to-air conductance, but it will increase the condenser air fan power and/or lower the air flow rate. These competing effects make it more difficult to determine the relative merit of a heat exchanger design. Many different heat exchanger figures-of-merit have been used. Their differences primarily depend on constraints imposed for the analysis.

II-D: Figures of Merit

The selection of an appropriate figure of merit is critical in the design optimization of heat exchangers due to the required trade off between increased heat transfer and increased frictional pressure drop. This is especially true on the air-side as interruptions are added to the fins. Some authors state that even a small increase in conductance can more than offset a large friction factor increase because flow velocity can then be decreased and air flow friction power varies with the cube of the velocity

(Kays & London 1964). However, this statement has not been quantitatively addressed with meaningful constraints and figures-of-merit.

In 1974 Bergles et al. reviewed the literature and found that there was no generally accepted performance criteria for evaluation of enhancement devices that permitted comparison between designs. Their article discusses the different factors which enter the decision making process to use an augmentative technique including: heat duty increase, area reduction, initial cost, pumping power, operating cost, and maintenance cost. Bergles et al. then developed eight performance criteria depending on what is held fixed in the comparison and the desired objective. These eight criteria are summarized in Table 2-1.

Table 2-1: Summary of Performance Criteria Evaluations (Bergles et al. 1974)

		Criterion Number							
		1	2	3	4	5	6	7	8
Fixed	Basic Geometry	X	X	X	X				
	Flow Rate	X						X	X
	Pressure Drop		X				X		X
	Pumping Power			X		X			
	Heat Duty				X	X	X	X	X
Objective	Increase Heat Transfer	X	X	X					
	Reduce Pumping Power				X				
	Reduce Exchanger Size					X	X	X	X

In 1978 Shah summarized over 30 different methods proposed in the literature to compare the heat transfer and pressure drop characteristics of different surfaces. Shah recommends that the selection criteria be as simple and direct as possible but meaningful, because in many cases the best performing surface may not be an optimum heat exchanger for a given application. Shah recommends the following methods:

1. j/f' vs. Re is recommended for flow "area goodness" comparison
2. h_{std} vs. E_{std} is recommended for selecting a surface where there are no system or manufacturing restraints.
3. $\eta_o h_{std} \beta_r$ versus $E_{std} \beta_r$ characterizes a surface best from a "volume goodness" viewpoint.
4. The performance ratio method of Bergles et al. (1974) is recommended for other design criteria.

Where j is the Colburn heat transfer modulus (St $Pr^{2/3}$), f' is the Fanning friction factor, h_{std} is the convective heat transfer coefficient at arbitrarily selected standard temperature and pressure conditions, E_{std} is the friction power expended per unit of surface area ($W\Delta p/\rho A$, W/m^2) at standard conditions, and β_r is the ratio of total transfer area on one side of the exchanger to total volume of the exchanger ($4\sigma/D_h$ (σ=minimum free-flow area/frontal area, D_h =hydraulic Diameter), m^2/m^3).

More recently, several authors have investigated whether interrupted fins actually improve the heat exchanger design by developing their own heuristic figure of merit. For

instance, Yun & Lee (2000) heuristically developed and proposed a ratio called *JF* to describe the relative goodness of a design (larger is better):

$$JF = \frac{j / j_R}{(f / f_R)^{1/3}} \tag{2.1}$$

The subscript *R* refers to a reference design (un-augmented case) with which to compare the augmented design.

All of these studies thus far neglected to look at the design of the heat exchanger in reference to the overall performance of the cycle in which it was designed to be used. Therefore, their figures of merit were not shown to be accurate nor indicative of predicting relative cycle performance. Shah & Sekulić (2003) state that from a system point of view, heat exchanger design must be based on design specifications that are in full accord with an optimization objective designed for the system as a whole.

As discussed in the introduction, the most common system figure-of-merit for comparing the relative energy efficiency of different air-conditioning system designs is the first law efficiency, which is expressed as the coefficient-of-performance (COP). More specifically, the seasonal COP (COP_{seas}) measures the average COP over a cooling season. However, for a heat exchanger optimization study, care must be taken in fixing the appropriate constraints of the system design for the comparison. The more important ones are generally the system's desired cooling capacity, physical size, and equipment cost.

II-D.1: Entropy Generation Minimization

Alefeld (1990) showed that COP and system entropy generation are directly related through fundamental equations (as shown in Chapter 3). Additionally, Bejan (1996) suggests that the point of minimum system entropy generation should coincide with optimum system performance. The technique of Entropy Generation Minimization (EGM) has been in use since the 1970s and is discussed in detail in Bejan (1982). According to Bejan & Pfister (1980):

> "the 'energy conservation' value of a heat transfer augmentation technique can be best measured in terms of the technique's ability to reduce the rate of entropy generation (irreversibility, exergy destruction) in the heat transfer device in which it is implemented."

The central theme of the EGM method is that by minimizing entropy generation, performance is optimized. Bejan (1980, 1982 & 1996) gives many examples of situations in which EGM can be used to optimize performance, however most cases are very basic in nature and have constraints that make their application to a real world design problem impractical.

Klein & Reindl (1997) considered the effect of heat exchanger optimization in relation to an entire cycle. The work explores the optimum allocation of heat exchanger area for both the reverse Carnot and the vapor compression refrigeration cycle models and a comparison was made between using system performance and minimum entropy generation as the figure of merit. The model used is very simplistic compared to the current study, using specific operating conditions to eliminate details. It was concluded that minimizing the total system entropy generation rate does not always result in the same design as maximizing system performance. It is believed that the discrepancies

found in the Klein & Reindl study are due to the evaporator cooling capacity not being fixed throughout the analysis.

Stemming from the fact that system entropy generation and COP are directly related, is the idea of thermoeconomic isolation. This terminology is rooted in a type of analysis known as thermoeconomic optimization, which involves a combination of an exergy/availability analysis of a system with an economical analysis for optimization of thermal systems. A value is placed on the "lost work" from irreversibilities in the system (Moran & Shapiro 2003). An early contribution to this field was by Tribus & Evans (1962). Thermoeconomic isolation, however, is defined by Muñoz & von Spakovsky (2003) as the ability to optimize independently each unit of a system and yet still arrive at the optimum system as a whole. A second law analysis using an availability, exergy, or minimum entropy generation analysis is required. In the current study, minimum entropy generation is investigated as a figure-of-merit in the isolated condenser component compared with maximum system COP (or minimum system entropy generation).

Tapia & Moran (1986) state that system components can be regarded as isolated (in thermoeconomic isolation) from one another when the proper value is assigned to the availability at the various component junctions. Under these conditions, Tapia & Moran state that thermoeconomic isolation guarantees that optimizing a component of an overall thermal system by itself coincides with optimization of the system as a whole. In the current study (as many others have found) these component junction values vary with changing component designs. This is because decreasing entropy generation, or irreversibility, in one component can cause an increase in another. Since the isolated model is lacking feedback from the rest of the system as the component design changes,

it is not possible to state that the resulting component design is the best from the system performance viewpoint by just looking at an individual component. This has been the issue with thermoeconomic isolation, and why its theoretical development has been limited. However, von Spakovsky & Evans (1988) wrote that:

> "although thermoeconomic isolation is an ideal condition that real-world systems can only approach, if approached closely enough both detailed and practical component and system optimizations are possible."

Therefore, by selecting appropriate variables and component junction values to fix, this ideal condition can be approached. In the current study, thermoeconomic isolation is explored as an alternative practical design tool for optimizing the finned-tube condenser heat exchanger component with the goal of optimizing the COP of the air-conditioning system they are designed for.

Many authors have assumed that thermoeconomic isolation is valid, investigating entropy generation minimization in just the heat exchanger component without regard to the system in which it is placed (Saboya & da Costa 2000; Hesselgreaves 2000; Sekulić 1986; Sekulić & Herman 1986; McClintock 1951; Witte & Shamsundar 1983; San & Jan 2000). Most of these analyses are for very simple heat exchanger types, not for finned tube heat exchangers. However, Lin & Lee (1998) used the analysis of Bejan & Pfister (1980) applied to a wavy plate finned-tube heat exchanger. Their analysis only studied a comparison of the inline vs. staggered tube array. Additionally, Schenone et al. (1991) performed a second law analysis to optimize the fin geometry of offset strip-fin heat exchangers. All of these studies assumed that by optimizing the heat exchanger component the entire system would be optimized, but none attempted to address the validity of this assumption.

On a similar note, Cavallini (2002) derives a Penalty Factor (PF, smaller is better) based on the product of two components that tend to penalize the condenser inlet saturation temperature. While the individual components are derived from an exergy analysis of a vapor-compression refrigeration cycle, the development of the Penalty Factor as a product of these values is heuristic. Cavallini continues to use this Penalty Factor to evaluate different refrigerants' relative potential for producing efficient refrigeration systems, as well as to determine optimum circuitry arrangements.

CHAPTER III

COMPONENT MODEL DEVELOPMENT

III-A: Vapor Compression Refrigeration Cycle

The air-conditioning system studied was based on a basic vapor compression refrigeration cycle, shown in Figure 3-1 on a Temperature-Entropy diagram and schematically. As the figure shows, low pressure, superheated refrigerant vapor from the evaporator enters the compressor (State 1) and leaves as high pressure, superheated vapor (State 2). This vapor enters the condenser where heat is rejected to outdoor air that is forced over the condenser coils. The refrigerant vapor is cooled to the saturation temperature (State 2b), condensed, and then cooled to below the saturation point until sub-cooled liquid is present (State 3). The high-pressure liquid then flows through the expansion valve into the evaporator (State 4) where it enters as a low pressure saturated mixture. The liquid refrigerant is evaporated (state 4a) and then superheated by heat transfer from warmer indoor air blown over the evaporator coils. The refrigerant then enters the compressor (State 1). The indoor air is cooled and dehumidified as it flows over the evaporator and is returned to the living space. These state point notations will be used throughout this section to denote properties of the fluids at these points in the system.

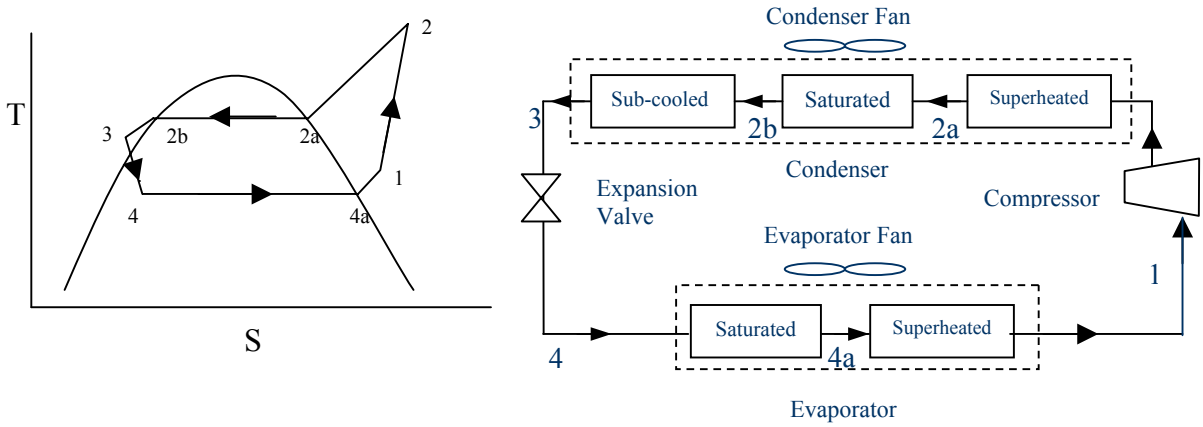

Figure 3-1: Vapor Compression Refrigeration Cycle Description

The complete set of the equations used in the current study is developed in this section. Additionally, improvements made by the current model compared to the model used by Wright (2000) and Aspelund (2001) are noted.

III-B: Compressor

The compressor is the major energy-consuming component of the refrigeration system, and its performance and reliability are significant to the overall performance of the HVAC system. For this study, scroll type positive displacement compressors, which dominate the residential air-conditioning industry, are considered.

The amount of specific work (work per unit mass of refrigerant) done by an ideal compressor ($w_{s,com}$) can be expressed by the change in enthalpy between state 1 and state 2s, where state 2s is a hypothetical state assuming an isentropic process from 1 to 2s (therefore $s_1=s_{2s}$).

For a non-ideal compressor, the actual amount of work done ($w_{a,com}$) depends on the compressor isentropic thermal efficiency η_c:

$$w_{a,com} = \frac{w_{s,com}}{\eta_{com}} = \left(h_2 - h_1\right) \tag{3.1}$$

Wright and Aspelund both used a thermal efficiency equation for an R-22 scroll type compressor formulated by Klein & Reindl (1997). In the current study a correlation relating the isentropic efficiency of R-410a scroll type compressors to the pressure ratio has been developed using manufacturer's data from Copeland (2002):

$$\eta_{com} = 0.0117P_r^3 - 0.155P_r^2 + 0.5487P_r + 0.1035 \tag{3.2}$$

where, P_r is the ratio of the saturated condenser pressure to the saturated evaporator pressure.

The compressor volumetric efficiency is defined by Threlkeld (1970) as the mass of vapor actually pumped by the compressor divided by the mass of vapor which the compressor could pump if it handled a volume of vapor equal to its piston displacement and if no thermodynamic state changes occurred during the intake stroke. The volumetric efficiency (η_{vol}) expression used can be found in Threlkeld (1970), assuming negligible pressure drop in the suction valve and negligible cylinder-wall heating effects:

$$\eta_{vol} = 1 + C_{com} - C_{com}P_r^{1/\gamma} \tag{3.3}$$

with experimental factors determined for this study also from manufacturer's data (Copeland 2002):

$$C_{com} = 0.0617 \tag{3.4}$$

$$\gamma = c_p / c_v \text{ for R410A} \tag{3.5}$$

The volumetric efficiency is used to determine the mass flow rate of the refrigerant though the compressor, $\dot{m}$, for a given compressor size:

$$\dot{m}_r = \frac{\eta_{vol} PD}{v_1} \tag{3.6}$$

where PD is the piston displacement (Threkeld, 1970) and v_1 is the refrigerant specific volume at the evaporator superheated outlet condition.

The entropy generation of the compressor is calculated by the following entropy balance:

$$\dot{S}_{gen,comp} = \dot{m}_r \left(s_2 - s_3 \right) \tag{3.7}$$

where $\dot{m}_r$ is the mass flow rate of the refrigerant.

III-C: Condenser

The condenser heat exchanger configuration used by Wright was of the cross-flow, plate-fin-and-tube type. Refrigerant flows through the tubes, and a fan forces air between the fins and over the tubes. A schematic of this heat exchanger is shown in Figure 3-2 showing some of the geometrical design parameters, while in Figure 3-3, the heat exchanger circuitry is shown. X_t is the transverse, or vertical tube spacing. X_l is the longitudinal, or horizontal tube spacing. F_P is the fin pitch. V_{ac} is the velocity of the air flowing over the condenser, and D is the tube diameter.

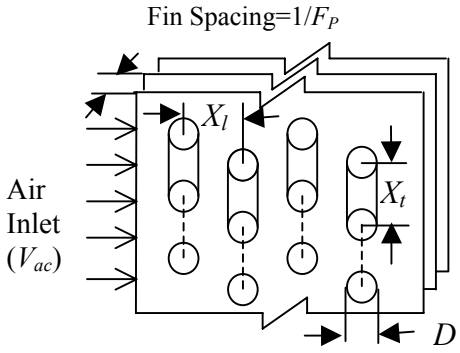

Figure 3-2: Finned Tube Heat Exchanger Schematic

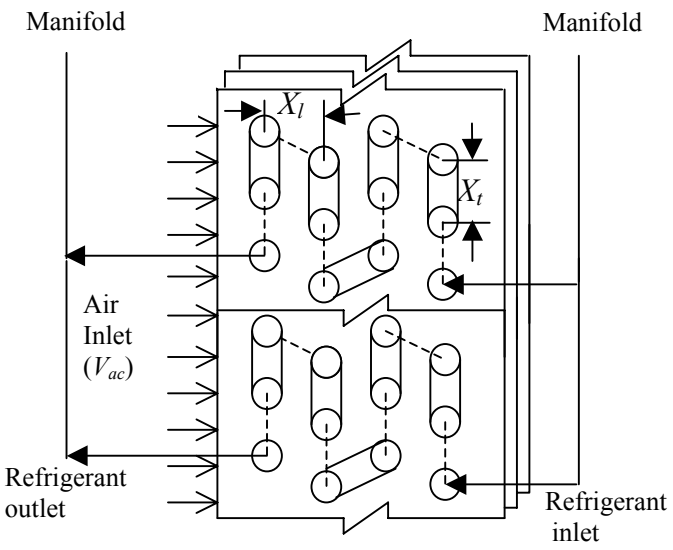

Figure 3-3: Finned-Tube Heat Exchanger Circuitry
(Shown: 4 rows, 2 circuits, 3 tubes per row/circuit)

When the refrigerant exits the compressor, it enters the condenser as a superheated vapor and exits as a sub-cooled liquid. The condenser is separated into three sections: superheated, saturated, and sub-cooled in the model. In the superheated and sub-cooled sections the fluid is in a single phase, while in the saturated section two-phase flow correlations are needed. An energy balance in each of these sections yields the following set of equations:

$$q_{cond,sh} = h_2 - h_{2a}\,, \quad q_{cond,sat} = h_{2a} - h_{2b}\,, \quad q_{cond,sc} = h_{2b} - h_3 \tag{3.8}$$

where $q_{cond,sh}$, $q_{cond,sat}$, and $q_{cond,sc}$ are the heat transfer per unit mass for the superheated, saturated, and subcooled sections, respectively.

The effective mass flow rates on the air-side over each section of the heat exchanger can be related through the individual lengths of each respective section weighted by the total tube length in the condenser (L_{tot}=L_{sh}+L_{sat}+L_{sc}):

$$\dot{m}_{a,sh} = \frac{L_{sh}}{L_{tot}}\dot{m}_{a,tot}\ ,\ \dot{m}_{a,sat} = \frac{L_{sat}}{L_{tot}}\dot{m}_{a,tot}\ ,\ \dot{m}_{a,sc} = \frac{L_{sc}}{L_{tot}}\dot{m}_{a,tot} \tag{3.9}$$

The next several basic heat exchanger equations can be found in Incropera & Dewitt (1996). The total heat transfer rate can be defined in terms of the heat exchanger effectiveness (ε), the minimum heat capacity (C_{min}, the lesser of the heat capacities of the refrigerant-side or the air-side) and the temperature difference between the inlets of the two fluids.

$$\dot{Q} = \varepsilon C_{\min}\left(T_{h,i} - T_{c,i}\right) \tag{3.10}$$

Where the heat exchanger effectiveness is defined as the ratio between the actual heat transfer and the maximum possible heat transfer.

$$\varepsilon = \dot{Q}/\dot{Q}_{\max} \tag{3.11}$$

Depending on the flow configuration, the effectiveness can also be related to a quantity known as the Number of Transfer Units (*NTU*), defined as:

$$NTU = \frac{UA}{C_{\min}} \tag{3.12}$$

Where *UA* is the overall heat transfer coefficient, *U*, times heat transfer area, *A*. Neglecting fouling & wall thermal resistance and assuming the refrigerant side surface efficiency is one (no internal enhancements) the *UA* is defined by the following relation:

$$UA = \left(\frac{1}{\eta_{s,a} \overline{h}_a A_o} + \frac{1}{\overline{h}_r A_r} \right)^{-1} \tag{3.13}$$

Where $\eta_{s,a}$ is the air-side surface efficiency (to be defined shortly), $\overline{h}_a$ & $\overline{h}_r$ are the air side and refrigerant side average convective heat transfer coefficients respectively, and A_r and A_a are the heat transfer areas on the refrigerant and air sides respectively. This total *UA* will be determined by summing the *UA* for each section of the condenser (superheated, saturated, and subcooled).

In the case of a heat exchanger undergoing a phase change in one of the fluids (as in the saturated region of the condenser), the ratio of the heat capacities, C_r:

$$C_r = \frac{C_{\min}}{C_{\max}} \tag{3.14}$$

goes to zero, since the maximum heat capacity fluid has an infinite heat capacity. In this situation the following ε-*NTU* relationship can be used:

$$\varepsilon = 1 - \exp\left(-NTU\right) \tag{3.15}$$

Note that Equation (3.15) is valid for any flow circuitry configuration.

The heat exchanger design shown in Figure 3-3 is a combination of cross-flow and counter flow, however since the majority (over 75%) of the condenser operates in the

saturated region, the counter-flow effect is neglected for the sub-cooled and saturated regions, allowing the use of pure cross flow relations (since there are no analytical relationships for the cross-counter flow configuration).

For a cross-flow heat exchanger, with both fluids unmixed, as in the superheated and sub-cooled sections, the following relationship is given by Incropera & Dewitt (1996):

$$\varepsilon = 1 - \exp\left\{\left(\frac{1}{C_r}\right)\left(NTU\right)^{0.22}\left[\exp\left(-C_r\left(NTU\right)^{0.78}\right)-1\right]\right\} \tag{3.16}$$

This equation, used by Wright & Aspelund, is actually valid for an infinite number of tube rows. For unmixed-unmixed flow with more than four tube rows, ESDU (1991) uses Equation (3.16) as a good approximation, however Wang et al. (2000c) reports that unacceptable results may occur when applying Equation (3.16) to reduce heat transfer coefficients without accounting for the number of tube rows (when less than four). The ε-NTU relationships for unmixed-unmixed cross-flow from ESDU (1991) are thus used and shown in Table 3-1.

Table 3-1: ε-NTU Relationships for unmixed-unmixed cross-flow (ESDU 1991)

# Tube Rows	C_{min} fluid	Formula
1	Air	$\varepsilon = \frac{1}{C_r}\left[1 - e^{-C_r\left(1-e^{-NTU}\right)}\right]$
	Tube	$\varepsilon = 1 - e^{-\frac{\left(1-e^{-NTU\cdot C_r}\right)}{C_r}}$
2	Air	$\varepsilon = \frac{1}{C_r}\left[1 - e^{-2KC_r}\left(1 + C_r K^2\right)\right] \quad (K = 1 - e^{-NTU/2})$
	Tube	$\varepsilon = 1 - e^{-2K/C_r}\left(1 + \frac{K^2}{C_r}\right) \quad (K = 1 - e^{-NTU\cdot C_r/2})$
3	Air	$\varepsilon = \frac{1}{C_r}\left[1 - e^{-3KC_r}\left(1 + C_r K^2\left(3 - K\right) + \frac{3C_r^2 K^4}{2}\right)\right] \quad (K = 1 - e^{-NTU/3})$
	Tube	$\varepsilon = 1 - e^{-3K/C_r}\left(1 + \frac{K^2\left(3-K\right)}{C_r} + \frac{3K^4}{2C_r^2}\right) \quad (K = 1 - e^{-NTU\cdot C_r/3})$
4	Air	$\varepsilon = \frac{1}{C_r}\left[1 - e^{-4KC_r}\left(1 + C_r K^2\left(6 - 4K + K^2\right) + 4C_r^2 K^4\left(2 - K\right) + \frac{8C_r^3 K^6}{3}\right)\right]$ $(K = 1 - e^{-NTU/4})$
	Tube	$\varepsilon = 1 - e^{-4K/C_r}\left(1 + \frac{K^2\left(6 - 4K + K^2\right)}{C_r} + \frac{4K^4\left(2-K\right)}{C_r^2} + \frac{8K^6}{3C_r^3}\right) \quad (K = 1 - e^{-NTU\cdot C_r/4})$
∞	-	$\varepsilon = 1 - \exp\left\{\left(\frac{1}{C_r}\right)\left(NTU\right)^{0.22}\left[\exp\left(-C_r\left(NTU\right)^{0.78}\right) - 1\right]\right\}$ Same as Eq. (3.16), *Note*: unmixed-unmixed formula

III-C.1: Air-side Surface Efficiency

III-C.1.a: Plain Fins

To determine the overall air-side surface efficiency for a finned tube heat exchanger, it is first necessary to determine the efficiency of a fin around a single tube. For a plate-fin-and-tube heat exchanger with multiple rows of staggered tubes, the plates can be symmetrically divided into hexagonal shaped fins as shown in Figure 3-4.

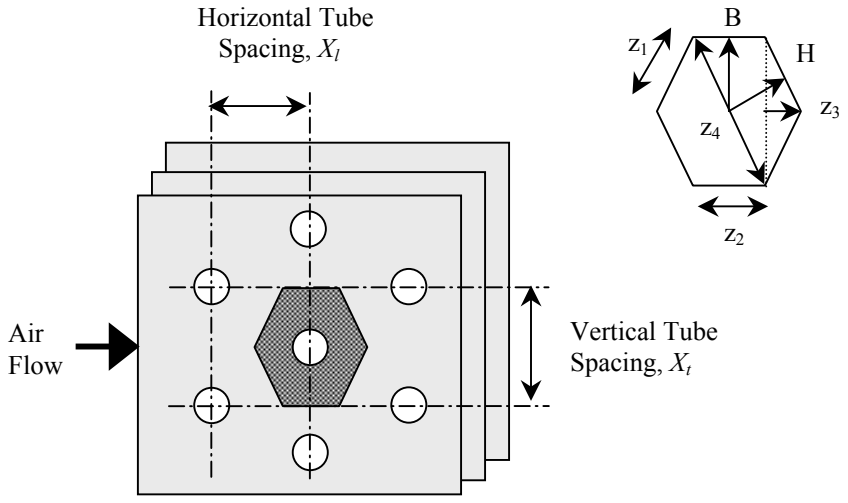

Figure 3-4: Staggered Tube Configuration

The air side surface efficiency is defined by Incropera & Dewitt (1996) as follows:

$$\eta_{s,a} = 1 - \frac{A_{fin}}{A_o}\left(1 - \eta_{fin}\right) \tag{3.17}$$

where A_{fin} is the surface area of the fins, A_o is the total air side heat transfer area (including the fin and the tubes) and η_{fin} is the fin efficiency of a circular fin, which Incropera & Dewitt (1996) define as:

$$\eta_{fin} = \frac{\tanh\left(m_{es} R\phi\right)}{m_{es} R\phi} \tag{3.18}$$

where R is the radius of a circular fin, m_{es} is the standard extended surface parameter, which is defined as:

$$m_{es} = \left(\frac{2\bar{h}_a}{k_a t_f}\right)^{1/2} \tag{3.19}$$

assuming the fin length is much larger than the fin thickness (k_a is the thermal conductivity of the air and t_{fin} is the fin thickness), and ϕ is the fin efficiency parameter for a circular fin.

Schmidt (1945) analyzed plain hexagonal fins and determined that they can be treated as circular fins by using an equivalent circular fin radius. Schmidt developed empirical correlations for the equivalent radius (R_e, to be used in Equation (3.18) in place of R), which Wright (2000) and Aspelund (2001) used:

$$\frac{R_e}{r_t} = 1.27\psi\left(\beta - 0.3\right)^{1/2} \tag{3.20}$$

where r_t is the outside tube radius and Ψ and β are:

$$\psi = \frac{B}{r_t} \tag{3.21}$$

$$\beta = \frac{H}{B} \tag{3.22}$$

For this analysis,

$$B = X_l \text{ if } X_l < X_t / 2, \text{ otherwise } B = X_t / 2 \tag{3.23}$$

$$H = \frac{1}{2}\sqrt{\left(\frac{X_t}{2}\right)^2 + X_l^2} \tag{3.24}$$

(these parameters are shown in Figure 3-4 assuming $B = X_t /2$). Where X_t is the transverse (vertical) tube spacing and X_l is the longitudinal (horizontal) tube spacing.

However, in Schmidt's study it is claimed that this approximation is limited to situations where β >1. From Aspelund's (2001) work the optimum tube spacing ratio may be much higher than conventionally used and outside of the range in which Schmidt's approximation is proven to be valid. Zeller & Grewe (1994) give an improved equation for the equivalent circular fin radius based on the relative perimeters of the circle and the hexagon. It was found that Zeller & Grewe's and Schmidt's correlations showed very good agreement with each other when β >1. Zeller & Grewe's equation was used in the current study, since it does not have the limitations of Schmidt's equation.

Therefore the relation for the equivalent radius, as defined by Zeller & Grewe is:

$$\frac{R_e}{r_t} = \frac{P_{hex}}{2\pi r_t} \tag{3.25}$$

where P_{hex} is the Perimeter of the hexagonal fin:

$$P_{hex} = 4z_1 + 2z_2 \tag{3.26}$$

The lengths z_1 and z_2, defined in Figure 3-4, can be found from iteratively solving the following four equations when the lengths B and H are known (Equations (3.23) and (3.24) still apply):

$$z_2^{\,2} + (2B)^2 = z_4^{\,2} \tag{3.27}$$

$$\left(\frac{z_1}{2}\right)^2 + H^2 = \left(\frac{z_4}{2}\right)^2 \tag{3.28}$$

$$H^2 + \left(\frac{z_1}{2}\right)^2 = \left(z_3 + z_2/2\right)^2 \tag{3.29}$$

$$z_1^{\,2} = z_3^{\,2} + B^2 \tag{3.30}$$

This equivalent circular fin radius can then be used to calculate the fin efficiency parameter using the circular fin relationship (as Wright & Aspelund used):

$$\phi = \left(\frac{R_e}{r_t} - 1\right)\left(1 + 0.35\ln\left(\frac{R_e}{r_t}\right)\right) \tag{3.31}$$

Perrotin & Clodic (2003), proposed using a modified ϕ parameter in Equation (3.31):

$$\phi_m = \left(\frac{R_e}{r_t} - 1\right)\left[1 + \left(0.3 + \left(\frac{m(R_e - r_t)}{2.5}\right)^{1.5 - \frac{1}{12}\frac{R_e}{r_t}}\left(0.26\left(\frac{R_e}{r_t}\right)^{0.3} - 0.3\right)\right)\ln\left(\frac{R_e}{r_t}\right)\right] \quad (3.32)$$

Perrotin & Clodic found that using this modified ϕ_m the error between their analytical solution and the approximation does not exceed 2% over the practical range of conditions $R_e/r_t \leq 6$ and $m(R_e\text{-}r_t) \leq 2.5$ for plain fins.

Additionally, Hong & Webb (1996) proposed to slightly modify Equation (3.18) in order to obtain better accuracy. Therefore Equation (3.18) becomes:

$$\eta_{fin} = \frac{\tanh(m_{es} R_e \phi)}{m_{es} R_e \phi}\cos(0.1 m_{es} R_e \phi) \quad (3.33)$$

III-C.1.b: Louvered Fins

For louvered fins, Perrotin & Clodic (2003) concluded that Schmidt's circular fin approximation analysis overestimates the fin efficiency, by up to 5%. This is because the addition of the enhancement can alter the conduction path through the fin. However, there is currently no approximation method available in the literature that claims to be valid for enhanced fins, therefore Zeller & Grewe's correlations were used for the louvered fin cases as well.

Now the airside fin surface efficiency can be calculated, however the heat transfer coefficients on the air and refrigerant sides of the heat exchanger are not specified in Equation (3.13).

III-C.2: Refrigerant Side Correlations

III-C.2.a: Heat Transfer Relations

The most important aspect of the condenser model is the equations used to describe the heat transfer coefficients and pressure drops on both the air-side and refrigerant-side of the heat exchanger. On the refrigerant side, the heat transfer coefficient in the single phase regions (sub-cooled and superheated) region are calculated by the correlation of Kays & London (1984):

$$\mathrm{St}\,\mathrm{Pr}^{2/3} = a_{st}\,\mathrm{Re}_{D_i}^{\,b_{st}} \tag{3.34}$$

where the coefficients a_{st} and b_{st} are:

Laminar	$\mathrm{Re_{Di}} < 3{,}500$	$a_{st} = 1.10647$,	$b_{st} = -0.78992$
Transition	$3{,}500 \le \mathrm{Re_{Di}} \le 6{,}000$	$a_{st} = 3.5194 \times 10^{-7}$,	$b_{st} = 1.03804$
Turbulent	$6{,}000 < \mathrm{Re_{Di}}$	$a_{st} = 0.2243$,	$b_{st} = -0.385$

and,

$$\mathrm{St} = \frac{\mathrm{Nu_D}}{\mathrm{Re}_{D_i}\,\mathrm{Pr}} = \frac{\bar{h}_{r,SP}}{Gc_p} \tag{3.35}$$

where, G is the total mass velocity, St is the Stanton number, $\mathrm{Nu_D}$ is the Nusselt number, $\mathrm{Re_{Di}}$ is the Reynolds number based on the inner tube diameter, and $\bar{h}_{r,SP}$ is the refrigerant side single phase average convective heat transfer coefficient.

For the two-phase portion of the condenser, Wright's model used the heat transfer coefficient calculated by the correlation of Shah (1979). In the current study, a new

model was used instead of Shah (1979) because Cavallini et al. (2001) found that Shah's model displayed discrepancies and limited application within its set of valid ranges when applied to the new "high pressure" fluids, such as R-410a. The predictive model by Cavallini et al. (2002) was chosen because it was developed to compute the heat transfer coefficient and pressure drop during condensation inside smooth tubes operating with pure or blended halogenated refrigerants, including the new high pressure HFC fluids.

Additionally, the Cavallini et al. (2002) model takes into consideration changes in flow regime including annular, stratified-wavy/transition, and slug flow. Based on the works of Breber et al. (1980), Sardesai et al. (1981), Tandon et al. (1982, 1985), Rabas and Arman (2000), Dobson and Chato (1998), and Wallis et al. 1977), Cavallini determines the transition criteria shown in Table 3-2:

Table 3-2: Refrigerant Flow Regime Transition Criteria (Cavallini et al. 2002)

Flow Regime	J_G	X_{tt}
Annular	≥ 2.5	-
Annular-stratified transition and stratified flow	< 2.5	<1.6
$G < G_W$ *stratified – wavy*	<2.5	>1.6
$G > G_W$ *slug flow*		

Where J_G is the dimensionless vapor mass velocity, defined in terms of quality, x, mass velocity, G, inside tube diameter, D_i, density of the gas phase, ρ_G, density of the liquid phase, and gravity, g:

$$J_G = \frac{xG}{\left[gD_i\rho_G\left(\rho_L - \rho_G\right)\right]^{0.5}} \tag{3.36}$$

X_{tt} is the Martinelli parameter, defined by:

$$X_{tt} = \left(\frac{\mu_L}{\mu_G}\right)^{0.1}\left(\frac{\rho_G}{\rho_L}\right)^{0.5}\left[\left(1-x\right)/x\right]^{0.9} \tag{3.37}$$

where μ_G and μ_L are the viscosities of the liquid and gas phases, respectively. And G_W is the transition flow rate given by Wallis (1977), defined by:

$$G_W = \left(0.54 - 0.06\mathrm{E}_\mathrm{O}^2 - 1.05\mathrm{E}_\mathrm{O}\right)\rho_L\left(gD_i\right)^{0.5} \tag{3.38}$$

where $\mathrm{E_O}$ is the Eötvos number:

$$\mathrm{E_O} = \frac{4\sigma}{\left[\left(\rho_L - \rho_G\right)gD_i^{\,2}\right]} \tag{3.39}$$

And σ is the surface tension of the liquid phase.

These transitions, as defined by Cavallini et al. (2002), are shown on the phase regime plot in Figure 3-5 along with a curve for a representative set of conditions in the saturated region of condensers of the current study. It can be seen that from saturated vapor (x=1) up to a quality of about 0.49, the flow is in the annular region. Upon further condensation, the flow is in the annular transition and wavy-stratified region, before

moving into the slug flow region at a quality, x, of about 0.17 down to saturated liquid (x=0).

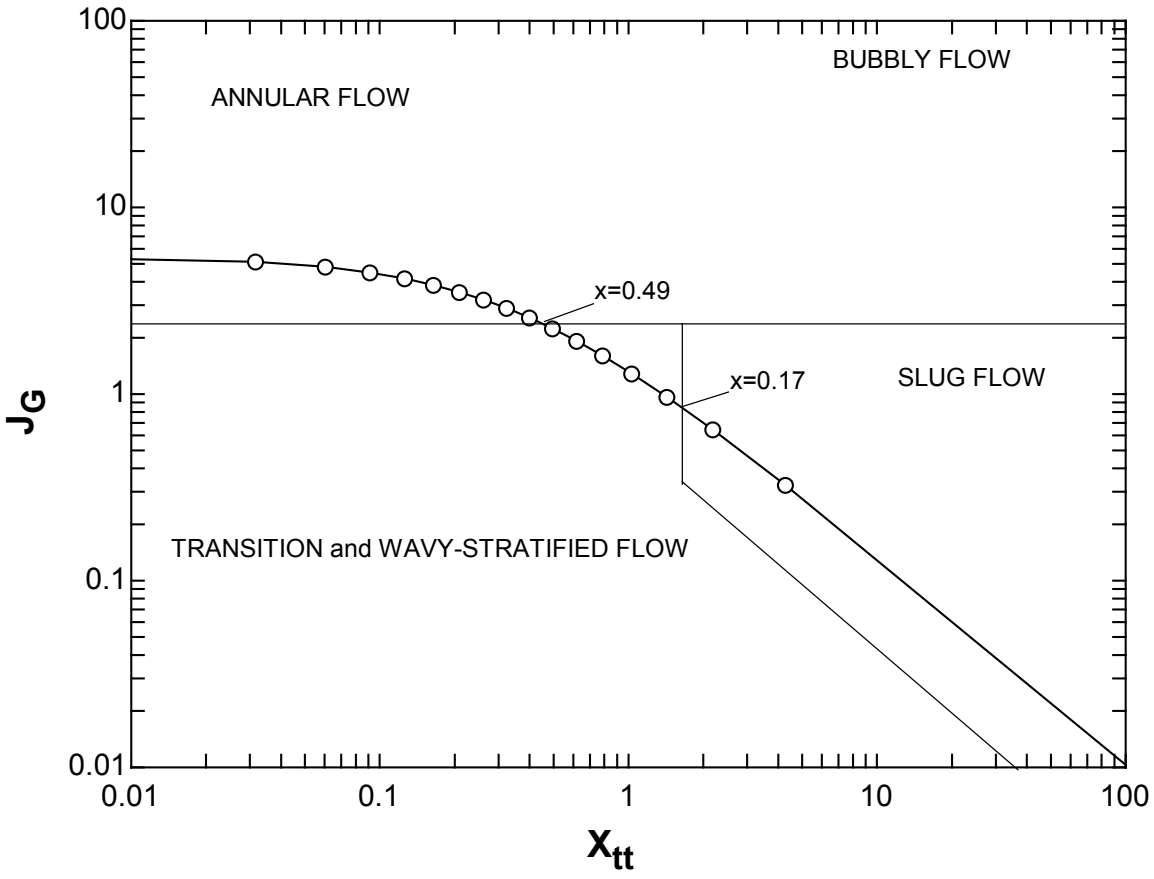

Figure 3-5: Two Phase Flow Regime Transitions

The equations used in Cavallini's heat transfer model are summarized in Tables 3-3 through 3-5. Any variables not defined here can be found in the Nomenclature section.

Table 3-3: Cavallini et al. (2002), Annular Flow Model to be Applied When J_G>2.5

Equation	Eq. #
$h_{TP} = \rho_L c_{pL} \left(\tau / \rho_L\right)^{0.5} / T^+$	(3.40)
$T^+ = \delta^+ \mathrm{Pr}_L \qquad \delta^+ \le 5$	(3.41)
$T^+ = 5\left\{\mathrm{Pr}_L + \ln\left[1 + \mathrm{Pr}_L\left(\frac{\delta^+}{5} - 1\right)\right]\right\} \qquad 5 < \delta^+ < 30$	(3.42)
$T^+ = 5\left\{\mathrm{Pr}_L + \ln\left(1 + 5\,\mathrm{Pr}_L\right) + 0.495 \ln\left(\frac{\delta^+}{30}\right)\right\} \qquad \delta^+ \ge 30$	(3.43)
$\mathrm{Re}_{Di} = \frac{4\dot{m}_L}{\pi D_i \mu_L} = \frac{G(1-x)D_i}{\mu_L}$	(3.44)
$\delta^+ = \left(\frac{\mathrm{Re}_{Di}}{2}\right)^{0.5} \qquad for\ \mathrm{Re}_{Di} \le 1145$	(3.45)
$\delta^+ = 0.0504\,\mathrm{Re}_{Di}^{7/8} \qquad for\ \mathrm{Re}_{Di} \le 1145$	(3.46)
$\tau = \left(\frac{dp}{dz}\right)_f \frac{D_i}{4}$	(3.47)
$\left(\frac{dp}{dz}\right)_f = \Phi_{LO}^2 \left(\frac{dp}{dz}\right)_{f,LO} = \frac{\Phi_{LO}^2 f'_{LO} G^2}{D_i \rho_L}$	(3.48)
$\Phi_{LO}^2 = E_{cav} + \frac{1.262 F_{cav} \cdot H_{cav}}{We^{0.1458}}$	(3.49)
$E_{cav} = (1-x)^2 + x^2 \left(\frac{\rho_L f'_{GO}}{\rho_G f'_{LO}}\right)$	(3.50)
$F_{cav} = x^{0.6978}$	(3.51)

$H_{cav} = \left(\frac{\rho_L}{\rho_G}\right)^{0.3278} \left(\frac{\mu_G}{\mu_L}\right)^{-1.181} \left(1-\frac{\mu_G}{\mu_L}\right)^{3.477}$		(3.52)
$We = \frac{G^2 D_i}{\rho_G \sigma_L}$		(3.53)
$f'_{LO} = 0.046\left[\frac{GD_i}{\mu_L}\right]^{-0.2}$	$GD_i / \mu_G > 2000$	(3.54)
$f'_{LO} = 16/\left[\frac{GD_i}{\mu_L}\right]$	$GD_i / \mu_G \leq 2000$	(3.55)
$f'_{GO} = 0.046\left[\frac{GD_i}{\mu_G}\right]^{-0.2}$	$GD_i / \mu_G > 2000$	(3.56)
$f'_{GO} = 16/\left[\frac{GD_i}{\mu_G}\right]$	$GD_i / \mu_G \leq 2000$	(3.57)

Where h_{TP} is the two-phase convective heat transfer coefficient, Pr_L is the Prandtl number for the liquid phase ($\mu_L c_{pl}/k_L$), τ is the wall shear stress, We is the Weber number, Φ_{LO}^2 is the two-phase frictional multiplier, f'_{LO} is the Fanning friction factor if the liquid only flowed in the tube, and f'_{GO} is the Fanning friction factor if the gas only flowed in the tube.

When J_G decreases below 2.5 and $X_{tt} > 1.6$ the flow enters the annular-stratified transition and stratified flow region. For this situation the heat transfer coefficient is calculated from a linear-interpolation between the heat transfer coefficient for annular flow at J_G =2.5 ($h_{TP,an,JG=2.5}$) and the heat transfer coefficient for stratified flow (Equation (3.60)). The heat transfer coefficient $h_{TP,an,JG=2.5}$ is evaluated with equations from Table

3-3 at the existing local vapor quality and fluid properties but with the fictitious value $G_{JG=2.5}$ of mass velocity relative to J_G =2.5:

$$G_{JG=2.5} = 2.5\left[gD_i\rho_G\left(\rho_L - \rho_G\right)\right]^{0.5} / x \tag{3.58}$$

Then the transition heat transfer coefficient can be calculated using Table 3-4 (Cavallini et al. 2002).

Table 3-4: Cavallini et al. (2002) Model for Annular-Stratified Transition and Stratified Flow to be Applied When J_G<2.5 and X_{tt}<1.6

Equation	**Eq. #**
$h_{TP,trans} = \left(h_{TP,an,JG=2.5} - h_{TP,strat}\right)\left(\frac{J_G}{2.5}\right) + h_{TP,strat}$	(3.59)
$h_{TP,strat} = 0.725\left\{1+0.82\left[\frac{1-x}{x}\right]^{0.268}\right\}^{-1}\left[\frac{k_L^3\rho_L\left(\rho_L-\rho_G\right)gh_{fg}}{\mu_L D_i\Delta T}\right]^{0.25} + \alpha_L\left(1-\frac{\theta}{\pi}\right)$	(3.60)
$\alpha_L = \alpha_{LO}\left(1-x\right)^{0.8}$	(3.61)
$\alpha_{LO} = 0.023\,\mathrm{Re}_{LO}^{0.8}\,\mathrm{Pr}_L^{0.4}\left(\frac{k_L}{D_i}\right) = \left(\frac{GD_i}{\mu_L}\right)^{0.8}\left(\frac{c_{pL}\mu_L}{k_L}\right)^{0.4}\left(\frac{k_L}{D_i}\right)$	(3.62)
$1-\frac{\theta}{\pi} = \frac{\left[\arccos\left(2\varepsilon_z - 1\right)\right]}{\pi}$	(3.63)
$\varepsilon_{v,z} = \frac{x}{\left[x+\left(1-x\right)\left(\frac{\rho_G}{\rho_L}\right)^{0.66}\right]}$ (Zivi void fraction)	(3.64)

The flow enters the stratified-slug transition and slug flow region as the Martinelli parameter becomes larger than 1.6, with J_G <2.5. The transition flow rate G_W, given by Wallis et al. (1977), is the flow rate needed for a tube to run full at the exit when discharging a liquid into a gas filled space. When the mass velocity is less than G_W, the heat transfer coefficient is calculated with the method presented for the annular-stratified region (Table 3-4). The ΔT in Equation (3.60) is the temperature difference between the refrigerant and the tube wall. This ΔT was calculated as an average value in the saturated region by the following equation:

$$\Delta T = \frac{Q_{2a2b}}{\left(\pi D_o L_{2a2b}\right)\bar{h}_{2a2b}} \tag{3.65}$$

When the mass velocity is greater than G_W, the heat transfer coefficient is calculated with a two-phase flow multiplier equation (Equation (3.67)).

Table 3-5: Cavallini et al. (2002) Model for Stratified-Slug Transition and Slug Flow to be Applied When J_G<2.5 and X_{tt}>1.6

Equation			**Eq. #**
$h_{TP} = h_{TP,trans}$	(Equations (3.59)-(3.64))	for $G < G_W$	(3.66)
$h_{TP} = h_{TP,slug} = \alpha_L \left\{ 1+2.87 \left[x^{0.9} \left(\frac{\rho_L}{\rho_G} \right)^{0.5} \left(\frac{\mu_G}{\mu_L} \right)^{0.1} \right]^{1.44} \right\}$		for $G > G_W$	(3.67)

Note that these equations give the local heat transfer coefficient. Therefore, the integral of these equations must be taken over the length of tubing in the saturated region

to obtain the average heat transfer coefficient. Unfortunately, it is difficult to predict the variation of the quality with length, *dx/dz*, therefore a linear profile is assumed for the work of this study. The integral function in EES, which is a second-order predictor-corrector algorithm, was used to perform this integration. To help increase the speed of calculations, a trapezoidal rule was used to approximate the integral in early stages of the search technique. This approximation did not have an effect on the optimum condenser design, however the more accurate EES Integral Function was used in the final stages of optimization for more accurate calculation of the seasonal COP.

Heat transfer in the finless tube bends has been neglected. The more important aspect of the tube bends is the significant pressure drops, which comprise about 30% of the total pressure drop on the refrigerant side in the system.

III-C.2.b: Pressure Drop Relations

III-C.2.b.i: Straight Tube Section

The pressure drop on the refrigerant side in the single-phase regimes are calculated by the standard equation for pressure drop in circular pipe flow:

$$\Delta p_{S,SP} = \frac{f G^2 L}{\rho} \tag{3.68}$$

using a Darcy friction factor for fully developed laminar flow (Munson et al. 1998) of:

$$f = \frac{64}{\mathrm{Re}_{Di}} \tag{3.69}$$

(where the Reynolds number is based on the inside tube diameter D_i) and the Colebrook equation (1938) is used for turbulent pipe flow:

$$\frac{1}{f^{1/2}} = -2\log_{10}\left[\frac{\varepsilon_{\mathrm{pr}}/D_i}{3.7} + \frac{2.51}{\mathrm{Re}_{D_i} f^{1/2}}\right]. \tag{3.70}$$

where ε_{pr} is the pipe roughness, for which a value of 0.000005 ft was used (for drawn copper tubes).

In the saturated (two-phase) portion of the condenser, Wright (2000) used the work of Hiller & Glicksman (1976) to find the pressure drop, which is an extension of the Lockhart & Martinelli (1949) method. However, in the current study the work of Cavallini et al. (2002) is used. As mentioned earlier, Cavallini's model was developed for higher-pressure refrigerants such as R-410a. Cavallini recommends the correlations summarized in Table 3-6 for the annular flow regime, when $J_G \geq 2.5$, and the correlations of Friedel (1979), as shown in Table 3-7, for J_G<2.5. Equation (3.71) shows how the pressure drop is split up into a frictional term and a momentum term. Equation (3.49) is to be used for calculation of the frictional pressure drop $\left(\frac{dp}{dz}\right)_f$.

Table 3-6: Cavallini et al. (2002) Pressure Gradient During Condensation to be used when $J_G \geq 2.5$ (Annular Flow)

Equation	Eq. #
$-\left(\frac{dp}{dz}\right) = -\left(\frac{dp}{dz}\right)_f - \left(\frac{dp}{dz}\right)_m$	(3.71)
$-\left(\frac{dp}{dz}\right)_m = G^2 D_i \left\{ \frac{x^2}{\rho_G \varepsilon_v} + \frac{(1-x)^2}{\rho_L (1-\varepsilon_v)} \right\} / dz$	(3.72)
$\varepsilon_v = \left(\frac{1-2\delta}{D_i}\right)^2$	(3.73)
$\delta = \frac{\delta^+ \upsilon_L}{u_\tau}$	(3.74)
$u_\tau = \left(\frac{\tau}{\rho_L}\right)^{0.5}$	(3.75)

where ε is the void fraction, ν_L is the kinematic viscosity of the liquid phase, δ^+ was defined in Equations (3.45) and (3.46), and τ was defined in Equation (3.47).

As was the case with the condensation heat transfer coefficient, a linear variation of quality with length is assumed. If the quality variation is divided in to small increments of Δx, the resulting pressure drops over each small increment can be summed to yield the total pressure drop over the entire length. The pressure drop per unit length as a function of the variation in quality for the frictional and momentum components are then integrated over the length of the tube, utilizing the aforementioned incremental procedure. As in the average heat transfer calculations, the EES integral function (second-order predictor-corrector algorithm) was used to perform this integral.

Table 3-7: Friedel (1979) Correlation for Pressure Drop for J_G<2.5

Equation	Eq. #
$\Phi_{LO}^2 = A_1 + \frac{3.24 A_2}{\mathrm{Fr}^{0.045}\mathrm{We}^{0.035}}$	(3.76)
$A_1 = (1-x)^2 + x^2 \left(\frac{\rho_L}{\rho_G}\right)\left(\frac{f'_{GO}}{f'_{LO}}\right)$	(3.77)
$A_2 = x^{0.78}(1-x)^{0.24}\left(\frac{\rho_L}{\rho_G}\right)^{0.91}\left(\frac{\mu_G}{\mu_L}\right)^{0.19}\left(1-\frac{\mu_G}{\mu_L}\right)^{0.70}$	(3.78)
$\mathrm{Fr} = \frac{G^2}{g D_i \rho_{TP}}$ (Froude number)	(3.79)
$\rho_{TP} = \left(\frac{x}{\rho_G} + \frac{1-x}{\rho_L}\right)^{-1}$ (two-phase density)	(3.80)
$\mathrm{We} = \frac{G^2 D_i}{\rho_{TP}\sigma_L}$	(3.81)

III-C.2.b.ii: <u>Tube Bends</u>

The method for calculating the pressure drop inside the tube bends was the same as that used by Wright, using the work of Chisholm (1983). For single-phase flow, the pressure drop in tube bends is calculated simply by assigning an equivalent length to each bend based on the flow diameter and the bend radius. For two-phase flow in tube bends, the pressure drop is calculated for liquid-only flow, and correction factors are applied to determine the approximate two-phase flow pressure drop. Instead of predicting the two-phase pressure drop in inclined bends that are found in most heat exchangers, this method

predicts the pressure drops for two-phase flow in horizontal bends. However, no accurate correlations are available for predicting the two-phase flow pattern in an inclined bend. Furthermore, the pressure gradients due to elevation changes caused by the incline are negligible compared to friction pressure losses. Hence, the horizontal bend model developed by Chisolm is used in this study. Since the bends are not finned and do not come into contact with air flow, the heat transfer in the bends is neglected.

The first step in computing the pressure drop in a tube bend is to determine the equivalent length of the bend. The equivalent tube length, y, is a function of the relative radius, r_r:

$$r_r = \frac{r_b}{D_i} \tag{3.82}$$

where r_b is the tube centerline radius of the bend. Most condensers utilize tubes with a relative radius between 1 and 3, which according to Chisolm's model corresponds to an equivalent length of between 12 to 15 diameters for 90° bends. The equivalent length for a 180° return bend is approximately twice the equivalent length of a 90° bend. Therefore, in this study, 180° return bends are assumed to have an equivalent length of 26 diameters.

Chisolm approximates the single-phase pressure drop in a bend by simply substituting the equivalent length of the bend, y, for the straight pipe length in the standard pressure drop equation,

$$\Delta p_{b,SP} = \frac{fG^2}{2\rho}\left[\frac{y}{D_i}\right]_e \tag{3.83}$$

where $\Delta p_{b,SP}$ is the single phase pressure drop in the bend.

For the two-phase flow pressure drop in bends, the calculations are more involved. Assuming homogeneous two-phase flow, the friction factor is determined by the same expressions that are used for single phase flow as shown in Equations (3.69) and (3.70). However, Chisolm's development uses a Reynolds number based on the two-phase flow viscosity.

$$\mathrm{Re}_{D_i} = \frac{GD_i}{\mu_{TP}} \tag{3.84}$$

The two-phase viscosity is a function of the quality and is determined by the following expression:

$$\mu_{TP} = \mu_G x + (1-x)\,\mu_L \tag{3.85}$$

Chisolm defines a two-phase flow bend pressure drop coefficient for a 90° bend, $k_{b,90^\circ}$, which is expressed as:

$$k_{b,90^o} = \left[\frac{\mathrm{y}}{D_i}\right]_e f \tag{3.86}$$

Another coefficient for 90° bends, B_{90° is also defined, and is expressed by:

$$B_{90^o} = 1 + \frac{2.2}{k_{b,90^o}\left(2 + R_b / D_i\right)} \tag{3.87}$$

where R_b is the bend recovery length. The B_θ coefficient for bends that are not 90° is expressed as:

$$B_\theta = 1 + \left[B_{90^o} - 1\right]\frac{k_{b,90^o}}{k_{b,\theta}} \tag{3.88}$$

In the case of 180° bends, the bend pressure coefficient $k_{b,180^\circ}$, is approximately twice the value of $k_{b,90^\circ}$, so B_{180° can be calculated by the following expression.

$$B_{180^o} = 0.5\left(1 + B_{90^o}\right) \tag{3.89}$$

Chisolm defines a two-phase multiplier, φ^2, for the pressure drop in a tube bend as:

$$\Phi^2_{b,lo} = 1 + \left(\Gamma^2_b - 1\right)\left(B_\theta x^{(2-n)/2}\left(1-x\right)^{(2-n)/2} + x^{(2-n)}\right) \tag{3.90}$$

where Γ_b^2 is the physical property coefficient for a tube bend and is determined by,

$$\Gamma^2_b = \frac{\rho_L}{\rho_G}\left(\frac{\mu_G}{\mu_L}\right)^{n_B} \tag{3.91}$$

and n_B is the Blausius coefficient, which is calculated by the following expression.

$$n_B = \frac{\ln\left(\dfrac{f_{LO}}{f_{GO}}\right)}{\left(\dfrac{\mu_G}{\mu_L}\right)} \tag{3.92}$$

The friction factors f_{LO} and f_{GO} are determined using Equation (3.69) for laminar flow inside a circular pipe, by assuming all of the mass is flowing alone as either a liquid or a vapor.

The two-phase pressure drop is then calculated as the product of the liquid-only single-phase pressure drop and the two-phase multiplier, $\Phi^2_{b,LO}$:

$$\Delta p_{b,TP} = \Delta p_{b,LO} \Phi^2_{b,LO} \tag{3.93}$$

The liquid-only bend pressure drop, $\Delta p_{b,LO}$ is then determined by Equation (3.83).

III-C.3: Air-side Correlations: Plain Fins

III-C.3.a: Analysis of Alternative Correlations from Studies of Wright & Aspelund

While the velocity distribution of the air over the coil is assumed to be uniform, the complex airflow pattern across the fin-and-tube surfaces makes the theoretical predictions of the heat-transfer coefficient and friction factor from first principles very difficult; therefore such relations are usually empirical in nature. However, these empirical correlations are limited by the range of data used in their development, and these ranges are not always published along with the correlations. Sometimes it required obtaining the experimental data from other publications and examining the ranges used in the correlations' development.

On the air-side, Wright used the work of McQuiston (McQuiston & Parker 1994) for the heat transfer coefficient and the work of Rich (1973) to calculate the air-side pressure drop, with the Euler number calculated from Zukauskas & Ulinskas (1998).

Aspelund's optimum design fell outside of the range of applicability of all of the heat transfer and friction correlations used on the air-side due to the large ratio of vertical to horizontal tube spacing it prescribed. Because of this, the works of Wang (1996 & 2000), McQuiston (1978) and Gray & Webb (1986) were investigated to determine if their ranges of applicability included Aspelund's design, which they did not either. Then all of the correlations were compared to see how they behaved outside of their range of applicability.

Many of the early studies that provide heat transfer and friction correlations for the airside of finned-tube heat exchangers were based on larger tube diameters and tube spacings than those more commonly used today. Heat exchanger manufacturers found that the use of smaller heat transfer tubes, smaller transverse tube pitch, and smaller longitudinal tube pitch can effectively reduce the airside resistance as well as saving resources and can lead to a much more compact fin-and-tube heat exchanger design. Benefits of using smaller diameter tubes include smaller form drag caused by the tube, higher refrigerant side heat transfer coefficients due to smaller hydraulic diameter, and less refrigerant inventory in the system (Wang et al. 2001).

While Wang's (2000) correlations were developed using tube diameters more appropriate for the current study, it was found that the friction and heat transfer correlations are unstable near the ends of its validity range. Additionally, Wang's (1996) heat transfer correlation always showed disagreement with the other correlations, so it was disregarded. However, the friction correlation from the same study did not have this problem. McQuiston's friction correlation did not behave well with the diameter of tubing used in the current study (5/16"), plus it received negative reviews by Gray &

Webb (1986). Webb's friction correlation also did not behave well at small diameters, but this may be more due to the fact that it, like the Rich equation (used by Wright & Aspelund), is used in conjunction with the work of Zukauskas and Ulinksas, which is reported to be a better correlation with larger diameter tubes (5/8" to 2")(Wang 2001b). Because of this, Wang (2001b) developed a modification to the Zukauskas and Ulinskas relation, expanding its range of applicability to larger X_t / D ratios, allowing for smaller diameter tubes to be used with constant vertical spacing.

From this current analysis, the equations originally used by Wright and Aspelund were deemed the most stable and appropriate with the correction from Wang (2001b) added. However limits have now been added to the program so that it is restricted to solving within the equations' ranges of data from which they were developed.

III-C.3.b: Heat Transfer Relations

The work of McQuiston (McQuiston and Parker, 1994) is used to evaluate the air-side convective heat transfer coefficient for a plate finned-tube heat exchanger with multiple rows of staggered tubes. The model is developed for dry coils. The heat transfer coefficient is based on the Colburn j-factor, which is defined as:

$$j = St \, \mathrm{Pr}^{2/3} . \tag{3.94}$$

Substituting the appropriate values for the Stanton number, *St*, gives the following relationship for the air-side convective heat transfer coefficient, $\overline{h}_a$,

$$\bar{h}_a = \frac{jc_p G_{\max}}{\Pr^{2/3}} \tag{3.95}$$

where c_p is the specific heat, and G_{max} is the mass velocity of air through the minimum flow area which is expressed as:

$$G_{\max} = \frac{\dot{m}_{air}}{A_{\min}}, \tag{3.96}$$

The minimum free flow area, A_{min}, is the passage height (fin spacing – fin thickness) multiplied by the minimum of the distances X_t or 2*X_{diag} (as shown in Figure 3-6).

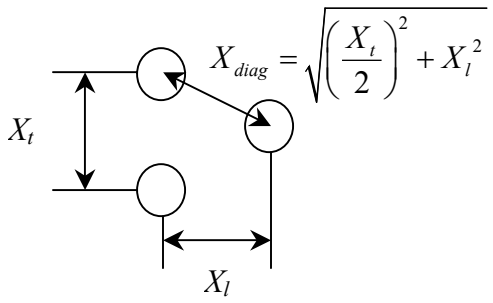

Figure 3-6: Diagram of Minimum Free Flow Area

McQuiston (McQuiston and Parker, 1994) used a 4-row finned tube heat exchanger as the baseline model, and define the Colburn j-factor for a 4-row finned-tube heat exchanger as:

$$j_4 = 0.2675JP + 1.325 \times 10^{-6} \tag{3.97}$$

and the parameter JP is defined as:

$$JP = \mathrm{Re}_{D_o}^{-0.4} \left(\frac{A_o}{A_t} \right)^{-0.15} \tag{3.98}$$

where A_t is the tube outside surface area, and A_o is the total air side heat transfer surface area (fin area plus tube area). The Reynolds number, Re_{Do} in the above expression is based on the tube outside diameter, D_o, and the maximum mass velocity, G_{max}. The area ratio can be expressed as:

$$\frac{A_o}{A_t} = \frac{4}{\pi} \frac{X_l}{D_h} \frac{X_t}{D_{depc}} \sigma \tag{3.99}$$

where X_l is the tube spacing parallel to the air flow (longitudinal), X_t is the tube spacing normal to the air flow (transverse), D_{depc} is the depth of the condenser in the direction of the air flow, D_h is the hydraulic diameter defined as:

$$D_h = \frac{4 A_{\min} D_{depc}}{A_o} \tag{3.100}$$

and σ is the ratio of the minimum free-flow area to the frontal area,

$$\sigma = \frac{A_{\min}}{A_{fr}} \tag{3.101}$$

The j-factor for heat exchangers with four or fewer rows can then be found using the following correlation:

$$\frac{j_z}{j_4} = \frac{1 - 1280 z \, \mathrm{Re}_l^{-1.2}}{1 - (1280)(4) \mathrm{Re}_l^{-1.2}} \tag{3.102}$$

where z is the number of rows of tubes, and Re_l is the Reynolds number based on the longitudinal tube spacing,

$$\mathrm{Re}_l = \frac{G_{\max} X_l}{\mu_{air}} \tag{3.103}$$

III-C.3.c: Pressure Drop Relations

According to Rich (1973), the air-side pressure drop can be divided into two components, the pressure drop due to the tubes, Δp_{tubes}, and the pressure drop due to the fins, Δp_{fin}. The work of Rich is used to evaluate the air-side pressure drop due to the fins, which is expressed as

$$\Delta p_{\mathrm{fin}} = f_{\mathrm{fin}} \mathrm{v}_{m_{air}} \frac{G_{\max}^2}{2} \frac{A_{\mathrm{fin}}}{A_{\min}} \tag{3.104}$$

where, f_{fin} is the fin friction factor, $\mathrm{v}_{m,air}$ is the mean air specific volume, and A_{fin} is the fin surface area. In experimental tests, Rich found that the friction factor is dependent on the Reynolds number, but it is independent of the fin spacing for fin spacing between 3 and 14 fins per inch. In this range of fin spacing, Rich expresses the fin friction factor as:

$$f_{\text{fin}} = 1.7\,\text{Re}_l^{-0.5} \tag{3.105}$$

To determine the pressure drop over the tubes, the relationships developed by Zukauskas and Ulinskas (1998) are used. The pressure drop over the banks of bare tubes is expressed as:

$$\Delta p_{\text{tubes}} = \text{Eu}\frac{G_{\max}{}^2}{2\rho_{air}} z \tag{3.106}$$

where z is again the number of rows, and Eu is the Euler number. Rich expresses the Euler number as a function of the Reynolds number and the tube geometry. For staggered, equilateral triangle tube banks with several rows, Rich expresses the Euler number by a fourth order inverse power series by the following:

$$\text{Eu} = q_{cst} + \frac{r_{cst}}{\text{Re}_{D_o}} + \frac{s_{cst}}{\text{Re}_{D_o}^2} + \frac{t_{cst}}{\text{Re}_{D_o}^3} + \frac{u_{cst}}{\text{Re}_{D_o}^4} \tag{3.107}$$

where Re_{Do} is the Reynolds number based on the outer tube diameter. The coefficients q_{cst}, r_{cst}, s_{cst}, t_{cst}, and u_{cst} are dependent on the Reynolds number and the parameter "a", which is defined as the ratio of the transverse tube spacing to the tube diameter (X_t/D_o). The coefficients for a range of Reynolds numbers and spacing to diameter ratios have been determined from experimental data by Zukauskas and Ulinskas (1998) and are expressed in Table 3-8.

For non-equilateral triangle tube bank arrays, the staggered array geometry factor k_1 must be used as a correction factor to the coefficients in Table 3-8. The staggered

array geometry factor is dependent on the Reynolds number based on: 1) the outer tube diameter; 2) the parameter "a", which again is defined as the ratio of the transverse tube spacing to the tube diameter; and 3) the parameter "b", which is defined as the ratio of the tube spacing in the direction normal to the air flow and the tube diameter (X_l/D_o). The equations for k_1 are found in Table 3-9.

Table 3-8: Coefficients for the Euler Number Inverse Power Series

a	Reynolds Number	q_{cst}	r_{cst}	s_{cst}	t_{cst}	u_{cst}
1.25	$3 < Re_{Do} < 10^3$	0.795	0.247×10^3	0.335×10^3	-0.155×10^4	0.241×10^4
	$10^3 < Re_{Do} < 2 \times 10^6$	0.245	0.339×10^4	-0.984×10^7	0.132×10^{11}	-0.599×10^{13}
1.5	$3 < Re_{Do} < 10^3$	0.683	0.111×10^3	-0.973×10^2	0.426×10^3	-0.574×10^3
	$10^3 < Re_{Do} < 2 \times 10^6$	0.203	0.248×10^4	-0.758×10^7	0.104×10^{11}	-0.482×10^{13}
2.0	$7 < Re_{Do} < 10^2$	0.713	0.448×10^2	-0.126×10^3	-0.582×10^3	0.000
	$10^2 < Re_{Do} < 10^4$	0.343	0.303×10^3	-0.717×10^5	0.880×10^7	-0.380×10^9
	$10^4 < Re_{Do} < 2 \times 10^6$	0.162	0.181×10^4	-0.792×10^8	-0.165×10^{13}	0.872×10^{16}
2.5	$10^2 < Re_{Do} < 5 \times 10^3$	0.330	0.989×10^2	-0.148×10^5	0.192×10^7	0.862×10^8
	$5 \times 10^3 < Re_{Do} < 2 \times 10^6$	0.119	0.848×10^4	-0.507×10^8	0.251×10^{12}	-0.463×10^{15}

Table 3-9: Staggered Array Geometry Factor

Re_D	a/b	k_1
10^2	1.25 < a/b < 3.5	$k_1 = 0.93\left(\frac{a}{b}\right)^{0.48}$
10^3	0.5 < a/b < 3.5	$k_1 = \left(\frac{a}{b}\right)^{-0.048}$
	1.25 < a/b < 3.5	$k_1 = 0.951\left(\frac{a}{b}\right)^{0.284}$
10^4	0.45 < a/b < 3.5	$k_1 = 1.28 - \frac{0.708}{(a/b)} + \frac{0.55}{(a/b)^2} - \frac{0.113}{(a/b)^3}$
10^5	0.45 < a/b < 3.5	$k_1 = 2.016 - 1.675\left(\frac{a}{b}\right) + 0.948\left(\frac{a}{b}\right)^2$ $-0.234\left(\frac{a}{b}\right)^3 + 0.021\left(\frac{a}{b}\right)^4$
10^6	0.45 < a/b < 1.6	

If the tube bank has a small number of transverse rows, an average row correction factor, C_z, must be applied because the pressure drop over the first few rows will be different from the pressure drop over the subsequent rows. C_z is the average of the individual row correction factors, c_z.

$$C_z = \frac{1}{z}\sum_{z=1}^{z} c_z \tag{3.108}$$

The equations for the individual row correction factors are given in Table 3-10. Once the average row correction factor is found, the corrected Euler number can be determined as:

$$Eu_{cor} = k_1 C_z Eu. \tag{3.109}$$

Table 3-10: Correction Factors for Individual Rows of Tubes

Re_D	Z	c_z
10	< 3	$c_z = 1.065 - \frac{0.18}{z - 0.297}$
10^2	< 4	$c_z = 1.798 - \frac{3.497}{z + 1.273}$
10^3	< 3	$c_z = 1.149 - \frac{0.411}{z - 0.412}$
10^4	< 3	$c_z = 0.924 - \frac{0.269}{z + 0.143}$
$> 10^5$	< 4	$c_z = 0.62 - \frac{1.467}{z + 0.667}$
For values of z greater than 4, $c_z = 1$		

The corrected Euler factor, Eu_{cor} can then be used in equation (3.106) to determine the pressure drop over the tubes. Since the relations in Table 3-8, Table 3-9, and Table 3-10, are given for discrete values of the "a" parameter and the Reynolds number, a linear interpolation is used for non-integer values to estimate the values of Eu, k_1, and c_z. The total pressure drop over the heat exchanger is then simply the sum of the pressure drop over the tubes and the pressure drop over the fins:

$$\Delta p_{tot,ac} = \Delta p_{\text{tubes}} + \Delta p_{\text{fin}}. \tag{3.110}$$

III-C.4: Air-side Correlations: Louvered Fins

III-C.4.a: Heat Transfer Relations

For the airside louvered fins, the heat transfer coefficient correlations used are from Wang (2000), as shown in Table 3-11. Wang's correlations are for the Colburn *j*-factor, which is related to the heat transfer coefficient by:

$$\bar{h}_a = \frac{j c_p G_{\max}}{\mathrm{Pr}^{2/3}} \tag{3.111}$$

where G_{max} is the mass flux of the air through the minimum flow area, and Pr is the Prandtl number of the air. Some terminology of the louver fin geometry can be seen in Figures 3-7 and 3-8.

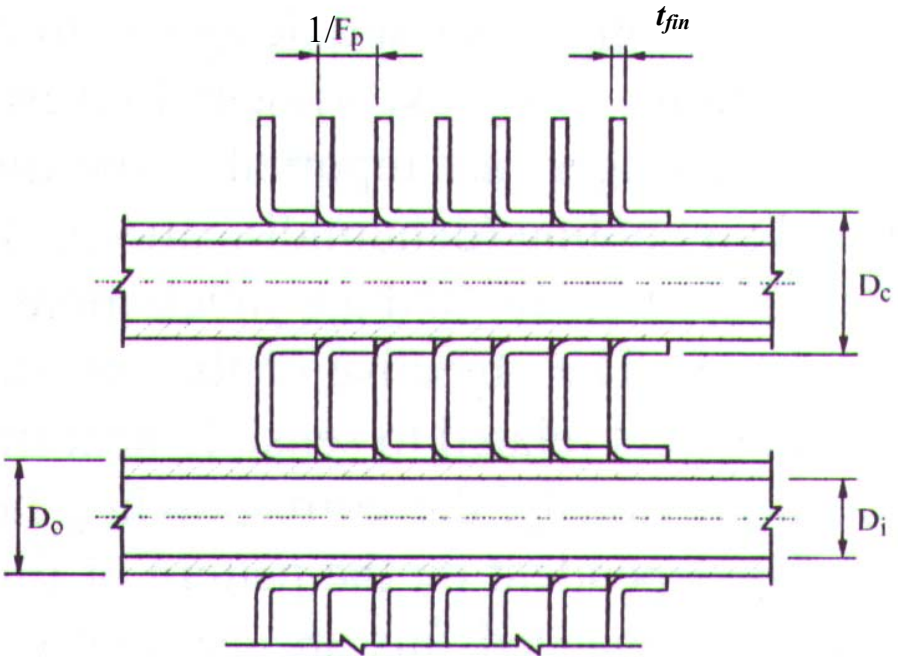

Figure 3-7: Finned-Tube Heat Exchanger Nomenclature

Where D_c is the collar diameter, t_{fin} is the fin thickness, and F_p is the fin pitch which is the inverse of the fin spacing, F_s.

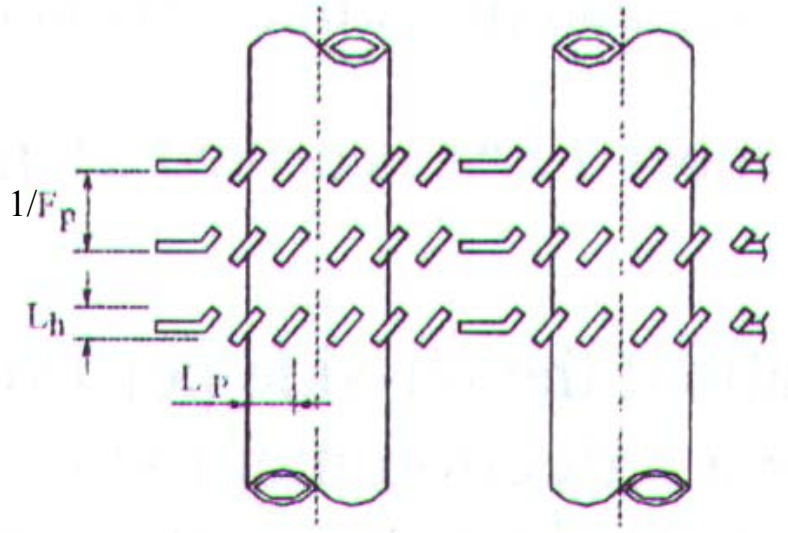

Figure 3-8: Louvered Fin Nomenclature

where L_h is the louver height and L_p is the louver pitch.

Table 3-11: Wang (1999b) Air-Side Heat Transfer Coefficient for Louvered Fins

For Re_{Dc}<1000:	**Eq.#**
$j = 14.3117\left(\mathrm{Re}_{D_c}\right)^{J1}\left(\frac{F_s}{D_c}\right)^{J2}\left(\frac{L_h}{L_p}\right)^{J3}\left(\frac{F_s}{X_l}\right)^{J4}\left(\frac{X_l}{X_t}\right)^{-1.724}$	(3.112)
$J1 = -0.991 - 0.1055\left(\frac{X_l}{X_t}\right)^{3.1}\ln\left(\frac{L_h}{L_p}\right)$	(3.113)

$$J2 = -0.7344 + 2.1059\left(\frac{z^{0.55}}{\ln\left(\mathrm{Re}_{D_c}\right) - 3.2}\right)$$	(3.114)
$$J3 = 0.08485\left(\frac{X_l}{X_t}\right)^{-4.4} z^{-0.68}$$	(3.115)
$$J4 = -0.1741\ln\left(z\right)$$	(3.116)
For $\mathrm{Re}_{Dc} \geq 1000$:	**Eq.#**
$$j = 1.1373\left(\mathrm{Re}_{D_c}\right)^{J5}\left(\frac{F_s}{X_l}\right)^{J6}\left(\frac{L_h}{L_p}\right)^{J7}\left(\frac{X_l}{X_t}\right)^{J8} z^{0.3545}$$	(3.117)
$$J5 = -0.6027 + 0.02593\left(\frac{X_l}{D_{h,W}}\right)^{0.52} z^{-0.5}\ln\left(\frac{L_h}{L_p}\right)$$	(3.118)
$$J6 = -0.4776 + 0.40774\left(\frac{z^{0.7}}{\ln\left(\mathrm{Re}_{D_c}\right) - 4.4}\right)$$	(3.119)
$$J7 = -0.58655\left(\frac{F_s}{D_{h,W}}\right)^{2.3}\left(\frac{X_l}{X_t}\right)^{-1.6} z^{-0.65}$$	(3.120)
$$J8 = 0.0814\left(\ln\left(\mathrm{Re}_{D_c}\right) - 3\right)$$	(3.121)
$$D_{h,W} = \frac{4A_{\min}}{L}$$	(3.122)

where z is the number of tube rows and L is the flow length (Depth of the coil).

III-C.4.b: Pressure Drop Relations

To calculate the pressure drop for the louvered fins, Wang (1999b) is again used. Like the plain fins, the airside pressure drop is split into two components, the fins and the bare tubes. Wang's equations are used for the fin component (see Table 3-12), while Zukauskas and Ulinskas (1998) is again used for the pressure drop across the bank of tubes.

Table 3-12: Wang (1999b) Air-side Friction Factor Correlation for Louvered Fins

For N=1:	**Eq. #**
$f = 0.00317\left(\mathrm{Re}_{D_c}\right)^{F1}\left(\frac{F_s}{X_l}\right)^{F2}\left(\frac{D_{h,W}}{D_c}\right)^{F3}\left(\frac{L_h}{L_p}\right)^{F4}\left(\ln\left(\frac{A_o}{A_t}\right)\right)^{-6.0483}$	(3.123)
$F1 = 0.1691 + 4.4118\left(\frac{F_s}{X_l}\right)^{-0.3}\left(\frac{L_h}{L_p}\right)^{-2}\left(\ln\left(\frac{X_l}{X_t}\right)\right)\left(\frac{F_s}{X_t}\right)^{3}$	(3.124)
$F2 = -2.6642 - 14.3809\left(\frac{1}{\ln \mathrm{Re}_{D_c}}\right)$	(3.125)
$F3 = -0.6816\ln\left(\frac{F_s}{X_l}\right)$	(3.126)
$\mathrm{F4}=6.4668\left(\frac{F_s}{X_t}\right)^{1.7}\ln\left(\frac{A_o}{A_t}\right)$	(3.127)
For N>1:	**Eq. #**
$f = 0.06393\left(\mathrm{Re}_{\mathrm{D_c}}\right)^{F5}\left(\frac{F_s}{D_c}\right)^{F6}\left(\frac{D_{h,W}}{D_c}\right)^{F7}\left(\frac{L_h}{L_p}\right)^{F8} z^{F9}\left(\ln\left(\mathrm{Re}_{D_c}\right) - 4.0\right)^{-1.093}$	(3.128)

$$F5 = 0.1395 - 0.0101\left(\frac{F_s}{X_l}\right)^{0.58}\left(\frac{L_h}{L_p}\right)^{-2}\left(\ln\left(\frac{A_o}{A_t}\right)\right)\left(\frac{X_l}{X_t}\right)^{1.9}$$	(3.129)
$$F6 = -6.4367\left(\frac{1}{\ln\left(\mathrm{Re}_{D_c}\right)}\right)$$	(3.130)
$$F7 = 0.07191\ln\left(\mathrm{Re}_{D_c}\right)$$	(3.131)
$$F8 = -2.0585\left(\frac{F_s}{X_t}\right)^{1.67}\ln\left(\mathrm{Re}_{D_c}\right)$$	(3.132)
$$F9 = 0.1036\left(\ln\left(\frac{X_l}{X_t}\right)\right)$$	(3.133)

III-C.5: Entropy Generation

The entropy generation in the condenser component ($\dot{S}_{gen,cond}$) is calculated from an entropy balance as the sum of entropy changes of the refrigerant and of the air as they pass through the condenser, plus the change in entropy of the air caused by mixing with the ambient air temperature ($T_{amb,c}$), plus the irreversibility due to heat transfer ($\dot{Q}_{cond}$) over a finite temperature difference. The result is:

$$\dot{S}_{gen,cond} = \dot{m}_r(s_3 - s_2) + \dot{m}_a \cdot c_{p,air}\left(\ln\left(\frac{T_{ac2}}{T_{ac1}}\right) + \ln\left(\frac{T_{amb,c}}{T_{ac2}}\right)\right) - \frac{\dot{Q}_{cond}}{T_{amb,c}} \quad (3.134)$$

where:

$$\dot{Q}_{cond} = \dot{Q}_{23} + \dot{W}_{fan,c} = \dot{m}_a \cdot c_{p,air}\left(T_{amb,c} - T_{ac2}\right) \quad (3.135)$$

(Note $\dot{Q}_{cond}$ will have a negative value), and $\dot{m}_a$ is the mass flow rate of the air flowing over the condenser, T_{ac1} is the temperature of the air as it enters the condenser and T_{ac2} is the temperature as it leaves, $T_{amb,c}$ is the outdoor ambient temperature of the air (notice T_{ac1}=$T_{amb,c}$ therefore the temperature natural log terms cancel in Equation (3.134)), $\dot{Q}_{23}$ is the heat transfer from the refrigerant to the air and $\dot{W}_{fan,c}$ is the power required to run the condenser fan.

III-C.6: Constraints

For proper comparison of the plain fin optimum condenser designs to the optimum interrupted fin condenser designs, the same parametric restrictions were used for each optimization. These restrictions were selected based on the ranges of data used to develop the air-side plain-fin (Rich 1973, Zukauskas & Ulinskas 1998, and McQuiston & Parker 1994) and louvered-fin (Wang 1999b and Zukauskas & Ulinskas) heat transfer and pressure drop correlations. Therefore the restrictions for the tube spacing used were:

$$12.7 \text{ mm } (0.5") < X_l < 28 \text{ mm } (1.1")$$

$$17.8 \text{ mm } (0.7") < X_t < 30.5 \text{ mm } (1.2")$$

Fin pitch was limited to the following range:

$$0.157 \text{ fins/mm } (4 \text{ fins/in}) < F_P < 0.71 \text{ fins/mm } (18 \text{ fins/in})$$

While the air velocity over the condenser was limited (determined by ranges of Reynolds numbers used in the experimental data) to:

$$0.91 \text{ m/s (3 ft/s)} < V_{ac} < 5.3 \text{ m/s (17.4 ft/s)}$$

Additionally, for the louvered fin model, the following restrictions were placed on the louver height (L_h) and louver pitch (L_p):

$$0.79\text{mm (0.031”)} < L_h < 1.4\text{mm (0.055”)}$$

$$1.7\text{mm (0.067”)} < L_p < 3.75\text{mm (0.147”)}$$

III-D: Condenser Fan

Natural convection is not sufficient to attain the heat transfer rate required on the air-side of the condenser used in residential air-conditioning systems. Therefore a fan is employed. Although much of the electrical power consumed by the total system is due to the compressor, the condenser fan also requires a significant amount of power. The power required by the fan ($\dot{W}_{fan}$) is directly related to the air-side pressure drop (ΔP_{air}) across the condenser, the frontal area of the condenser (A_{fr}) and to the velocity of air through the condenser (V_{air}):

$$\dot{W}_{fan} = \frac{V_{ac} A_{fr} \Delta P_{air}}{\eta_{fan}} \tag{3.136}$$

Therefore, since adding interruptions to the fins of the condenser increases the pressure drop on the air-side, the fan power also increases, possibly decreasing system

efficiency. The correlations for the air-side pressure drop are given in the previous section. This fan power is included in the model with a fan and motor isentropic efficiency (η_{fan}) of 65%. As the design changes, it assumes a different fan and motor will be chosen based on the required air flow and pressure rise with the 65% isentropic efficiency. The entropy generation of the condenser fan is taken into consideration in the condenser entropy generation term.

III-E: Expansion Valve

A thermostatic expansion valve is used to control the refrigerant flow through the system. The energy equation shows that the enthalpy is constant across the expansion valve.

$$h_3 = h_4 \tag{3.137}$$

Under normal operating conditions, the expansion valve opens and closes in order to maintain a fixed amount of superheat at the exit of the evaporator. In this study, the superheat is set at the typical 5.5° C (10° F). Because the expansion valve can not pass a significant quantity of refrigerant gas, it cannot maintain the specified superheat at the evaporator exit if the refrigerant at the condenser outlet is not completely condensed into liquid. In actual practice, if incomplete condensation in the condenser occurs, the vapor refrigerant backs up behind the expansion valve and the condenser pressure increases until the increased refrigerant-air ΔT increases the heat transfer to fully condense the refrigerant. As a result, in some cases the expansion valve cannot regulate the refrigerant mass flow rate to maintain a superheated condition at the evaporator exit. Wright (2000)

found that this can occur when the air-conditioner is run at low ambient temperature. In that case the evaporator superheat varies above the desired 5.5° C. Under this condition, the evaporator superheat specification is then replaced with a zero subcool condenser exit condition. The model accounts for this condition.

Finally, the entropy generation in the expansion valve ($\dot{S}_{gen,valve}$) was calculated by the following entropy balance equation:

$$\dot{S}_{gen,valve} = \dot{m}_r \left(s_4 - s_3 \right) \tag{3.138}$$

III-F: Evaporator

The evaporator transfers heat from the house air in order to remove the house heat gain and moisture. Since the refrigerant enters the evaporator as a saturated mixture, it is only necessary to divide the component into two sections, saturated and superheated. Otherwise, the analysis of the evaporator in the model is nearly identical to that of the condenser. The only modifications are due to the wet coils on the air-side in the evaporator and different correlations in the saturated region for evaporation instead of condensation.

III-F.1: Effective Specific Heat

Since the evaporator is not the focus of the current study, and its heat transfer load and design will be held essentially constant throughout the condenser optimization, it is desired to keep the evaporator model simple, to save on computation time. Therefore, the evaporator coil is assumed to be dry in calculating the air-side heat transfer coefficient.

However, because the air flowing over the evaporator is cooled to a temperature below the wet bulb temperature, some of the heat rejected by the air causes water to condense out of the air rather than simply lowering the sensible temperature of the air. The total enthalpy change of the air water vapor mixture is thus the sum of the enthalpy change due to the decrease in temperature (sensible heat), and the enthalpy change due to condensation (latent heat):

$$\Delta h_{tot} = \Delta h_{sens} + \Delta h_{lat} \tag{3.139}$$

Note that these enthalpies are on a per unit mass of dry air basis, as is common in psychometrics.

Because of this latent heat, if a specific heat for dry air is used in the model for the evaporator, the resulting exit temperatures will be unrealistically low. Therefore, an effective specific heat that takes into account both the latent heat and the sensible heat should be used. Using an effective specific heat will result in a more accurate determination of the evaporator exit temperature without the complications associated with using heat exchanger equations for air-water mixtures. This approximation is not expected to affect the condenser optimization results.

The ratio of the sensible heat enthalpy change to the temperature change is by definition, the specific heat, c_p. Therefore, dividing through by the change in temperature, substituting c_p and rearranging, the following expression is obtained:

$$c_{p,eff} = c_p + \frac{\Delta h_{lat}}{\Delta T} \tag{3.140}$$

where c_p is the specific heat ratio for dry air and $c_{p,eff}$ is the effective specific heat. To maintain indoor humidity, the latent heat typically accounts for 25% of the total enthalpy change of the air flowing over an evaporator. The effective specific heat can thus be expressed in terms of the specific heat for dry air only,

$$c_{p,eff} = c_p + \left(\frac{0.25\Delta h_{lat}}{\Delta T}\right)\left(\frac{\Delta h_{sens}}{0.75\Delta h_{tot}}\right) = 1.33c_p \tag{3.141}$$

III-F.2: Saturated Refrigerant-Side Heat Transfer

Another difference between the condenser and evaporator models is that in the saturated region an evaporative heat transfer correlation is needed instead of one based on condensation. The expression for the average evaporative two-phase heat transfer coefficient is taken from Tong (1965). This relationship assumes a constant temperature difference between the wall and the fluid along the length of the pipe and is expressed as:

$$\begin{aligned}\bar{h}_{evap} = &(0.0186875)\frac{k_L}{D_i^{0.2}}\left(\frac{G}{\mu_L}\right)^{0.8}\left(\frac{\mu_L C_{p,L}}{k_L}\right)^{0.4}\left(\frac{\rho_L}{\rho_G}\right)^{0.375} \\ &\times\left(\frac{\mu_G}{\mu_L}\right)^{0.075}\left(\frac{x_e - x_i}{x_e^{0.325} - x_i^{0.325}}\right)\end{aligned} \tag{3.142}$$

where x_i is the inlet quality to the condenser, and x_e is the exiting quality.

III-F.3: Saturated Refrigerant-Side Pressure Drop

For the two-phase pressure drop calculation in the evaporator, the Lockhart & Martinelli (1949) method as described by Hiller & Glicksman (1976) was used. This method is not as accurate as the Cavallini et al. (2002) method used in the condenser, but

it requires much less computation time. Since the evaporator design is fixed, this has little effect on the optimal condenser design.

Although, various other general correlations have since been proposed, the original Lockhart-Martinelli approach is still one of the simplest methods to calculate two-phase pressure drop, as discussed by Chen and Spedding (1981). Again, one of the biggest advantages of this procedure is that it can be used for all flow regimes. While the cost of this flexibility is decreased accuracy, subsequent general correlations do not appear to be substantially more accurate than the Lockhart-Martinelli model. Therefore, the method of Lockhart and Martinelli is used to determine the two-phase flow refrigerant-side pressure drop for evaporator in this study.

The Lockhart-Martinelli method is derived from the separated flow model of two-phase flow. This model considers the phases to be artificially segregated into two streams; one of liquid and one of vapor (Collier and Thome, 1996). The separated flow model is based on assuming that the velocities of the vapor and liquid phases are constant but necessarily equal and that phases are in thermodynamic equilibrium.

Hiller and Glicksman (1976) expound on the method of Lockhart-Martinelli in the following manner. The total two-phase pressure drop is divided into frictional, gravitational, and momentum components as follows (as was done by Cavallini et al. 2002 in the condenser):

$$\frac{dP}{dz} = \left(\frac{dP}{dz}\right)_f + \left(\frac{dP}{dz}\right)_g + \left(\frac{dP}{dz}\right)_m \tag{3.143}$$

Since the flow in the evaporator is in the horizontal direction, the gravitational term is neglected. The following expression for the frictional component is defined by Hiller & Glicksman,

$$\left(\frac{dP}{dz}\right)_f = \frac{-\left(\frac{G_G^2}{\rho_G}\right)}{g_{cs}D_{i,evap}}(0.09)\left(\frac{\mu_G}{G_G D_{i,evap}}\right)^{0.2}\left(1+2.85X_{tt}^{0.523}\right)^2 \tag{3.144}$$

where g_{cs} is a units conversion constant, and X_{tt} is again the Martinelli parameter (Equation (3.37)). While the momentum pressure drop component is:

$$\left(\frac{dP}{dz}\right)_m = \frac{-G^2}{g_{cs}\rho_G}\left(\frac{dx}{dz}\right)\left[2x+(1-2x)\left(\frac{\rho_G}{\rho_L}\right)^{1/3}+(1-2x)\left(\frac{\rho_G}{\rho_L}\right)^{2/3}-2(1-x)\left(\frac{\rho_G}{\rho_L}\right)\right] \tag{3.145}$$

Once again, the variation of quality with tube length is assumed to be linear. The pressure drop per unit length as a function of the variation in quality for the frictional and momentum components are then integrated over the length of the tube in the evaporator two-phase region reducing to the following expression for the frictional pressure drop:

$$\begin{aligned}\Delta p_f = -C_{2HG}\Big[&0.357x^{2.8}+2C_{3HG}\left(0.429-0.141x-0.288x^2\right)x^{2.33}\\&+C_{3HG}^2\left(0.538-0.329x\right)x^{1.86}\Big]_{x_i}^{x_e}\end{aligned} \tag{3.146}$$

where the constants C_{3HG}, C_{2HG}, and C_{1HG} are determined by:

$$C_{3HG} = 2.85\left(\frac{\mu_L}{\mu_G}\right)^{0.0523}\left(\frac{\rho_G}{\rho_L}\right)^{0.262} \tag{3.147}$$

$$C_{2HG} = \frac{0.09\mu_G G^{1.8}}{C_{1HG} g \rho_G D_i^{1.2}} \tag{3.148}$$

$$C_{1HG} = \frac{x_e - x_i}{z_e - z_i} \tag{3.149}$$

And for the momentum pressure drop in the two-phase region:

$$\Delta p_m = \frac{G^2}{\rho_G g}\left\{\left[1+\left(\frac{\rho_G}{\rho_L}\right)-\left(\frac{\rho_G}{\rho_L}\right)^{1/3}-\left(\frac{\rho_G}{\rho_L}\right)^{2/3}\right]x - \left[2\left(\frac{\rho_G}{\rho_L}\right)-\left(\frac{\rho_G}{\rho_L}\right)^{1/3}-\left(\frac{\rho_G}{\rho_L}\right)^{2/3}\right]x\right\}\Bigg|_{x_i}^{x_e} \tag{3.150}$$

Hence, the total two-phase refrigerant pressure drop in the straight tube section of the evaporator is simply the sum of the momentum and frictional pressure drop components.

$$\Delta p_{e,S,TP} = \Delta p_m + \Delta p_f \tag{3.151}$$

III-F.4: Entropy Generation

The entropy generation in the evaporator component ($\dot{S}_{gen,evap}$) is the sum of entropy change of the refrigerant and of the air as they pass through the evaporator, plus the irreversibility due to heat transfer ($\dot{Q}_{evap}$) over a finite temperature difference, plus the change in entropy of the air caused by mixing with the ambient air temperature ($T_{amb,e}$):

$$\dot{S}_{gen,evap} = \dot{m}_r \left(s_1 - s_4 \right) + \dot{m}_{ae}\, c_{p,air} \ln\left(\frac{T_{ae,2}}{T_{ae,1}} \right) - \frac{\dot{Q}_{evap}}{T_{amb,e}} + \dot{m}_{ae}\, c_{p,air} \ln\left(\frac{T_{amb,e}}{T_{ae,2}} \right) \quad (3.152)$$

where $T_{ae,1}$ is the temperature of the air as it enters the evaporator and $T_{ae,2}$ is the air temperature as it exits the evaporator, and $\dot{m}_{a,e}$ is the mass flow rate of the air over the evaporator.

III-G: Evaporator Fan

As discussed above, because the evaporator is not the primary focus of this study, introducing wet coils would present unwelcome complications in the overall. In addition to affecting the heat transfer calculations, wet coils also have an effect on the air-side pressure drop. Although there are correlations available for determining the pressure drop over wet coils, they are cumbersome to use and the evaporator is fixed in design, heat load, and air flow rate.

After the air flows over the evaporator, it enters a series of ducts to the conditioned space. The power required by the evaporator fan depends on the losses in these ducts and can vary from installation to installation. Therefore, the default power requirement for the evaporator fan in the air handler specified by the Air-conditioning and Refrigeration Institute (ARI, 1989) of 365 Watts per 1000 ft^3/minute of air was used. Varying the condenser design does not affect this fan power. The entropy generation of the evaporator fan is included in the evaporator entropy generation calculation.

III-H: Calculation of COP_{seas}

The seasonal COP takes into account the effect of varying outside temperatures on the performance of the system. It is the ratio of the average cooling load for the system during its normal usage or "cooling load hours" to the average electricity required by the system over all cooling load hours. Cooling load hours are defined as hours when the temperature is above 65° F, which is when air-conditioning systems are typically operated. In warmer climates, there are more cooling load hours per year than in cooler climates. In Atlanta, for example, the total cooling load hours are approximately 1300 hours per year, while in Detroit, MI the cooling hours are about 700 per year.

The air-conditioning system actually runs fewer hours than the cooling load hours since at ambient temperatures below 95° F, the system usually cycles on and off, as regulated by a thermostat. (The cycling inefficiencies that result from the system cycling on and off are neglected in this study.) The distribution of temperature during these cooling hours is approximately the same for all major cities in the United States. Therefore, the Air-Conditioning Refrigeration Institute, ARI, has developed a temperature distribution model based on cooling load hours that is used throughout the United States. This is shown in Table 3-13 as the distribution of fractional hours in temperature "bins" (ARI, 1989). Table 3-13 shows for example that the outside temperature will be between 80° F and 84° F (temperature bin # 4) approximately 16.1% of the time that the ambient temperature is above 65° F.

Table 3-13: Distribution of Cooling Load Hours, i.e. Distribution of Fractional Hours in Temperature Bins

Bin # I	Bin Temperature Range (°F)	T_i, Representative Temperature for Bin (°F)	fr_i, Fraction of Total Temperature Bin Hours
1	65-69	67	0.214
2	70-74	72	0.231
3	75-79	77	0.261
4	80-84	82	0.161
5	85-89	87	0.104
6	90-94	92	0.052
7	95-99	97	0.018
8	100-104	102	0.004

Again, the seasonal COP is therefore the ratio of the average cooling load for the system over all cooling load hours to the average electricity required by the system over all cooling load hours, and is expressed as:

$$COP_{seas} = \frac{Q_{ave,seas}}{W_{ave,seas}} \tag{3.153}$$

The average cooling over all cooling load hours is calculated by summing the hourly "house" cooling load over all cooling load hours, and is expressed as:

$$Q_{ave,seas} = \sum_{i=1}^{8} UA_{house} \left(T_i - 65^{o}F\right) fr_i \tag{3.154}$$

where UA_{house} is the overall "house" heat transfer coefficient, i is the temperature bin number, T_i is the representative temperature bin, and fr_i is the fraction of total

temperature bin hours (as shown in Table 3-13). The average electricity required by the system over all cooling load hours is expressed as:

$$W_{ave,seas} = \sum_{i=1}^{8} \left[\frac{UA_{house} \left(T_i - 65^{o}F \right) \; fr_i}{COP_i} \right] \tag{3.155}$$

where COP_i is the COP at each representative temperature bin.

Since the overall "house" heat transfer coefficient, UA_{house}, is common to both expressions, dividing Equation (3.154) by Equation (3.155) yields the following expression for the seasonal COP:

$$COP_{seas} = \frac{\sum_{i=1}^{8} \left(T_i - 65^{o}F \right) \; fr_i}{\sum_{i=1}^{8} \left[\frac{\left(T_i - 65^{o}F \right) \; fr_i}{COP_i} \right]} \tag{3.156}$$

The numerator of the above expression is a constant. Since the air-conditioning system of this study is sized to deliver a specified amount of cooling at 95 °F (35 ºC) ambient temperature, the indoor temperature will rise when the ambient temperature is greater than 95 °F. As a result, the temperature difference of (T_i - 65°F) is limited to a maximum of 30 °F (16.67 ºC) for this study.

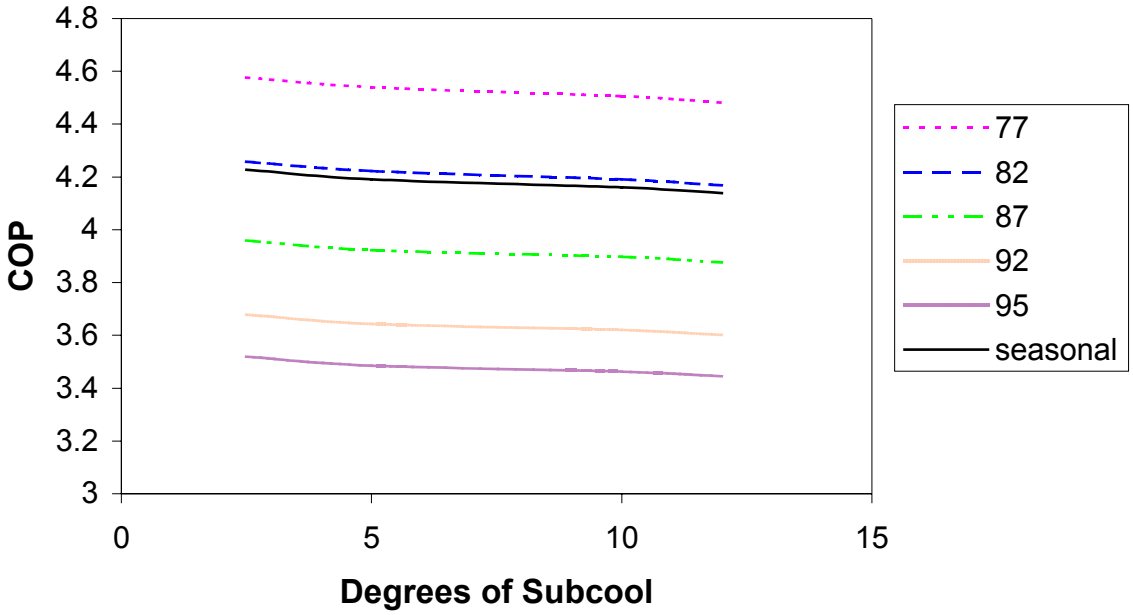

Figure 3-9: COP vs. Degrees of Sub-cool for Varying Ambient Temperatures

Figure 3-9 shows COP versus subcool for various ambient temperatures. Note from this figure that the COP's obtained using an ambient temperature of 82˚F, were essentially identical to the seasonal COP's. The U.S. Department of Energy, which requires a seasonal energy efficiency rating, SEER=3.412xCOP_{seas}, to be placed on a yellow sticker on all air-conditioning systems sold in the United States, also allow use of an ambient temperature of 82˚F to develop these ratings. Aspelund (2001) used $COP_{@82°F}$ as the figure of merit instead of the seasonal COP because it required fewer calculations and therefore increased calculation speed and stability. An ambient temperature of 82˚F is assumed to approximate seasonal conditions for the current study as well.

III-I: Refrigerant Mass Inventory

The magnitude of sub-cooling at the condenser exit is controlled by the system operating conditions and the quantity of refrigerant mass in the system. Equipment manufacturers specify refrigerant mass charge to attain a specified sub-cool (typically 5 ˚C (9˚F)) at a condenser outside air temperature of 35˚C (95°F). The optimum amount of sub-cool, at all conditions, was found to be 0˚C, which can be seen in Figure 3-9 as the lines are slightly sloped with higher COP's being obtained at lower sub-cools. However, since subcool varies with outside air temperature, systems are usually designed with some excess sub-cool to be certain that under all operating conditions there is enough refrigerant charge to maintain some subcool at the expansion valve inlet. In the model, the refrigerant mass charge was calculated as that coinciding with a 5˚C subcool at the 35˚C air inlet temperature. The sub-cool then varies at other ambient temperatures. Hence, the air velocity over the condenser and the sub-cool in the condenser at 35˚C (95˚F) ambient conditions are the two operating parameters that are optimized for each condenser geometric configuration investigated during this study.

The mass of refrigerant in the piping connecting the components is neglected. Since the compressor contains only vapor, the mass of refrigerant in the compressor is also neglected. Therefore the calculated total mass of refrigerant in the system includes the mass in the condenser and in the evaporator.

The following text outlines the procedure for finding the refrigerant mass in the saturated portion of the evaporator. The mass of refrigerant can be expressed as:

$$m = \int_0^L \frac{A_{ci}\,dl}{\mathrm{v}_r} \tag{3.157}$$

where, A_{ci} is the cross sectional area of the refrigerant-side of the tube, and v_r is the refrigerant specific volume, which at saturated conditions is a function of quality expressed as

$$v_r(x) = v_{r,f}(1-x) + v_{r,g}x \tag{3.158}$$

The boundary conditions for the saturated portion of the evaporator are

$$x(l=0) = x_i \tag{3.159}$$

and

$$x(l=L) = 1 \tag{3.160}$$

where l is the integral variable for evaporating tube length, and L is the total evaporating tube length. Using the boundary conditions and assuming the quality varies linearly with tube length, the following expression results.

$$x(l) = \frac{1-x_i}{L}l + x_i \tag{3.161}$$

Substituting (3.161) into (3.158) yields an expression for the specific volume as a function of length (dropping the subscript r),

$$v(l) = v_f + x_i(v_g - v_f) + l\left(\frac{1-x_i}{L}\right)(v_g - v_f) \tag{3.162}$$

For a uniform cross sectional area, substituting (3.162) into (3.157) yields

$$m_{sat,evap} = A_{ci} \int_{l=0}^{l=L} \left(\frac{1}{\mathrm{v}_f + x_i \left(\mathrm{v}_g - \mathrm{v}_f \right) + l \left(\frac{1 - x_i}{L} \right) \left(\mathrm{v}_g - \mathrm{v}_f \right)} \right) dl \tag{3.163}$$

Integrating (3.163) yields the following expression

$$m_{sat,evap} = \left\{ \frac{A_{ci} L}{\left(1 - x_i\right)\left(\mathrm{v}_g - \mathrm{v}_f\right)} \ln \left[\mathrm{v}_f + x_i \left(\mathrm{v}_g - \mathrm{v}_f \right) + l \left(\frac{1 - x_i}{L} \right) \left(\mathrm{v}_g - \mathrm{v}_f \right) \right] \right\}_{l=0}^{l=L} \tag{3.164}$$

Substituting for l, the expression for the final mass in the saturated portion of the evaporator is expressed as:

$$m_{sat,evap} = \frac{A_{ci} L_{sat,evap}}{\left(1 - x_i\right)\left(\mathrm{v}_g - \mathrm{v}_f\right)} \ln \left[\frac{\mathrm{v}_g}{x_i \left(\mathrm{v}_g - \mathrm{v}_f \right) + \mathrm{v}_f} \right] \tag{3.165}$$

The same procedure is also used to determine the mass of refrigerant in the saturated portion of the condenser, however the boundary conditions are different since the refrigerant enters as a saturated vapor and exits as a saturated liquid:

$$x\left(l = 0\right) = 1 \tag{3.166}$$

and

$$x(l = L) = 0 \tag{3.167}$$

Using these boundary conditions and assuming the quality varies linearly with tube length, the following expression results for the quality as a function of tube length:

$$x(l) = 1 - \frac{l}{L} \tag{3.168}$$

Again assuming a uniform cross sectional area and plugging Equation (3.168) into Equation (3.158) and then back into Equation (3.157) and integrating, as before, the resulting mass in the saturated region of the condenser is:

$$m_{sat,cond} = \frac{-A_{ci} L_{sat,cond}}{v_g - v_f} \ln\left(\frac{v_f}{v_g}\right) \tag{3.169}$$

The mass of refrigerant in the superheated portions of the condenser and evaporator are expressed simply as:

$$m_{con,sh} = \rho_G A_{ci} L_{con,sh} \tag{3.170}$$

and

$$m_{evap,sh} = \rho_G A_{ci} L_{evap,sh} \tag{3.171}$$

Finally, the mass of refrigerant in the sub-cooled section of the condenser is expressed as

$$m_{con,sc} = \rho_L A_{ci} L_{con,sc} \tag{3.172}$$

III-J: Heat Exchanger Material Cost

For calculation of the material costs of the condenser and the evaporator, the price of copper used was US$1.76/kg and the price of aluminum used was US$1.54/kg both from the London Metals Exchange (October 2003). While these values have remained nearly constant over the last five years, it should be noted that future prices of aluminum and copper might change. The volume of each metal was calculated and multiplied by its density and cost per pound to determine the material cost for each heat exchanger. Condenser finned tube heat exchanger prices are typically based on a multiple of material cost assuming mass production. The fact that coil cost is taken as a constant in this study makes knowledge of the multiplier unimportant, but it is typically in the range of three to five.

III-K: Basic Model Summary

By using the above relations for the air-conditioning system components in a system simulation program, it is possible to evaluate the detailed performance of a total air-conditioning system for varying condenser design parameters. Cycling efficiency degradations were neglected because their inclusion would be expected to have little effect on determination of the optimum design.

III-L: Isolated Condenser Model

In order to perform thermoeconomic isolation, the component of interest must be entirely "isolated" from the rest of the system. By doing this, the component ceases to give or receive feedback from the rest of the system. However, in order to produce a

properly posed and complete model, additional operating constraints are required. A total of five constraints are needed to complete the isolated condenser model. Referencing Figure 3-10, the options from which to choose are:

$$P_{ac1},\ P_{ac2},\ P_2,\ P_3,\ T_{ac1},\ T_{ac2},\ T_2,\ T_3,\ \dot{Q}_{cond}\ ,\ \dot{m}_r\ ,\ \Delta T_{SH},\ \Delta T_{SC},\ and\ T_{sat}\ .$$

where ΔT_{SC} is the degrees of subcool exiting the condenser, which is a parameter used to measure the refrigerant charge in the system. Also, T_{sat} is the saturation temperature in the condenser and ΔT_{SH} is the degrees of superheat entering the condenser. Note that this is not the normal definition of superheat in an air conditioning system, which usually describes the superheat exiting the evaporator.

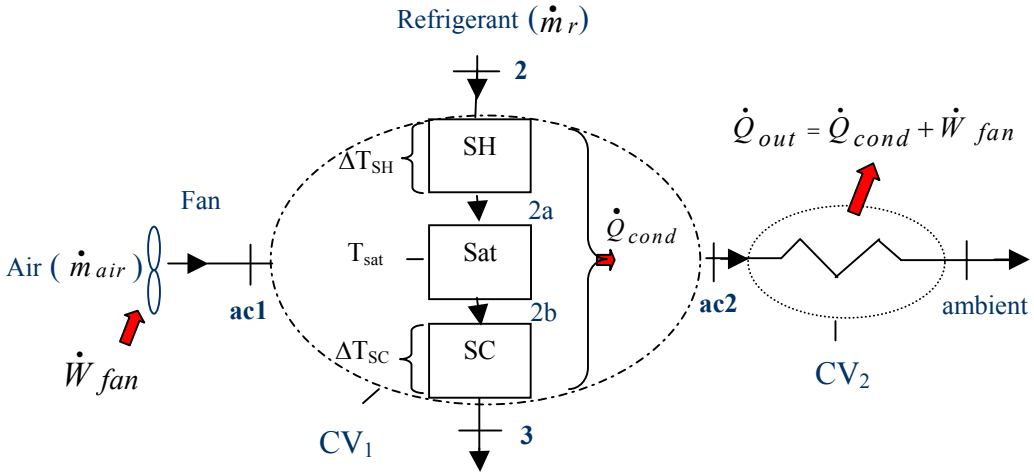

Figure 3-10: Detailed Condenser Flow Diagram

For the isolated condenser of a residential air-conditioning system, two of the needed five constraints are rather straightforward; i.e. the inlet air pressure and temperature are assumed to be ambient. Therefore, the P_{ac1} is taken as 1 bar, and T_{ac1} was taken as 27.8°C (82°F), which was found earlier to give a nearly identical COP as

the seasonal COP used by the U.S. Department of Energy in rating residential air conditioners. These values were used in the overall system model as well. The pressure drop and temperature increase on the air side are then calculated by the model.

Three additional constraints are needed to complete the isolated model. The appropriate selection of these three constraints is extremely important, therefore the decision making process is detailed here. Ideally, one parameter would give information about the refrigerant side entrance conditions (P_2, T_2, T_{sat}, ΔT_{SH}), the second parameter would give information about the refrigerant side exit conditions (P_3, T_3, T_{sat}, ΔT_{SC}), and the third would give information about the heat transfer scaling between the air side and the refrigerant side. While almost any combination of three additional parameters will result in a working model, certain combinations will not give as good a set of results due to their variation with changing condenser design. To find the best combination of parameters the following requirements should be met: 1.) the parameters should not require detailed non-condenser system information to arrive at a value, and 2.) they should not vary greatly with different heat exchanger designs when operating in the system. Because of these two requirements, explicit temperature and pressure information are not good options, therefore P_2, P_3, T_2, T_3 and even the saturation temperature in the condenser are taken out of consideration as it will vary with heat exchanger design. The remaining options for the refrigerant inlet and outlet conditions are ΔT_{SH} and ΔT_{SC} , respectively. With these temperature differences chosen, the only decision left to be made is the size scaling parameter, which could be either the refrigerant mass flow rate or the heat transfer rate between the refrigerant and the air. Both of these situations were investigated in more detail.

Prescribing the mass flow rate of the refrigerant in the isolated condenser model does not fix the total heat transfer rate in the heat exchanger. This is due to the fact that as the saturation pressure varies with heat exchanger design, the heat of condensation varies. Taken with fixed inlet superheat and exit subcool, the heat transfer rate increases as the saturation pressure decreases. In the system model, the refrigerant mass flow rate varies to compensate for this, while the total heat transfer rate stays relatively constant. Therefore, fixing the heat transfer rate is a more appropriate size scale constraint.

As shown by Equations (3.173) (neglecting the work of the fans) and (3.174), the heat transfer rate is dependent only on the COP and the desired evaporator cooling capacity, e.g., size, of the system that the condenser is being designed for:

$$COP = \frac{\text{Desired Output}}{\text{Required Input}} = \frac{\dot{Q}_{evap}}{\dot{W}_{comp}} = \frac{\dot{Q}_{evap}}{\dot{Q}_{cond} - \dot{Q}_{evap}} \tag{3.173}$$

Rearranging and solving for $\dot{Q}_{cond}$:

$$\dot{Q}_{cond} = \dot{Q}_{evap}\left(1 + \frac{1}{COP}\right) \tag{3.174}$$

With a refrigerating capacity fixed at 8.8 kW and a typical COP of approximately 4, this gives $\dot{Q}_{cond}$ = 11kW. Note that $\dot{Q}_{cond}$ is only weakly dependent on COP; e.g., a 25% change in COP produces only a 4-6% change in $\dot{Q}_{cond}$.

The value for the sub-cool used in the system model was set at 5˚C (9˚F) at an ambient temperature of 35˚C (95˚F). The optimum sub-cool is actually 0˚. However for practicality reasons, systems are usually designed with some excess sub-cool to be certain that for varying operating conditions no vapor will enter the expansion valve. Using this

design condition the system model then calculates the sub-cool for the actual ambient condition of 27.8˚C (82˚F). The resulting calculated sub-cool at 27.8˚C was slightly higher than 5˚C depending on the condenser design, so for the isolated model the value was fixed at 5˚C for simplicity.

The value for the condenser inlet superheat was set at 25˚C (45˚F) in the isolated model. This value was determined by looking at some typical model results from system designs.

CHAPTER IV

OPTIMIZATION METHODOLOGY

IV-A: Fitness Factors

In order to quantitatively evaluate the performance of any air-conditioning system, a figure of merit must be established. For an air-conditioning system utilizing a vapor compression refrigeration cycle, the efficiency is expressed in terms of the cooling coefficient of performance or the COP. The coefficient of performance is a dimensionless quantity. It is the ratio of the rate of cooling or refrigeration capacity (heat transfer to the evaporator), to the electrical or mechanical power used to drive the system (compressor power, condenser fan power, and evaporator fan power). The COP is expressed as:

$$COP = \frac{\dot{Q}_e}{\dot{W}_{com} + \dot{W}_{fan,cond} + \dot{W}_{fan,evap}} \tag{4.1}$$

As defined in the previous chapter, the weighted average of the COP over a cooling season is referred to as the seasonal COP (COP_{seas}). The seasonal COP is the system based figure of merit used in this study.

IV-B: Software Tools

The air-conditioner model was programmed in Engineering Equation Solver (EES, Klein and Alvarado 2003), a software tool that iteratively solves transcendental equations and has built-in thermodynamic and transport property relations for many different fluids, including R-410a. The model developed incorporates over 1800 equations in many large iterative solution blocks. While EES is useful for simulating the air-conditioning cycle it is not suitable for performing the design optimization search on multiple design parameters. However, EES does have the ability to communicate with other programs using Dynamic Data Exchange (DDE) supported by many other programs. Therefore, in the current study the optimization search scheme was programmed in Visual Basic (VB) using Microsoft Excel to organize the inputs and the outputs of the search. EES is then used as function, called on by VB to calculate the fitness value, the COP, when needed.

IV-C: The Nelder-Mead Simplex Search Method

In selection of an optimization algorithm the fact that the model of the air-conditioner is highly non-linear and iteratively solved in EES must be considered. The Simplex search method presented by Nelder and Mead (1965) has been widely used to optimize complex functions. This method was chosen over possibly more efficient techniques because it is very robust (converges consistently), relatively simple to implement, does not require derivatives, and moves toward the optimum in small enough increments that the EES model converges consistently in each iteration (see discussion of optimization techniques in Chapter II). Even though the Simplex search method will find

a good solution for the design of the condenser, like all non-exhaustive search methods it cannot be proven that it is the global optimum design.

Because the Nelder-Mead algorithm uses only function values, COP in this study, to optimize a scalar-value function of n real variables, it falls into the class of *Direct Search Methods* (Reklaits et. al. 1983). Each kth iteration ($k \geq 0$) of the simplex direct search method begins with a simplex, specified by its n+1 vertices and the associated function values. Since the desired solution is the maximum seasonal COP of the air-conditioner, the COP_{seas} is calculated for all the vertices and they are then ordered and labeled $\mathbf{x}_1^{(k)}, \ldots, \mathbf{x}_{n+1}^{(k)}$ such that:

$$COP_{seas}(\mathbf{x}_1^{(k)}) \geq COP_{seas}(\mathbf{x}_2^{(k)}) \geq \ldots \geq COP_{seas}(\mathbf{x}_{n+1}^{(k)}) \tag{4.2}$$

where $\mathbf{x}_1^{(k)}$ is the *best* vertex or design in the simplex while the $\mathbf{x}_{n+1}^{(k)}$ is the worst.

To start the search, one base design is chosen. The other vertices of the starting simplex are then determined by adding τ% to one parameter at a time so the initial simplex will span the search space. In this study the τ used was +/- 10%-30%. The percentage was decreased as the search narrowed in on the optimum point.

In the Nelder-Mead method there are four scalar parameters defined: coefficients of *reflection* (ρ_c), *expansion* (χ_c), *contraction* (γ_c) and *shrinkage* (σ_c). The recommended values by Nelder and Mead (1965), nearly universally used in the standard algorithm (Lagarias, et. al., 1998), are:

$$\rho_c = 1, \ \chi_c = 2, \ \gamma_c = 0.5, \ \text{and} \ \sigma_c = 0.5 \tag{4.3}$$

An example of the calculations used in one iteration of the Nelder-Mead Simplex search method, as explained by Lagarias et al. (1998), is shown in Table 4-1, while it is shown graphically in Figure 4-1 for the example case of a two-dimensional simplex.

The Simplex search algorithm was programmed in Visual Basic. As shown schematically in Figure 4-2, when starting the Simplex search, the initial simplex is sent from Excel to EES, where the COP values for each of the vertices are calculated. This COP information is then sent back to Excel and a new vertex is calculated by the VB program, which is sent again to EES. Nelder and Mead did not discuss any tie-breaking rules, however, in this study points with the same value are ordered so that the newest vertex is ranked higher. The Simplex search program will send vertex information from Excel to EES and the COP back to Excel until the simplex has converged. The search comes to a halt when the design changes by less than a prescribed tolerance (1/2000) over the latest two iterations. This does not necessarily mean that the volume of the simplex is getting close to zero, *i.e.* the vertices are converging to the same point, but rather that the simplex is not changing between the latest two iterations. It has been noted that this criteria might be fooled by a single anomalous step that, for one reason or another, failed to get anywhere. Therefore, it is frequently a good idea to restart a multidimensional optimization routine at a point where it claims to have found an optimum (Numerical Recipes). This was done in this study and repeated until the best point design in the restarted solution is the same as the base point design.

As the search scheme progressed through the steps shown in Table 4-1, in each stage the constraints imposed on the system were checked in the VB program. If a design parameter of a vertex didn't fall within the design constraints, the design information was

not sent to EES. Instead the COP was assigned to be a very small number, i.e., a penalty value was imposed, so that it would be eliminated as an optimum design.

Table 4-1: Nelder-Mead Simplex search algorithm

1. Order	Order the $n+1$ vertices using Equation [1] and calculate the center of the n best points: $\overline{\mathbf{x}} = \sum_{i=1}^{n} \mathbf{x_i} / n$ (4.4)
2. Reflect	Compute reflection point $\mathbf{x}_r$ from: $\mathbf{x}_r = \overline{\mathbf{x}} + \rho_c(\overline{\mathbf{x}} - \mathbf{x}_{n+1}) = (1+\rho_c)\overline{\mathbf{x}} - \rho_c \mathbf{x}_{n+1}$ (4.5) Calculate COP for $\mathbf{x}_r$. -If $COP_1 \leq COP_r > COP_n$ accept $\mathbf{x}_r$ as new point and terminate the iteration.
3. Expand	If $COP_r > COP_1$ calculate the expansion point $\mathbf{x}_e$ and $COP(\mathbf{x}_e)$ where: $\mathbf{x_e} = \overline{\mathbf{x}} + \chi_c(\mathbf{x}_r - \overline{\mathbf{x}}) = \mathbf{x} + \rho_c\chi_c(\overline{\mathbf{x}} - \mathbf{x}_{n+1}) = (1+\rho_c\chi_c)\overline{\mathbf{x}} - \rho_c\chi_c\mathbf{x}_{n+1}$ (4.6) -If $COP_e > COP_r$ accept $\mathbf{x}_e$ and terminate the iteration. -Else accept $\mathbf{x}_r$ and terminate the iteration.
4. Contract	**a.) Outside**. If $COP_n \leq COP_r > COP_{n+1}$ calculate: $\mathbf{x}_c = \overline{\mathbf{x}} + \gamma_c(\mathbf{x}_r - \overline{\mathbf{x}}) = (1+\gamma_c\rho_c)\overline{\mathbf{x}} - \gamma_c\rho_c\mathbf{x}_{n+1}$ (4.7) -If $COP_c \leq COP_r$ then accept $\mathbf{x_c}$ and terminate the iteration. -Else perform shrinking **b.) Inside**. If $COP_r \leq COP_{n+1}$ calculate: $\mathbf{x}_{cc} = \overline{\mathbf{x}} - \gamma_c(\overline{\mathbf{x}} - \mathbf{x}_{n+1}) = (1-\gamma_c)\overline{\mathbf{x}} + \gamma_c\mathbf{x}_{n+1}$ (4.8) -If $COP_{cc} > COP_{n+1}$ accept $\mathbf{x}_{cc}$ and terminate the iteration. -Else perform shrinking.
5. Shrink	Calculate $COP(\mathbf{v}_i)$ where: $\mathbf{v}_i = \mathbf{x}_1 + \sigma_c(\mathbf{x}_i - \mathbf{x}_1)$ and i = 2, …, n+1 (4.9) Then next simplex has vertices: $\mathbf{x}_1, \mathbf{v}_2, \ldots, \mathbf{v}_{n+1}$

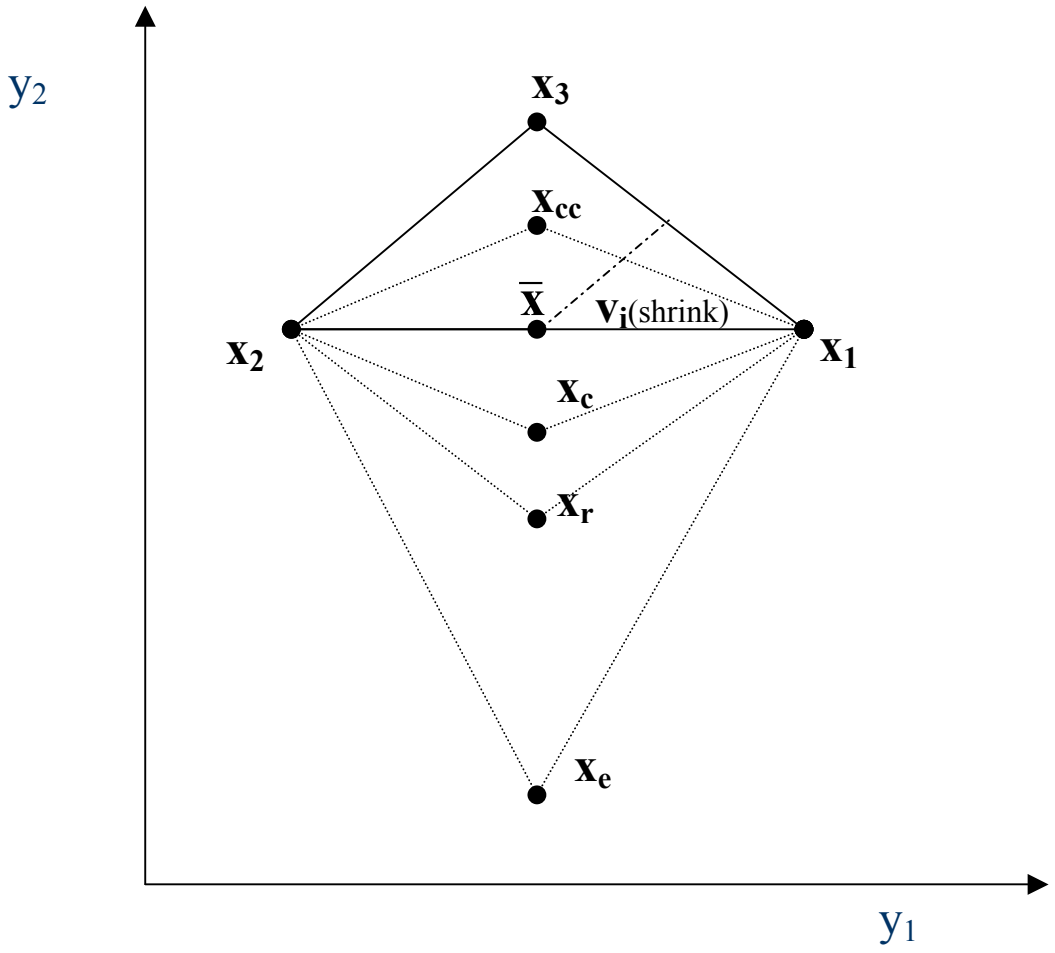

Figure 4-1: 2-D Simplex Diagram

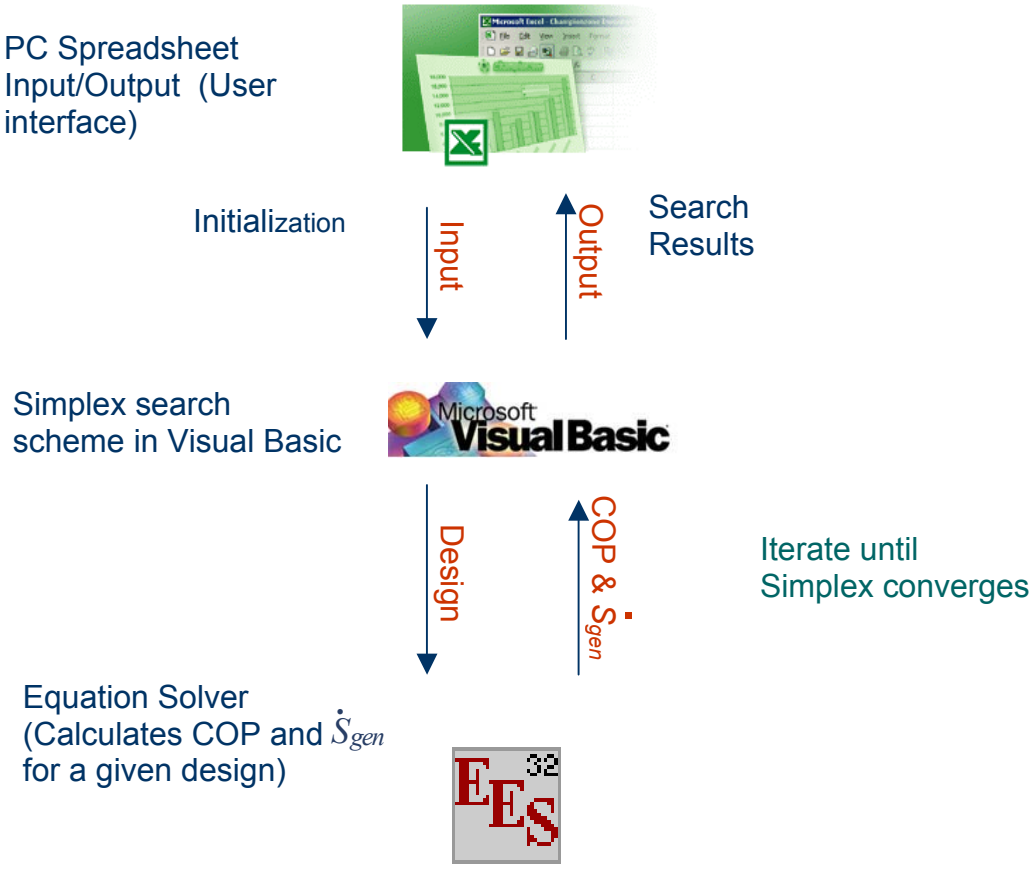

Figure 4-2: Optimization Flow Chart

IV-D: Finding Discrete Parameter Solutions

Initially, the optimization methodology developed finds designs using continuous parameters, however several of the design parameters are required to be discrete values (number of rows, tubes per row, and number of circuits). Therefore the optimization scheme gives a solution for the optimal design of a hypothetical finned-tube condenser with decimal values that should be close to the optimal integer design.

The second step of the optimization methodology involves a separate VB optimization program that only allows integer design values for the number of rows, number of circuits, and number of tubes per row. With this limitation the rows, circuits, and tubes per row are not used in the convergence criteria in this program since the variance between designs can be quite large if even one or more of the vertices(designs) has a different value (e.g. 4 or 5 circuits). By eliminating these values from the convergence criteria, this altered program can search through the possible upper and lower integer bounds around the hypothetical optimum found from the initial program, while re-optimizing the remaining continuous parameters (e.g. air velocity, tube spacing, fin spacing, louver height, louver pitch) for their integral parameter values.

Because the number of rows (or depth of the coil) largely affects the material cost of the condenser, these parameters (rows & cost) are highly dependent on each other. Therefore, if one is fixed, the other can be solved for. Note that in the initial program, cost is an input parameter, whereas the number of rows is solved for by EES for the specific design. Therefore, in order to make sure that the number of rows is an integer value in the "second step" integer VB program, it must now be fixed, which relaxes the cost constraint, allowing cost to be solved for. An additional design constraint is added

to the VB program in this case, limiting the possible designs to those whose cost is less than or equal to the original fixed cost associated with the hypothetical optimum design.

Otherwise, this discrete parameter VB simplex search program solves similarly to the continuous program. The result is a realistic optimum finned-tube condenser design for the given set of inputs (cost & frontal area).

CHAPTER V

ENTROPY GENERATION MINIMIZATION METHODOLOGY

V-A: COP vs. System EGM

Basic fundamental thermodynamic equations can show that entropy generation is inversely related to system COP. This means that the maximum COP will always correspond to the minimum entropy generation. Alefeld (1990) developed this relationship and it is summarized here:

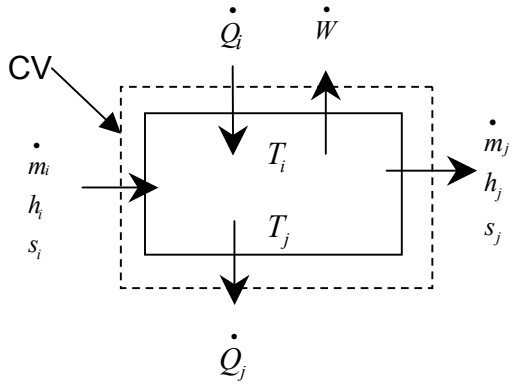

Figure 5-1: Example Control Volume

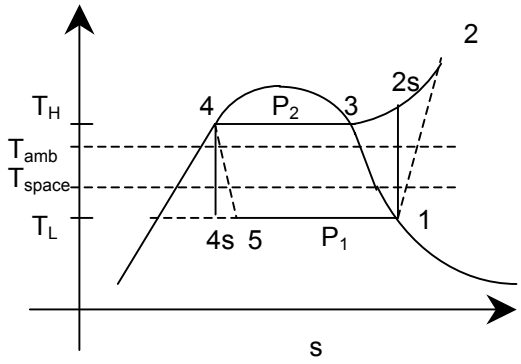

Figure 5-2: Vapor Compression Refrigeration Cycle

Based on the generic control volume shown in Figure 5-1, the first and second laws of thermodynamics, respectively, are applied for steady state conditions:

First Law of Thermodynamics:

$$\sum_{out} \dot{Q}_j + \sum_{out} \dot{m}_j h_j + \dot{W} = \sum_{in} \dot{Q}_i + \sum_{in} \dot{m}_i h_i \qquad (5.1)$$

Second Law of Thermodynamics:

$$\sum_{out} \frac{\dot{Q}_j}{T_j} + \sum_{out} \dot{m}_j s_j = \sum_{in} \frac{\dot{Q}_i}{T_i} + \sum_{in} \dot{m}_i s_i + \sum_{k} \dot{S}_{gen,k} \qquad (5.2)$$

The terms $S_{gen,k}$, which are always positive, represent the entropy production for the irreversible process. The sign of the heat transfer out, $\dot{Q}_j$, is positive in the out direction while the heat transfer in, $\dot{Q}_i$, is positive in the in direction. Also, the work is assumed to be positive out of the system. The temperatures T_i and T_j are entropic averages (Alefeld, 1987a,b, 1989b). An entropic average temperature is used when the boundary temperature across which heat transfer (Q_i) is occurring is not constant and/or uniform. It can be calculated by dividing the entropy change of the heat reservoir (ΔS_i) due to the heat transfer by the amount of heat transferred:

$$\overline{T}_{i,s} \equiv \frac{Q_i}{\Delta S_i} = \frac{Q_i}{Q_i / T_i} \qquad (5.3)$$

By multiplying the second law equation (5.2) by a free choosable parameter, T_x, and subtracting the resulting equation from the first law equation (5.1), the result is:

$$\dot{W} = \sum_{in} \dot{Q}_i \frac{T_i - T_x}{T_i} - \sum_{out} \dot{Q}_j \frac{T_j - T_x}{T_j} + \sum_{in} \dot{m}_i \left(h_i - T_x s_i \right) - \sum_{out} \dot{m}_j \left(h_j - T_x s_j \right) - T_x \sum_{k} \dot{S}_{gen,k} \qquad (5.4)$$

For the case of a vapor compression refrigeration cycle (Figure 5-2), work is added to the system and the sign convention is changed to be positive for work into the system. Now, $\dot{Q}_i=\dot{Q}_L$ (refrigeration load), $\dot{Q}_j=\dot{Q}_H$ (condenser heat), and $\dot{m}_i=\dot{m}_j=0$. Additionally, the boundaries of the control volume are chosen to include the heat transfer irreversibilities across the finite temperature difference with the environment. Therefore $T_i=T_{space}$ (temperature of the refrigerated space) and $T_j=T_{amb}$ (temperature of the environment) are external temperatures, i.e. entropically averaged temperatures of the transfer fluid. For this case:

$$\dot{W}=\dot{Q}_H\left(\frac{T_{amb}-T_x}{T_{amb}}\right)-\dot{Q}_L\left(\frac{T_{space}-T_x}{T_{space}}\right)+T_x\sum_k\dot{S}_{gen,k} \tag{5.5}$$

Note that this equation is not the same as an exergy balance, since T_x is a free parameter, which can be arbitrarily chosen to be any value between zero and infinity, positive or negative.

By judiciously setting the free parameter $T_x=T_{amb}$ and solving for the *COP*:

$$COP=\frac{\dot{Q}_L}{\dot{W}}=\frac{\dfrac{T_{space}}{T_{amb}-T_{space}}}{1+\dfrac{T_{space}T_{amb}}{T_{amb}-T_{space}}\displaystyle\sum_k\frac{\dot{S}_{gen,k}}{\dot{Q}_L}}=\frac{COP_{reversible}}{1+\dfrac{T_{space}T_{amb}}{T_{amb}-T_{space}}\displaystyle\sum_k\frac{\dot{S}_{gen,k}}{\dot{Q}_L}} \tag{5.6}$$

The numerator is the efficiency of a reversible refrigerator; the denominator takes into account the reduction due to the irreversibilities in the process, like pressure drops, throttling, de-superheating, irreversible compression, etc. In Alefeld (1987a), analytic equations are derived and quantitative details are given for these contributions. Alefeld

(1990) showed that this equation is as precise for COP calculations as the common Equation (4.1), in which only enthalpy differences are used. The same result was found in the current study, where the COP calculated from both equations was the same.

One might notice a contradiction here; Equation (4.1) is developed from 1st Law principles whereas Equation (5.6) uses the 1st & 2nd Law in its development. The link between the two is in the calculation of the properties (enthalpies) in the model. While Equation (4.1) only requires enthalpy information, many of these values are calculated through isentropic efficiencies or related through entropy values, implicitly introducing the 2nd Law.

As seen in Figure 5-3, as the COP is calculated and maximized during the optimization search, the system entropy generation is correspondingly minimized for the original non-augmented case. Additionally, as seen in Figure 5-4, as the COP is calculated and maximized, the condenser component entropy generation is also correspondingly minimized, though there are some spurious values at the beginning of the search. This indicates that entropy generation minimization in the condenser component alone may also correspond quite closely with maximum COP. However, note that the situation shown in Figure 5-4 is not for an "isolated" condenser. It was integrated into the rest of the system, and the components' entropy generation was recorded throughout the optimization procedure; i.e., there is feedback between the condenser component and the rest of the system via changing inlet and outlet conditions.

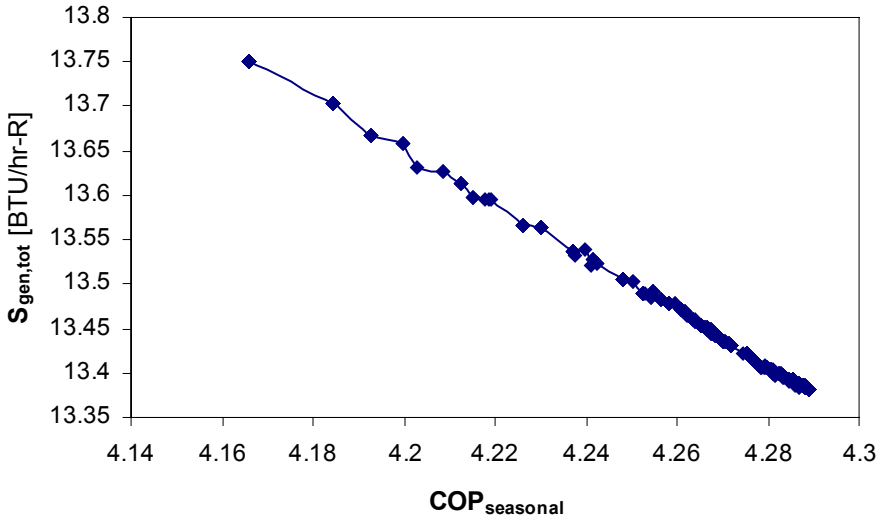

Figure 5-3: Total System Entropy Generation vs. Seasonal COP

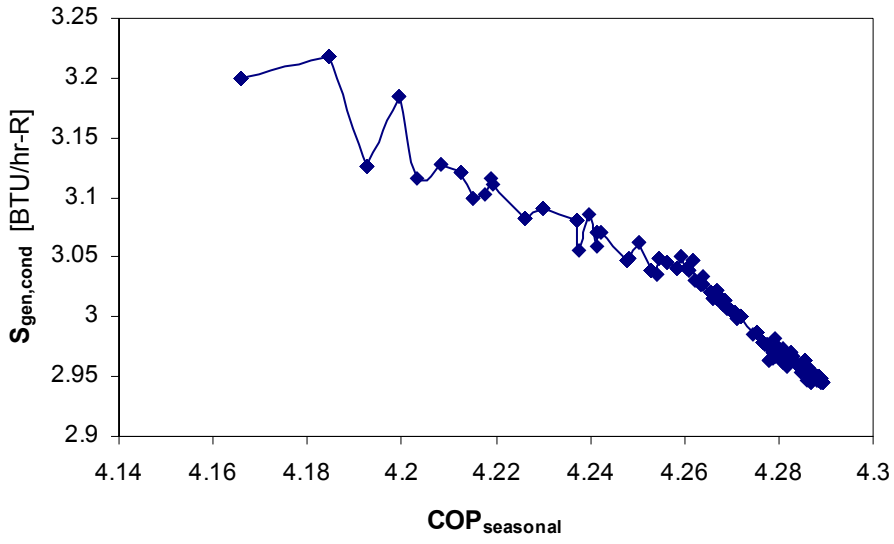

Figure 5-4: Condenser Entropy Generation vs. Seasonal COP

V-B: Smooth vs. Roughened Tubes Entropy Generation: Case Study

For many years now, the industry standard has been to manufacture finned-tube heat exchangers with augmented fins as well as augmentations on the inside surface of the tubes. Since there are competing effects of this augmentation (increased heat transfer and increased frictional pressure drop), it is not readily apparent whether or not the augmentation helps or hurts the overall system performance and, to date, no one has investigated this effect in finned-tube heat exchangers with an appropriate figure of merit.

In this chapter it has been shown that minimum entropy generation for the individual condenser component correlates with the maximum COP for the entire air-conditioning system. Therefore, by minimizing the entropy generation due to the heat transfer and friction irreversibilities in the finned tube condenser for the augmented and non-augmented cases, these two situations can be effectively compared to each other and related to their effect on the system performance. Initially this methodology is applied here to the simple problem of flow *inside* a tube of a simple heat exchanger consisting of a single tube at a fixed wall temperature. The augmentation in this case will involve sand grain roughening the insides of the tubes versus the non-augmented case of smooth tubes. There is detailed information available in the literature regarding friction and heat transfer effects of flow through both of these types of tubes. The hypothesis is that by optimizing the rough tube design, the total entropy generation for both the heat transfer and pressure drop can be minimized over an optimized smooth tube.

The basis for this analysis is from Bejan (1996). Bejan develops a relation for entropy generation per unit length ($\dot{S}'_{gen}$) of a tube with fixed heat transfer rate per unit

length (q') and fixed mass flow rate ($\dot{m}$), while the independent design parameter is the diameter. In one case, the study looks strictly at smooth tubes and uses this equation (minimizing $\dot{S}'_{gen}$) to optimize the diameter of the tube (or Reynolds number, since mass flow rate is fixed) under the constraints imposed. Then in a separate analysis augmentation (sand grain roughening) is applied to these tubes and the entropy generation (per unit length) for the smooth tube is compared with the entropy generation in a roughened tube of the same geometry. Plots are given which display the limiting Re number below which the augmentation will reduce the entropy generation compared to the smooth case.

There are several problems with Bejan's analysis regarding using it for design decisions. The first is that fixing the heat transfer rate per unit length allows the total heat transfer rate to change when optimizing the length of the tube. This method does not penalize for a longer tube at the same diameter, which would, in reality cost more. A more costly heat exchanger can always reduce the entropy generation by increasing the surface area. A more appropriate constraint would be to fix the heat transfer rate (service factor) and the surface area ($\dot{Q}/A_s$), which would approximate a fixed cost heat exchanger, i.e., assuming heat exchanger cost, is proportional to heat transfer area.

The second problem with Bejan's analysis is that in the augmented versus smooth comparisons there is no optimization of each design case performed before comparison. In fact, the smooth and the augmented cases both have the same tube length and diameter dimensions, when the optimum geometry for each smooth and roughened case would not be the same.

A more meaningful comparison could be made if an optimized smooth tube design were compared with an optimized roughened tube design. Additionally, the plots developed by Bejan do not give any useful information for designing the heat exchanger for optimum performance using augmentation.

Bejan's analysis is purely on a per unit length basis, making it more mathematically elegant, however it is also less useful in design application. Therefore, in the current study, the intent is to improve upon Bejan's (1996) work to gain some meaningful insight into the effect of augmentation on the heat exchanger performance for design decisions. The developed analysis is shown below.

First consider a duct of arbitrary cross section A_c as shown in Figure 5-5 (Bejan 1996). Heat ($\dot{Q}$) is transferred to the stream flowing through the duct with a flow rate of $\dot{m}$. At steady state the heat crosses the temperature gap ΔT formed between the wall temperature ($T+\Delta T$) and the bulk temperature of the stream (T). The stream flows with friction in the x-direction.

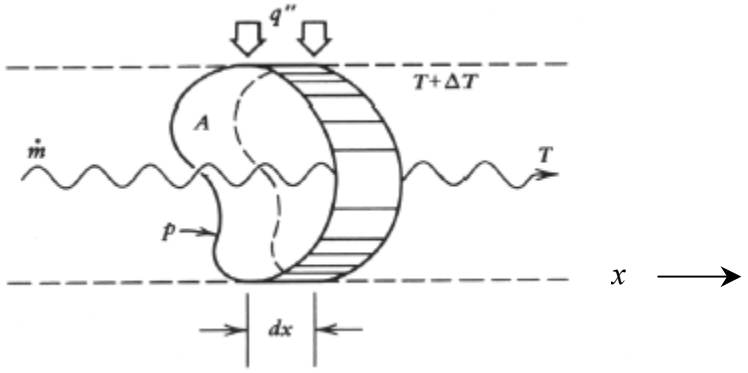

Figure 5-5: Forced Convection Heat Transfer in a Duct of Arbitrary Geometry

Applying the first law of thermodynamics to this system, noting that there is no work in this system:

$$\delta \dot{Q} = \dot{m}\, dh \tag{5.7}$$

Now, applying the second law of thermodynamics to this control volume, noting that the temperature at which heat transfer crosses the boundary is $T+\Delta T$:

$$\delta \dot{S}_{gen} = \dot{m}\, ds - \frac{\delta \dot{Q}}{T + \Delta T} \geq 0 \tag{5.8}$$

Combining (5.7) and (5.8) and using the second Gibbs equation ($Tds=dh-vdp$), the following relation for the entropy generation rate results:

$$\delta \dot{S}_{gen} = \delta \dot{Q}\left(\frac{1}{T} - \frac{1}{T + \Delta T}\right) - \frac{\dot{m}\, vdp}{T} = \delta \dot{Q}\left(\frac{\Delta T}{T^2\left(1 + \Delta T / T\right)}\right) - \frac{\dot{m}\, vdp}{T} \tag{5.9}$$

Assuming that ΔT is much less than T ($\Delta T/T$ is << 1) and using density (ρ) instead of specific volume, this equation becomes:

$$\delta \dot{S}_{gen} = \delta \dot{Q}\left(\frac{\Delta T}{T^2}\right) + \frac{\dot{m}\left(-dp\right)}{\rho T} \tag{5.18}$$

Now heat transfer terminology is employed as defined below for the Darcy friction factor (f), Stanton number (St), average convective heat transfer coefficient ($\bar{h}$),

mass velocity (G), Reynolds number (Re_D), hydraulic diameter (D_h), Nusselt number (Nu), and Prandtl number (Pr):

$$f = \frac{\rho D_h}{2G^2}\left(\frac{-dp}{dx}\right) \tag{5.10}$$

$$G = \frac{\dot{m}}{A_c} \tag{5.11}$$

$$\bar{h} = \frac{\dot{Q}}{A_s \Delta T} \tag{5.12}$$

$$Nu = \frac{\bar{h} D_h}{k} = \mathrm{St}\,\mathrm{Re}_D\,\mathrm{Pr} \tag{5.13}$$

Where:

$$D_h = \frac{4A_c}{P_w} \tag{5.14}$$

$$\mathrm{Re}_D = \frac{GD_h}{\mu} = \frac{4\dot{m}}{\pi \mu D} \tag{5.15}$$

$$\mathrm{St} = \frac{\bar{h}}{c_p G} \tag{5.16}$$

And

$$\mathrm{Pr} = \nu / \alpha \tag{5.17}$$

Where P_w is the wetted perimeter, μ is the fluid viscosity, ν is the kinematic viscosity, c_p is the specific heat, k is the fluid thermal conductivity, α is the thermal diffusivity, A_s is the surface area, and A_c is the cross sectional area.

Using Equation (5.10) and Equation (5.11) in Equation (5.18) results in the following relation:

$$\delta \dot{S}_{gen} = \delta \dot{Q}\left(\frac{\Delta T}{T^2}\right) + \frac{2\dot{m}^3 f}{\rho^2 A_c^2 D_h T} dx \tag{5.19}$$

Integrating this equation, with the assumptions that ΔT, T, $\dot{m}$, f, A_c, D_h, and ρ (assuming $\Delta P \ll P$) are constant through the integration, and then using Equations (5.12) and(5.13), the result is:

$$\dot{S}_{gen} = \frac{\dot{Q}^2 D_h}{A_s k T^2 Nu} + \frac{2\dot{m}^3 f L}{\rho^2 T D_h A_c^2} \tag{5.20}$$

Now assuming the channel is circular, thereby reducing one degree of freedom (since perimeter and area are related through the diameter), equation (5.20) becomes:

$$\dot{S}_{gen} = \frac{\dot{Q}^2}{\pi L k T^2 \mathrm{Nu}} + \frac{32\dot{m}^3 f L}{\pi^2 \rho^2 T D^5} \tag{5.21}$$

This is a general equation for the total entropy generation rate in a circular channel. The first term in this equation is the entropy generation due to heat transfer

($\dot{S}_{\Delta T}$) and the second term is the entropy generation due to pressure drop ($\dot{S}_{\Delta P}$) (Bejan 1996). An irreversibility distribution ratio, Φ, can be defined as the ratio of these two entropy generations:

$$\Phi = \dot{S}_{\Delta P} / \dot{S}_{\Delta T} \tag{5.22}$$

Notice that making a design change in equation (5.21), e.g., L, induces changes of opposite signs in the two entropy generation components. Therefore as in the finned-tube condenser, there is an optimal trade-off between the two irreversibility contributions, for which the overall measure of exergy destruction ($\dot{S}_{gen}$) is a minimum while the system continues to serve its specified function ($\dot{Q}/A_s$, $\dot{m}$).

The case of constant surface area (A_s), which approximates a condition of fixed material cost, will be considered from here on; $A_s = \pi DL$, therefore:

$$L = \frac{A_s}{\pi D} \tag{5.23}$$

Using this equation in Equation (5.21) and eliminating D in favor of $\mathrm{Re_D}$ using the second part of Equation (5.15) the following relationship for the total entropy generation is obtained:

$$\dot{S}_{gen} = \frac{4\dot{m}\dot{Q}^2 \mathrm{Re}_D^{-1}}{\pi A_s k \mu^2 T^2 \mathrm{Nu}} + \frac{\pi^3 A_s \mu^6 f \mathrm{Re}_D^{\,6}}{128 \rho^2 T \dot{m}^3} \tag{5.24}$$

In order to proceed, correlations for the Nusselt number and the friction factor are needed. For smooth tubes, the following fully turbulent relations are used, as also used by Bejan (1996), the Dittus Boelter equation for heating:

$$\mathrm{Nu}_s = 0.023\,\mathrm{Re}_D^{0.8}\,\mathrm{Pr}^{0.4} \quad (0.7<\mathrm{Pr}<160;\ \mathrm{Re}_D>10^4) \tag{5.25}$$

And the fully turbulent friction factor:

$$f_s = 0.046\,\mathrm{Re}_D^{-0.2} \quad (10^4<\mathrm{Re}_D<10^6) \tag{5.26}$$

For the case of roughened tubes, the fully turbulent correlations developed from Nikuradse (1950) and Dipprey and Sabersky (1963) are used:

$$\mathrm{St}_r = \frac{f_r/2}{1+\sqrt{\frac{f_r}{2}}\left[\bar{g}(e^+)-B(e^+)\right]} \tag{5.27}$$

$$\sqrt{\frac{f_r}{2}} = \frac{1}{2.5\left(1.2-\ln\frac{\varepsilon}{D}\right)} \tag{5.28}$$

where, St is the Stanton number defined by:

$$\mathrm{St}=\frac{\mathrm{Nu}}{\mathrm{Re}_D\,\mathrm{Pr}}, \tag{5.29}$$

and e^+ is the "roughness Reynolds number":

$$e^+ = \frac{\varepsilon_r}{D} \mathrm{Re}_D \sqrt{f_r / 2}\,, \tag{5.30}$$

The function $\bar{g}(e^+)$ is graphically expressed by Dipprey and Sabersky (1963). For fully rough conditions ($e^+ > 70$) it can be expressed in equation form as:

$$\bar{g}(e^+) = k_f (e^+)^{0.2} \mathrm{Pr}^{0.44} \tag{5.31}$$

where, k_f is a constant and depends only on the particular type of roughness shape. It has a value of 5.19 for sand grain roughness, which is the roughness type considered in the current study. The function $B(e^+)$ is also graphically expressed by Dipprey and Sabersky as shown in Figure 5-7, and takes on a value of 8.48 for the fully rough conditions.

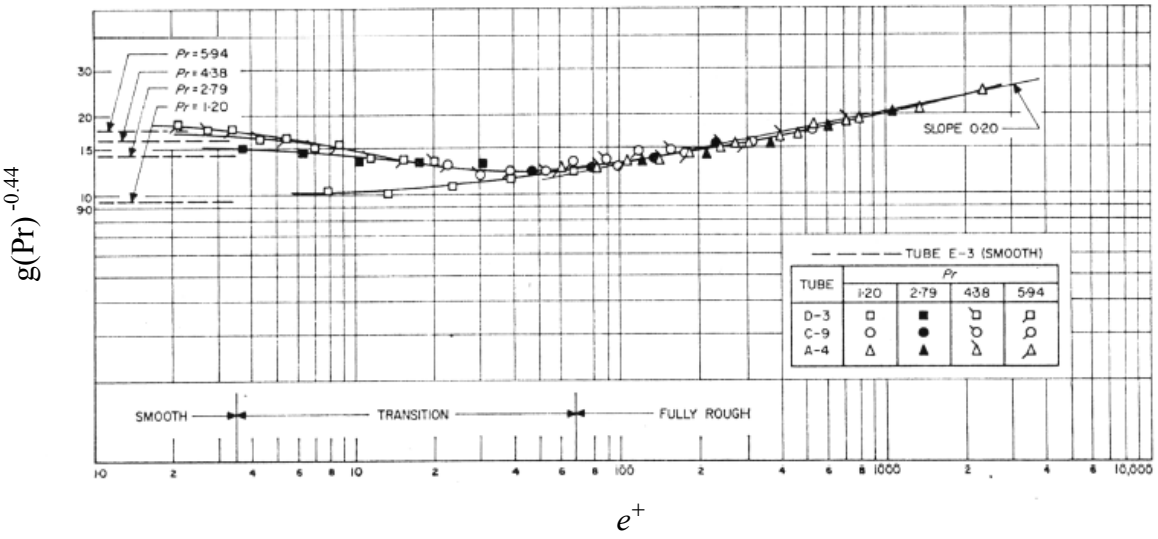

Figure 5-6: Dipprey & Sabersky (1963) $\bar{g}(e^+)$ vs. e^+

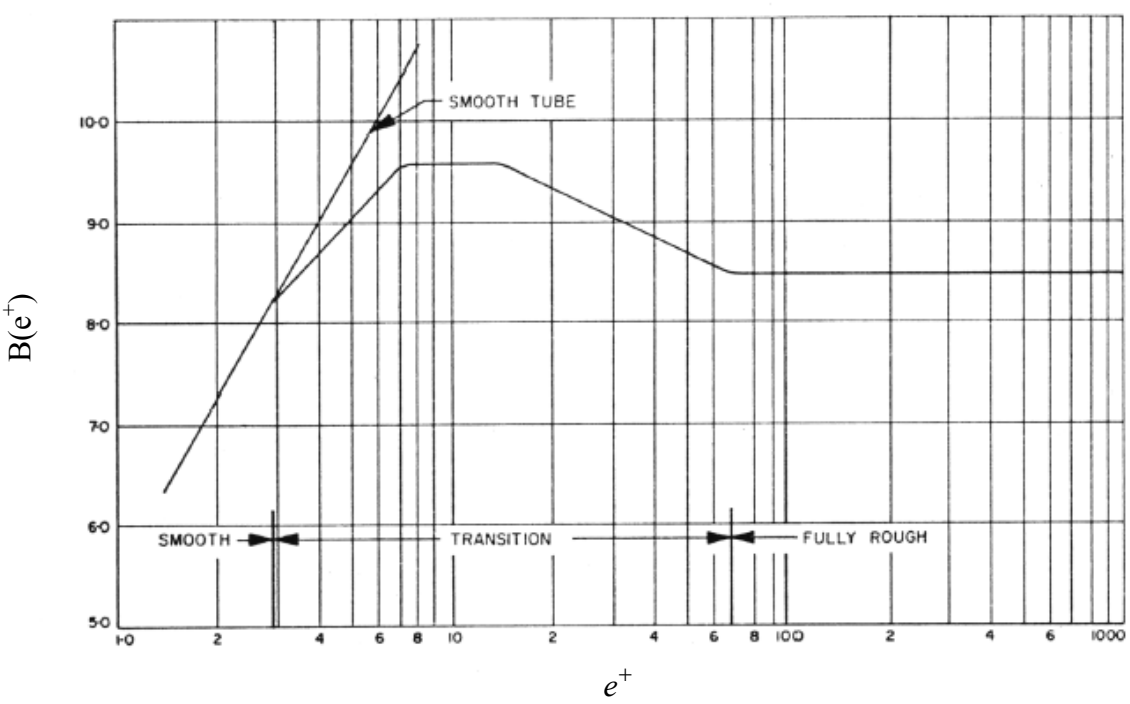

Figure 5-7: Dipprey & Sabersky (1963) $B(e^+)$ **vs.** e^+

V-B.1: Smooth Tube Optimization

For the smooth case, the optimum Reynolds number can be calculated in closed form by taking the derivative of the entropy generation rate with respect to Reynolds number and setting this value equal to zero. The optimum Reynolds number value obtained for fixed surface area is then:

$$\mathrm{Re}_{D_{opt}} = 2.6271 Bo_{A_s}^{\ 0.263} \mathrm{Pr}^{-0.053} \tag{5.32}$$

where:

$$Bo = \frac{\rho \dot{Q} \dot{m}^2}{A_s \left(\mu^7 kT\right)^{1/2}} \tag{5.33}$$

Because of the different constraints used, this equation is different from Bejan's (1996) but has the same form.

The irreversibility distribution ratio takes on an optimum value when $\dot{S}_{gen} = \dot{S}_{gen,\min}$, at $\mathrm{Re}_D = \mathrm{Re}_{D_{opt}}$. This optimum value for Φ can be calculated in closed form for all smooth cases (with fixed surface area) to be:

$$\Phi_{opt} = 0.3103 \tag{5.34}$$

Note this states that the optimum design has an entropy generation due to friction irreversibilities that is 31% of the entropy generation due to heat transfer irreversibilities.

V-B.2: Rough Tube Optimization

For the rough case, the mathematical manipulation of solving for the optimum Reynolds number, and hence calculating the optimum irreversibility distribution ratio, is much more complicated. Its value must be investigated by specifying conditions and fluids.

This model was run for water at 10°C, 2 bars, with a ΔT of 5°C, diameter range of 6 to 14mm, and a mass flow rate of 0.6 kg/s, as well as air at 10°C, 2 bars, with a ΔT of 5°C, diameter range of 20-45 mm, and a mass flow rate of 0.06 kg/s. The constant used for A_s was 0.0314 m^2. Roughness values ranging from ε/D=0.0024 to 0.05 were investigated in addition to the smooth case. Care was taken at low roughnesses to make sure that the roughness Reynolds number, e^+, was always greater than 70 (fully rough

conditions). For situations where e^+ was lower than this value (transitional roughness) the Dipprey and Sabersky (1963) plots were used to find $B(e^+)$ and $\bar{g}\left(e^+\right)$. Results are shown in Figures 5-8 and 5-9, the solid markers are fully rough and the hollow markers are transitional cases, while the unmarked line is the smooth case.

It was found under the conditions investigated, that using consistent constraints for the smooth and roughened case (e.g. constant A_s), the optimum irreversibility distribution ratio for the rough case was the same as that for the smooth case (Φ_{opt}=0.3103). This information can be used to easily find the optimum design of a fully sand grain roughened tube, under fully turbulent flow conditions, for a fixed surface area tube, approximating fixed cost.

It can be seen from Figures 5-8 (for water) and 5-9 (for air) that under these conditions roughness can reduce entropy generation, when it is optimized. Note that there is an optimum amount of roughness shown in Figure 5-8, for the higher Prandtl number fluid, water, and this optimum seems to occur around the transition to fully rough. Also, note that for the higher Prandtl number fluid the advantages of adding roughness are more profound. Similarly, by comparing only heat transfer coefficients, Dipprey & Sabersky (1963) found a maximum near the start of fully roughened behavior, while the maximum was more pronounced for higher Prandtl numbers.

The result that higher Prandtl numbers reap more benefits from augmentation may be attributed to the fact that Prandtl number gives an indication of the relative size of the thermal boundary layer compared to the viscous boundary layer. For Pr >> 1 the thermal boundary layer is much thinner than the viscous boundary layer. Therefore, because the

relative size of the roughness is larger with respect to the thinner thermal boundary layer, the augmentation has a larger impact on the thermal boundary layer (increasing the heat transfer coefficient) in the case of Pr >> 1 than the thicker viscous boundary layer.

For air with the lower Prandtl number an optimum degree of roughness is not reached. Instead, Figure 5-9 indicates that extremely high roughnesses (> 5%) beyond those investigated may in fact produce an optimum. In contrast to this, Dipprey & Sabersky (1963) used as a figure of merit the ratio of heat transfer coefficient to friction coefficient, and concluded that no improvement could be attained by roughening at low Prandtl numbers (< 3). This is not the case in Figure 5-9, where in many cases the entropy generation is reduced by the addition of roughness. This shows that the figure of merit used by Dipprey & Sabersky was not successful in determining the effectiveness of the augmentation. Note also that for air small amounts of roughness actually reduce the performance.

Therefore, in general the heat transfer augmentation technique in these situations produced lower system entropy generations, however optimization of the geometry is instrumental in assuring any, or the maximum, benefit.

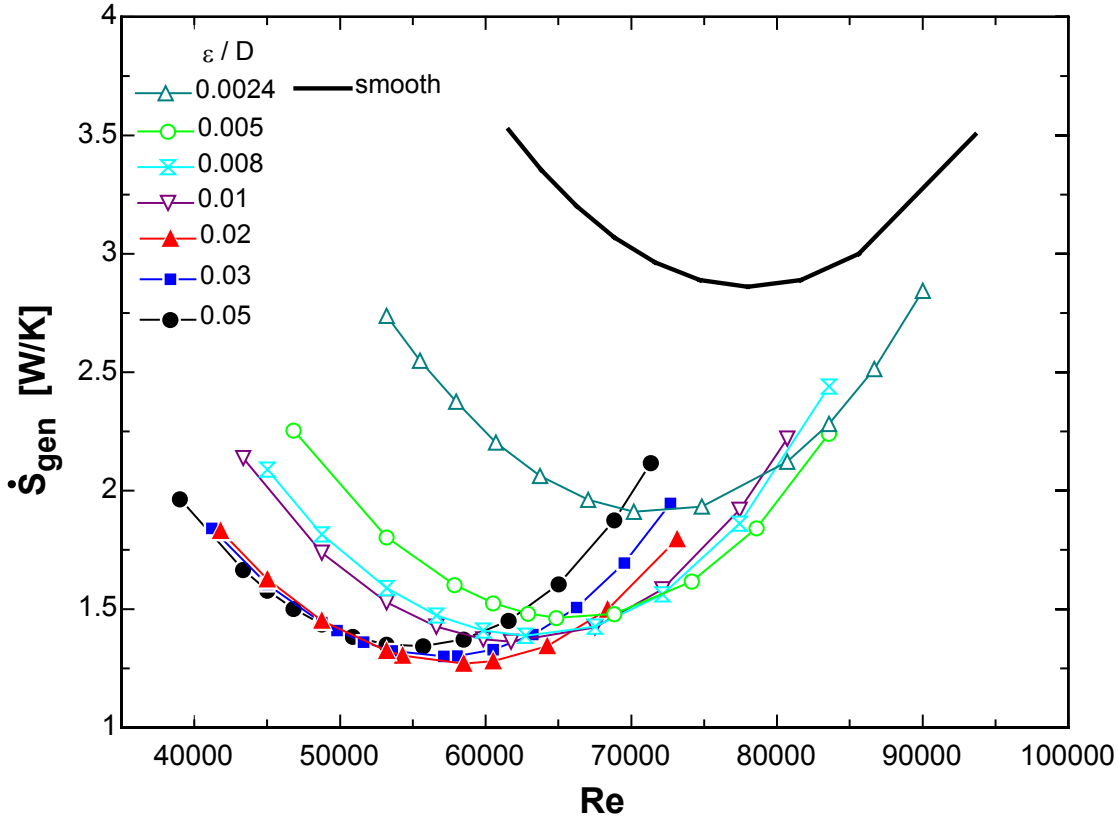

Figure 5-8: Entropy Generation vs. Reynolds Number for Water (Pr=9.39) Flow Through Tubes.

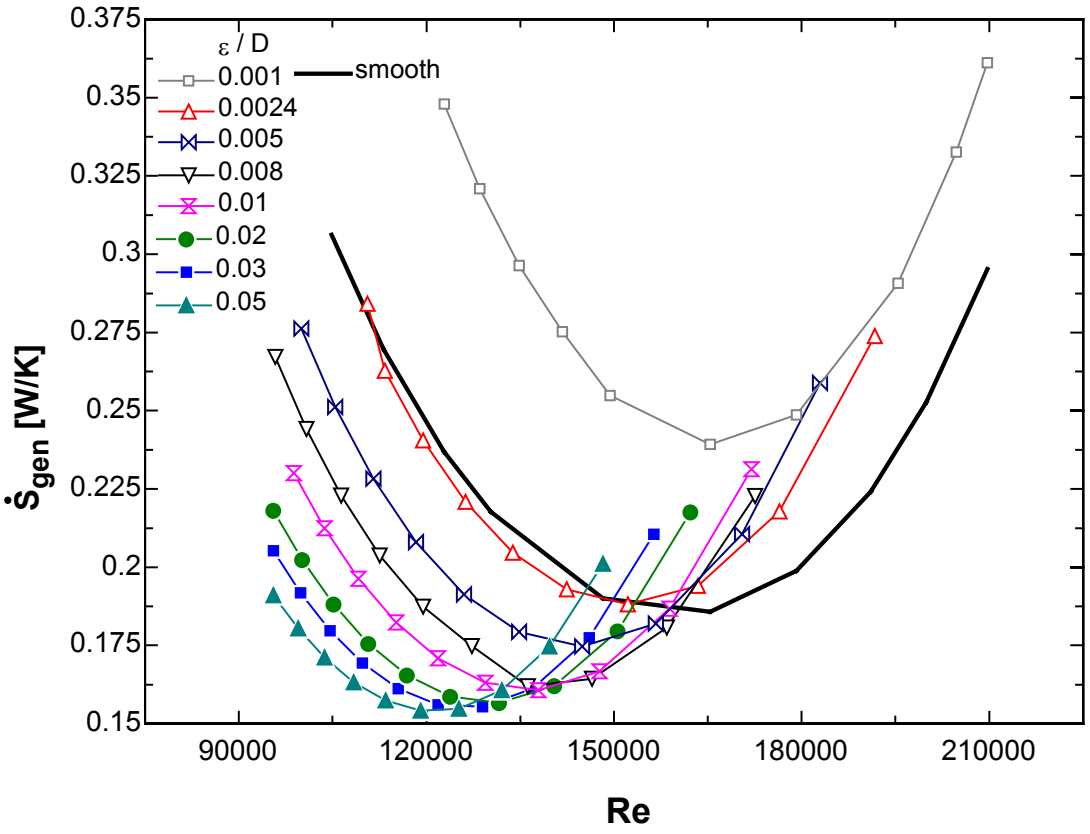

Figure 5-9: Entropy Generation vs. Reynolds Number for Air (Pr=0.7) Flow Through Tubes.

CHAPTER VI

RESULTS

VI-A: Introduction

As shown in Table 6-1, 12 design parameters are necessary to define a plain fin design, while the addition of louver enhancements creates an additional two parameters. In this heat exchanger design optimization, a single objective function is used in the optimization procedure. Initially, this objective function is seasonal COP, while later minimum condenser entropy generation is considered as an alternative to COP. Initially, the design parameters were not constrained in the optimization procedure except for those that were limited by the range of experimental data used to develop the empirical correlations employed by this study as discussed in Chapter III and shown in Table 6-1. As expected, some variables optimized to their limits. Since the purpose of the study is to arrive at practical designs, in the cases where these limits were zero or infinity these design parameters were then constrained to practical limits as discussed below and the remaining variables optimized to produce the maximum seasonal COP for a fixed cost condenser.

Since increasing material cost of a heat exchanger tends to increase the COP, the cost must be constrained to a maximum value for each optimization. The costs of the materials are based on current (October 2003) values of aluminum and copper from the

London Metals Exchange (2003). While these costs have remained nearly constant over the last five years, it should be noted that they might change in the future.

Table 6-1: Condenser Design Parameter Constraints

Lower Limit	Design Parameters	Upper Limit
	Geometric:	
0	Frontal Area (A_f) [m^2]	∞
0	Aspect Ratio (AR)	∞
0	Fin Thickness (t_{fin}) [mm]	∞
7.94	Tube Diameter (D) [mm]	7.94
0.157	Fin Pitch (F_p) [mm^{-1}]	0.71
17.8	Transverse Tube Spacing (X_t) [mm]	30.5
12.7	Longitudinal Tube Spacing (X_l) [mm]	28
1	Number of Rows (rows)	∞
1	Tubes per Row (tpr)	∞
1	Number of Circuits (circ)	∞
	Operational:	
0.91	Air Velocity (V_{ac}) **[m/s]**	5.3
0	Sub-cool (T_{sc}) [˚C]	∞
	Louvers:	
0.79	Louver Height (L_h) [mm]	1.4
1.7	Louver Pitch (L_p) [mm]	3.75

VI-B: Practical Design and Correlation Limitations

Constraints for the longitudinal and transverse tube spacing, fin pitch, air velocity, and louver height and pitch were based on the range of experimental data used to develop the empirical correlations employed in this study, as discussed in Chapter II-C.6.

When frontal area is not constrained, the fixed cost design leads to the largest frontal area ($A_f \rightarrow \infty$) corresponding to one row. This situation yields the minimum air pressure drop. Therefore, the larger the frontal area the better, if space and cost allow (as will be shown in Figure 6-2). Because of this, the frontal area is specified, or

constrained, for each optimization, while the effects of varying frontal area are investigated by comparing optimum designs using different frontal area constraints, (0.5, 0.75, 1.0, and 1.25 m^2) at the same condenser cost ($25).

Additionally, the overall heat exchanger aspect ratio (width divided by height) was limited by a maximum of three; since the outside A/C condensing/compressor unit is typically a cube in shape with the condenser bent around three sides (refer to Figure 1-1). If the aspect ratio were not restricted, the design converges to a single very long finned tube ($AR \rightarrow \infty$), since tube bends have pressure drop but no heat transfer

For all of the optimizations the tube diameter was fixed at 7.94 mm (5/16”). This is because Aspelund (2001) found that the smaller the tube ($D \rightarrow 0$), the better the COP, with little improvement beyond 7.94 mm. Additionally, as mentioned in the model section, heat exchanger manufacturers found that the use of smaller heat transfer tubes, smaller transverse tube spacing, and smaller longitudinal tube spacing can effectively reduce the airside resistance as well as saving resources and can lead to a much more compact fin-and-tube heat exchanger design. Benefits of using smaller diameter tubes include smaller form drag caused by the tube, higher refrigerant side heat transfer coefficients due to smaller hydraulic diameter, and less refrigerant inventory in the system (Wang et al. 2001).

Also, the fin thickness was ultimately fixed at 0.15 mm (0.006”). When left in as a search parameter, the solution always converged to a design with thinner and thinner fins ($t_{fin} \rightarrow 0$) while making the fin pitch larger and decreasing the air velocity to adjust for the increased pressure drop. This makes sense theoretically, however, in reality extremely thin fins are not structurally durable, and dirt and dust will clog the fins when

the fin spacing is too small. Because of this, the fin thickness was constrained to a practical minimum value of 0.15 mm.

As discussed in Chapter III-I, the optimum amount of sub-cool was found to be 0˚C. In practical application, a small change in operating conditions can result in a liquid-vapor mixture exiting the condenser, which, instead of passing through the expansion valve, would back up behind the valve until a high enough pressure is reached to fully condense the vapor. The expansion valve would than be wide open and have no control over the evaporator superheat. To avoid this situation under the normal range of operating conditions, the subcool was specified as 5˚C when operating at 35˚C ambient temperature.

The number of rows multiplied by the longitudinal tube spacing determines the depth of the condenser, while the tubes per row multiplied by the transverse tube spacing determines the height. The number of circuits determines the number of parallel tube passages the refrigerant mass flow rate is divided amongst by the manifold. Note that the number of tubes per circuit, tubes per row, and number of rows all must be discrete values. Initially in the optimization process, this restriction was not considered. However, once the optimum 'continuous' design was found, the integer designs on either side of the optimum were considered for each of the discrete parameters and the optimum of these integer value designs was determined as discussed in Chapter IV. These circuitry parameters were not constrained, besides being limited to integer values in the discrete optimization.

VI-C: Optimization

Figure 6-1 shows the general importance of heat exchanger design optimization. This figure shows a single optimized plain fin design with a fixed cost of $25and a fixed frontal area of 0.75m^2, with the air velocity over the fins varied around the optimum. It can be seen from the figure that varying one parameter from an otherwise optimized design, has a large effect on the systems' COP_{seas}, varying from its optimum design COP_{seas} by as much as 12%. If none of the heat exchanger design parameters were optimized, the systems' degradation in COP_{seas} from its optimum could be quite large. Therefore, optimization for each situation is always recommended.

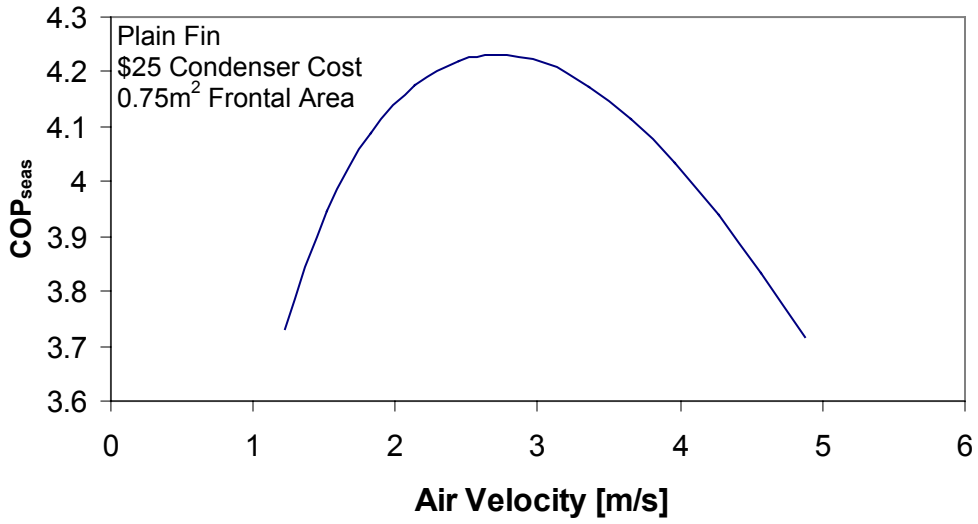

Figure 6-1: COP_{seas} vs. Air Velocity

Table 6-2 shows three different base designs from which the optimization scheme was started for the case of a fixed frontal area of 0.5 m^2 and a cost of $25. From all three starting points, the optimum design shown in bold was obtained from the optimization scheme. This shows that the techniques used were not prone to getting entrenched in

local minima. Note that tprc is the number of tubes per row in a circuit, which is the number of tubes per row (tpr) divided by the number of circuits (circ).

Table 6-2: Optimization Starting Points

Design	V_{ac} [m/s]	F_P [1/mm]	# circ	# rows	# tprc	X_t [mm]	X_l [mm]	Width [m]	COP_{seas}
1	2.5	0.65	1.5	3.7	9.2	24.2	22.6	0.87	3.90
2	1.5	0.4	4	6.2	4.2	27.9	17.8	1.07	2.75
3	4	0.7	6	3.1	3.5	19.1	27.9	1.20	3.70
Opt.	**3.08**	**0.556**	**2.24**	**4.0**	**7.8**	**24.03**	**23.88**	**1.19**	**4.05**

VI-C: Plain Fins

Under the conditions described above, the resulting model and optimization scheme were first used to analyze some general optimization trends for plain fins. Table 6-3 shows all of the optimum designs calculated for the plain fin configuration under the given cost and frontal area constraints using continuous variables for all parameters, while Table 6-4 shows the designs re-optimized with discrete parameters for the number of circuits, number of rows, and number of tubes per row in a circuit with the remaining parameters re-optimized. The continuous parameter results are more useful for showing general designs trends, therefore they are displayed along with the discrete designs in most of the following figures.

Table 6-3: Optimum Plain Fin Continuous Designs

Cost [US$]	Frontal Area [m^2]	V_{ac} [m/s]	F_p [mm^{-1}]	# circ	# rows	# tprc	X_t [mm]	X_l [mm]	Width [m]	COP_{seas}
15	0.75	3.25	0.709	1.84	1.9	12.65	21.59	14.08	1.488	4.033
25		2.70	0.568	2.63	3	8.85	22.25	18.67	1.445	4.232
35		2.44	0.499	3.20	4	6.64	23.55	23.53	1.498	4.309
45		2.29	0.454	3.61	5	5.57	25.50	27.88	1.459	4.344
55		2.23	0.386	4.84	7	3.67	28.23	27.94	1.495	4.376
25	0.5	3.08	0.56	2.24	4	7.81	24.03	23.88	1.189	4.049
	0.75	2.70	0.57	2.63	3	8.85	22.25	18.67	1.445	4.232
	1	2.43	0.68	2.87	2	9.53	21.11	18.57	1.732	4.340
	1.25	2.16	0.71	3.04	2	9.74	22.97	13.25	1.836	4.418

Table 6-4: Optimum Plain Fin Discrete Designs

Cost [US$]	Frontal Area [m^2]	V_{ac} [m/s]	F_p [mm^{-1}]	# circ	# rows	# tprc	X_t [mm]	X_l [mm]	Width [m]	COP_{seas}
15	0.75	3.16	0.707	2	2	12	22.57	13.09	1.385	3.986
25		2.63	0.552	3	3	8	21.00	18.39	1.488	4.200
35		2.38	0.511	3	4	7	23.85	23.12	1.498	4.290
45		2.29	0.451	4	5	5	25.01	27.80	1.499	4.327
55		2.24	0.382	5	7	4	27.87	27.91	1.345	4.335
25	0.5	3.04	0.568	2	4	9	24.06	23.36	1.154	4.022
	0.75	2.63	0.552	3	3	8	21.00	18.39	1.488	4.200
	1	2.37	0.689	3	2	9	21.39	18.55	1.731	4.310
	1.25	2.06	0.706	3	2	10	22.51	13.09	1.851	4.394

Figure 6-2 shows the optimum seasonal COP for varying frontal areas at a fixed cost of $25. This figure shows that increasing the frontal area always increases the COP at fixed cost. Alternatively, Figure 6-3 shows the optimum seasonal COP for varying condenser material costs, at a fixed frontal area of $0.75m^2$. In this case, it can be seen that at costs higher than about $30 the benefits of increased material cost on the system COP are lessened. This effect can be explained by exploring how the optimized design parameters vary with condenser cost and frontal area. Additionally, note that the discrete designs have slightly lower COP's than the continuous designs. This is because the optimum is a fictitious heat exchanger with a decimal number of rows, tubes per row and circuits. By altering these values from their optimums (to make them whole numbers) the fictitious optimum is not attainable, even with re-optimization of the remaining continuous parameters.

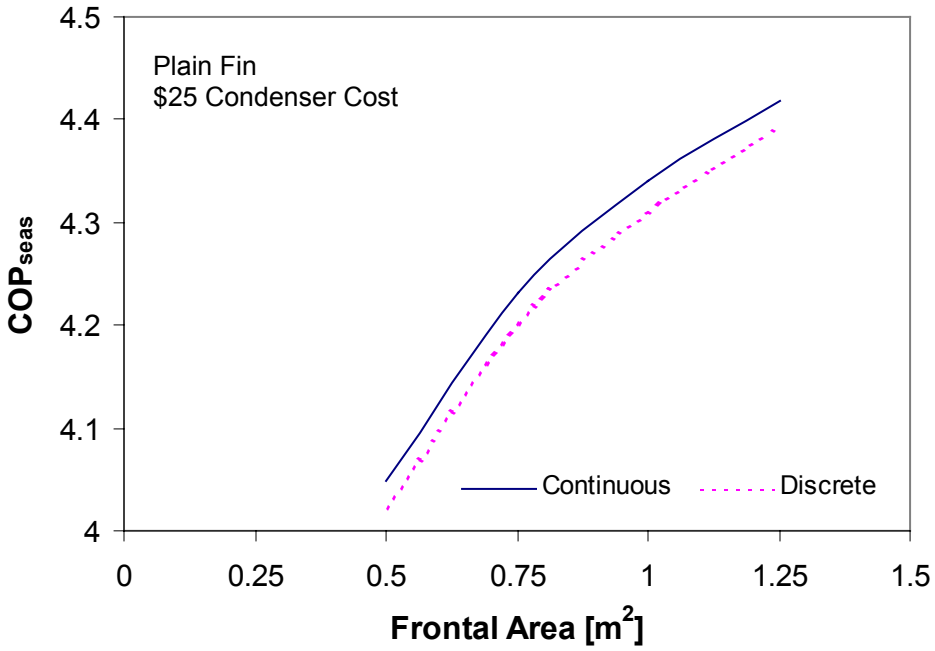

Figure 6-2: Optimum COP_{seas} vs. Frontal Area

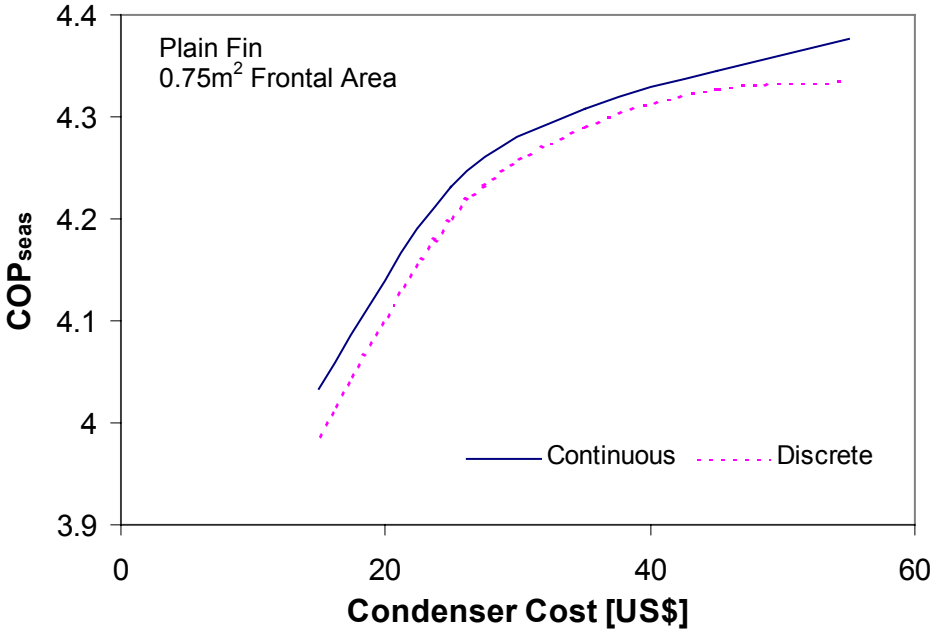

Figure 6-3: Optimum COP_{seas} vs. Condenser Cost

Figure 6-4 shows the optimal number of discrete tube rows superimposed on Figure 6-2's discrete optimum COP_{seas} versus frontal area at a fixed cost of $25. This figure shows that as the frontal area is increased at a fixed cost, the optimum number of tube rows decreases, while the COP_{seas} increases. This illustrates that, as mentioned in the previous section, as the frontal area is increased, the optimum design approaches the case of a single row.

Figure 6-5 shows that the depth of the condenser coil increases with increasing condenser cost almost linearly. Since the depth of the condenser coil is merely the number of tube rows multiplied by the longitudinal tube spacing, this shows that the depth of the coil has a large effect on the condenser coil cost.

Figures 6-6 and 6-7 show that the air velocity and the fin pitch, respectively, decrease with increasing condenser cost, which implies increasing coil depth (at a fixed frontal area). The added coil depth increases the frictional pressure drop on the air-side, therefore to help balance this increase in pressure drop the optimum design seeks to slow the velocity of the air passing over the coils while increasing the gap between fins so as to reduce their frictional effect. Also note that the slope of the air velocity versus cost in Figure 6-6 seems to change around $30, as was observed in Figure 6-3 for the COP_{seas} versus condenser cost. Therefore the change in air velocity (and fin pitch) more than offset the pressure drop effects of increased coil depth occurring with increased cost up to a certain point (approximately $30 in this case) after which the fan power effect is greater than the reduced condenser pressure and corresponding compressor power due to the larger condenser overall *UA*.

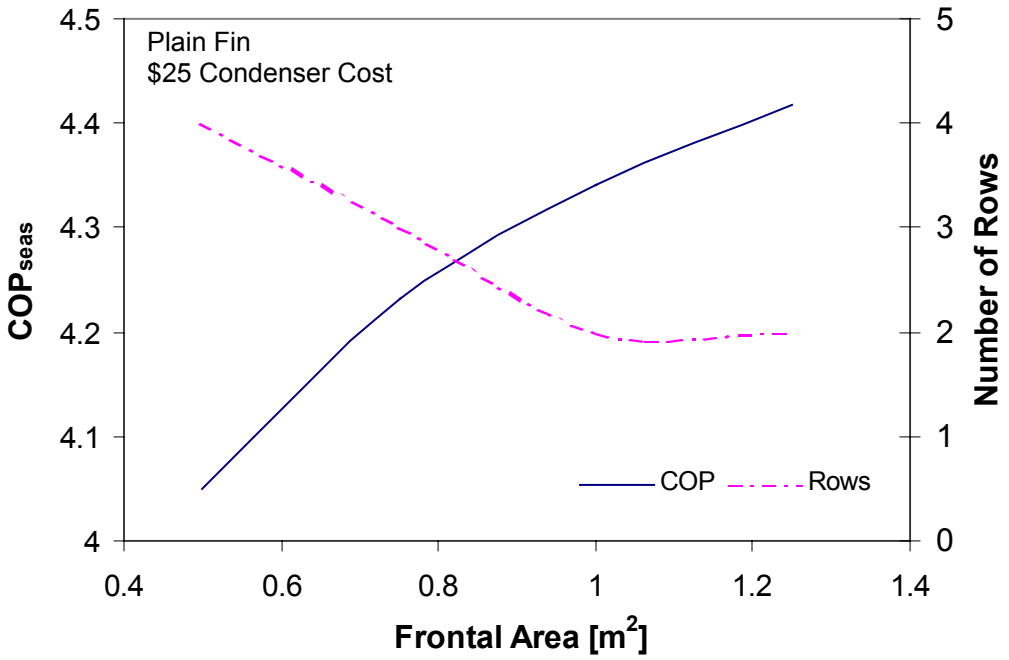

Figure 6-4: Optimum COP_{seas} and Number of Tube Rows vs. Frontal Area

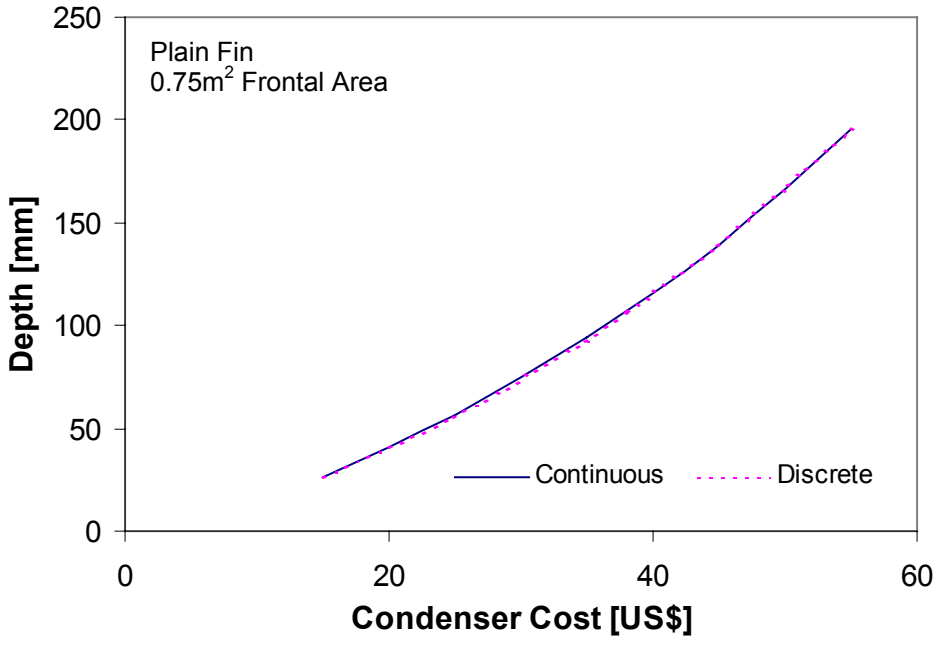

Figure 6-5: Optimum Coil Depth vs. Condenser Cost

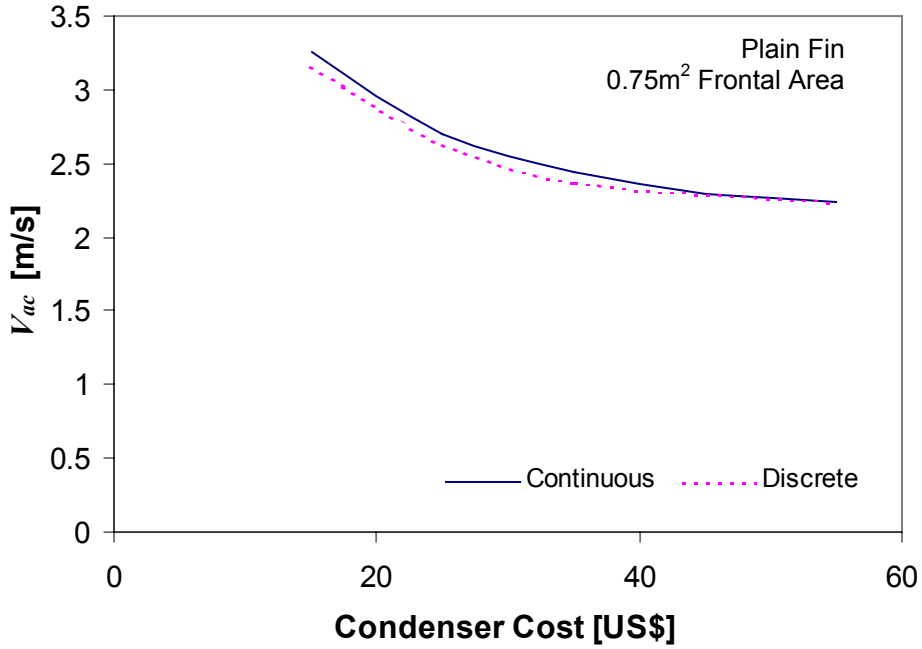

Figure 6-6: Optimum Air Velocity vs. Condenser Cost

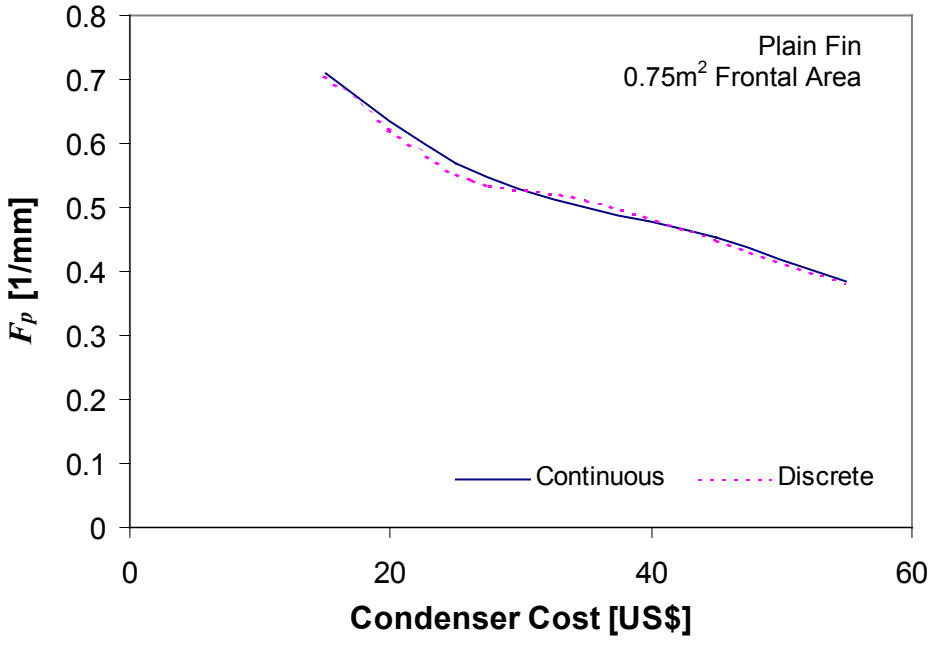

Figure 6-7: Optimum Fin Pitch vs. Condenser Cost

Additionally, as Figures 6-8 and 6-9 show, the longitudinal and transverse tube spacings both increase with increasing condenser cost as well. These effects also assist in offsetting the increasing pressure drop of deeper coils. Note in Figure 6-9, that the longitudinal spacing levels off around $50. This is because these designs have reached the maximum longitudinal tube spacing allowed in this study (as determined by the experimental data used in the air-side heat transfer coefficient and friction factor correlations' development as discussed in Chapter III).

Figure 6-10 shows the optimum number of tubes per row for the plain fins versus condenser cost at a fixed frontal area of $0.75m^2$. The plot shows that the number of tubes per row decreases with increasing cost. This is because the height is approximately constant, due to the fixed frontal area and aspect ratio constraint, while the optimum transverse (vertical) tube spacing increases with increasing cost (Figure 6-8), allowing for less tubes to fit in the same condenser height. Meanwhile, the number of circuits (Figure 6-11), which is the number of parallel flow paths the refrigerant flow is split between, increases with increasing cost. With the tubes per row decreasing this means that the number of tubes per row in a circuit decreases as well. These effects reduce the refrigerant side pressure drop by reducing the total flow length in each individual tube as the coil gets deeper with increased cost.

It should be noted that in several cases, where an optimum continuous design value fell well between integer values, e.g. 3.6 circuits, upon re-optimizing the continuous parameters, the new optimum designs had to adjust to this change. This is best shown between Figures 6-9 and 6-10/6-11. It can be seen where the number of tubes per row (6-10) and number of circuits (6-11) increased (having rounded up from the

continuous optimum value), the transverse tube spacing (6-9) decreased, and vice-versa. This is because for fixed cost, fixed frontal area, and fixed aspect ratio the heat exchanger height is approximately constant, so the transverse tube spacing had to adjust for the changes in tubes per row and number of circuits to maintain the same height.

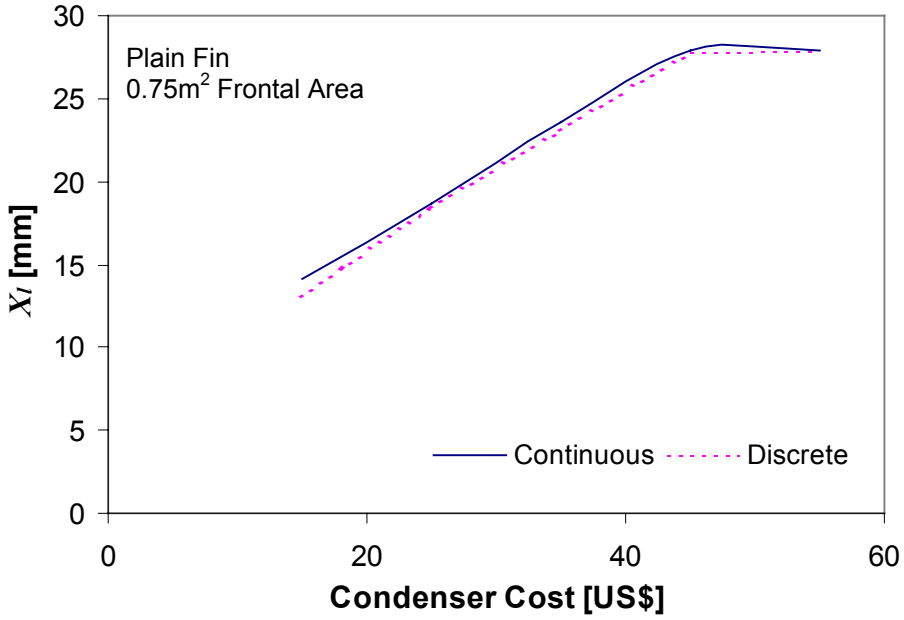

Figure 6-8: Optimum Longitudinal Tube Spacing vs. Condenser Cost

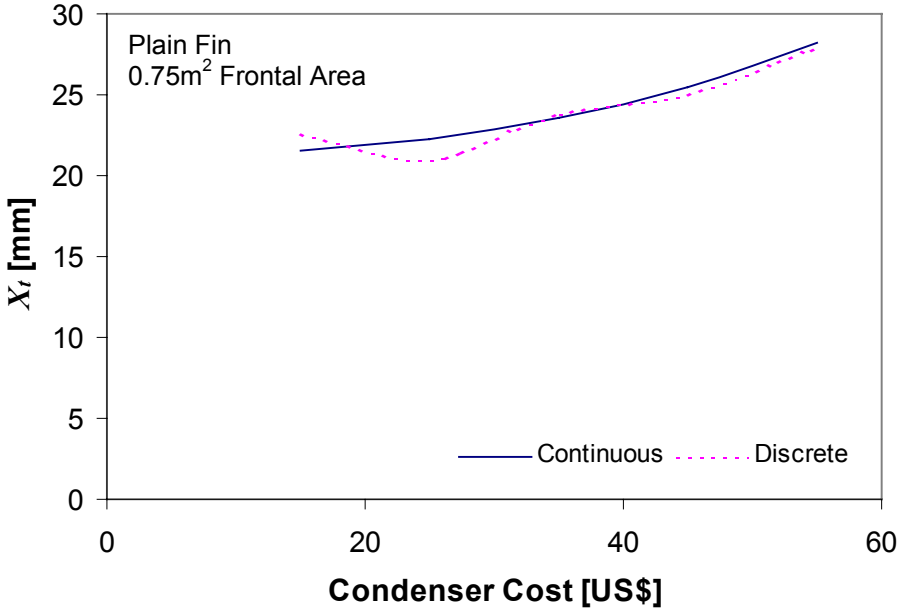

Figure 6-9: Optimum Transverse Tube Spacing vs. Condenser Cost

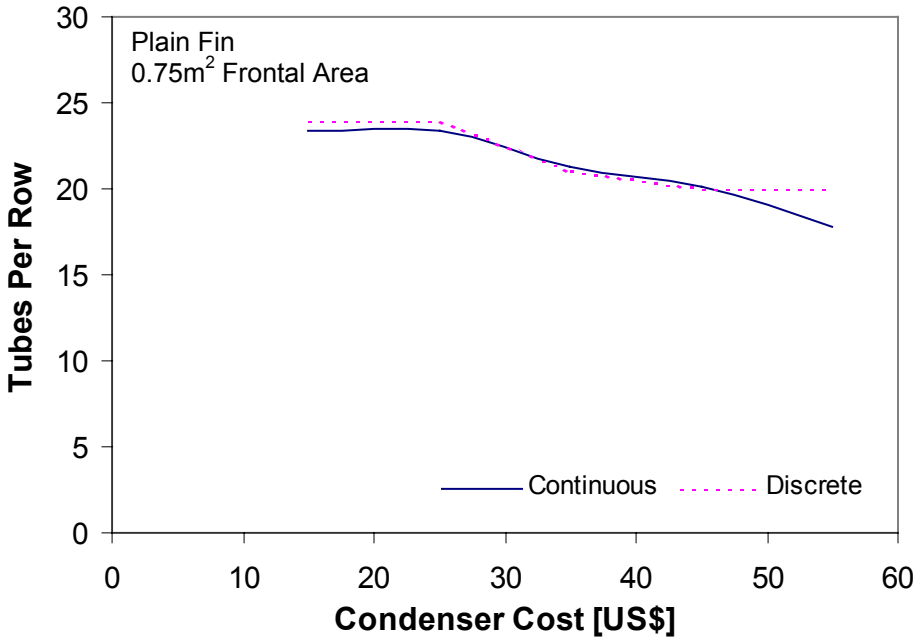

Figure 6-10: Optimum Tubes per Row vs. Condenser Cost

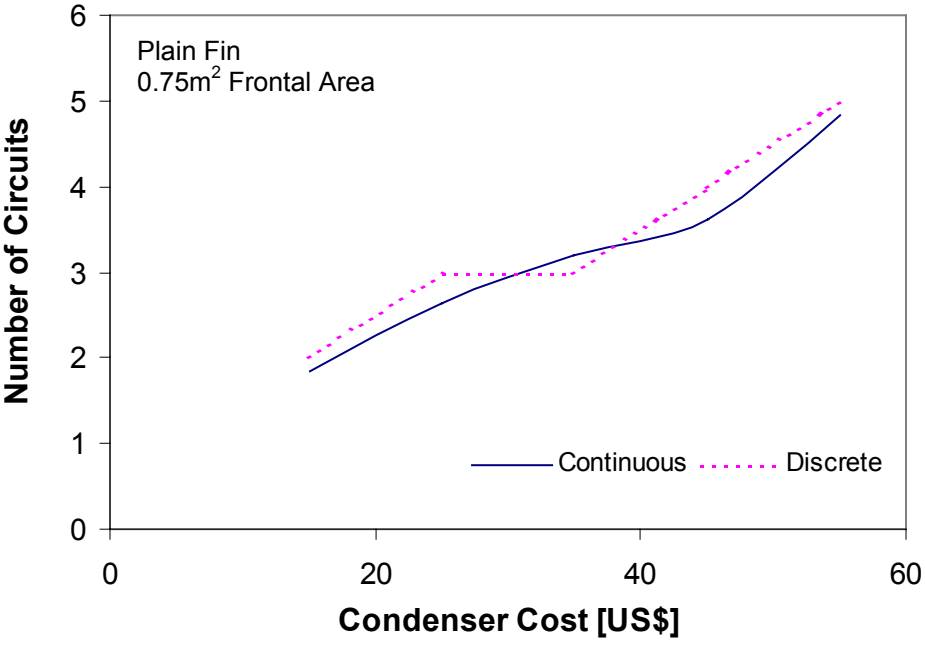

Figure 6-11: Optimum Number of Circuits vs. Condenser Cost

VI-D: Augmented Fins

The continuous optimum designs for the louvered-fin cases studied are shown in Table 6-5, while the discrete optimum louvered-fin designs are shown in Table 6-6, where A_f is the frontal area and W_c is the width of the condenser. As done with the plain fin cases, the louvered-fin continuous optimum designs are compared with the optimum designs found with discrete values for the number of rows, number of circuits, and number of tubes per row in a circuit.

Figure 6-12 shows the optimum louvered-fin COP plotted versus varying condenser material cost at a fixed frontal area of $0.75m^2$, while Figure 6-13 shows the COP plotted versus varying frontal area at a fixed cost of $25. Both plots show that the discrete designs came very close to the continuous optimums.

Again, the largest discrepancies between the continuous and discrete optimums occur when the optimum number of rows, number of circuits, and/or the number of tubes per row in a circuit from the continuous optimization had a design value well in between integer numbers, as can be seen in Figures 6-14 to 6-16. The effects of these changes in the design on some of the remaining continuous parameters are portrayed in Figures 6-17 and 6-18. Note that as the number of refrigerant circuits in the condenser increased above the continuous optimum, the number of tubes per row in a circuit decreased slightly, the air velocity of the condenser increased slightly, and the fin pitch decreased, while the opposite trends are true as well. This shows that these effects balanced each other in the optimization scheme to find the best possible solution under the given constraints.

Table 6-5: Optimum Louvered-Fin Continuous Designs

Cost [$]	A_f [m^2]	V_{ac} [m/s]	F_p [mm^{-1}]	# circ	# rows	# tprc	X_t [mm]	X_l [mm]	L_h [mm]	L_p [mm]	W_c [m]	COP_{seas}
15	0.75	3.39	0.409	2.08	1.54	13.5	17.78	27.91	0.79	3.74	1.50	4.282
25		2.60	0.400	3.43	2.60	8.18	17.82	27.93	0.79	3.74	1.50	4.467
35		2.33	0.406	4.61	3.61	6.06	17.92	27.94	0.79	3.74	1.50	4.519
45		2.18	0.381	6.01	4.78	4.68	17.78	27.93	0.79	3.74	1.49	4.517
25	0.5	2.92	0.539	2.61	3.32	9.00	17.80	27.94	0.79	3.74	1.20	4.307
	0.75	2.60	0.400	3.43	2.60	8.18	17.82	27.93	0.79	3.74	1.50	4.478
	1	2.59	0.38	4.00	2.00	9.00	17.95	27.74	0.79	3.74	1.55	4.57
	1.25	2.38	0.400	3.97	1.56	10.2	17.78	27.91	0.79	3.74	1.74	4.588

Table 6-6: Optimum Louvered-Fin Discrete Designs

Cost [$]	A_f [m^2]	V_{ac} [m/s]	F_p [mm^{-1}]	# circ	# rows	# tprc	X_t [mm]	X_l [mm]	L_h [mm]	L_p [mm]	W_c [m]	COP_{seas}
15	0.75	3.28	0.403	2	2	7	17.78	27.94	0.79	3.74	1.49	4.28
25		2.62	0.290	4	3	8	17.78	27.94	0.79	3.74	1.32	4.45
35		2.26	0.327	5	4	7	17.90	27.94	0.79	3.74	1.20	4.48
45		2.18	0.345	6	5	5	17.78	27.94	0.79	3.74	1.41	4.51
25	0.5	2.92	0.373	3	4	8	17.78	27.94	0.79	3.74	1.17	4.28
	0.75	2.62	0.290	4	3	8	17.78	27.94	0.79	3.74	1.32	4.45
	1	2.59	0.383	4	2	9	17.95	27.74	0.79	3.74	1.55	4.57
	1.25	2.19	0.227	4	2	9	18.05	27.89	0.79	3.74	1.92	4.51

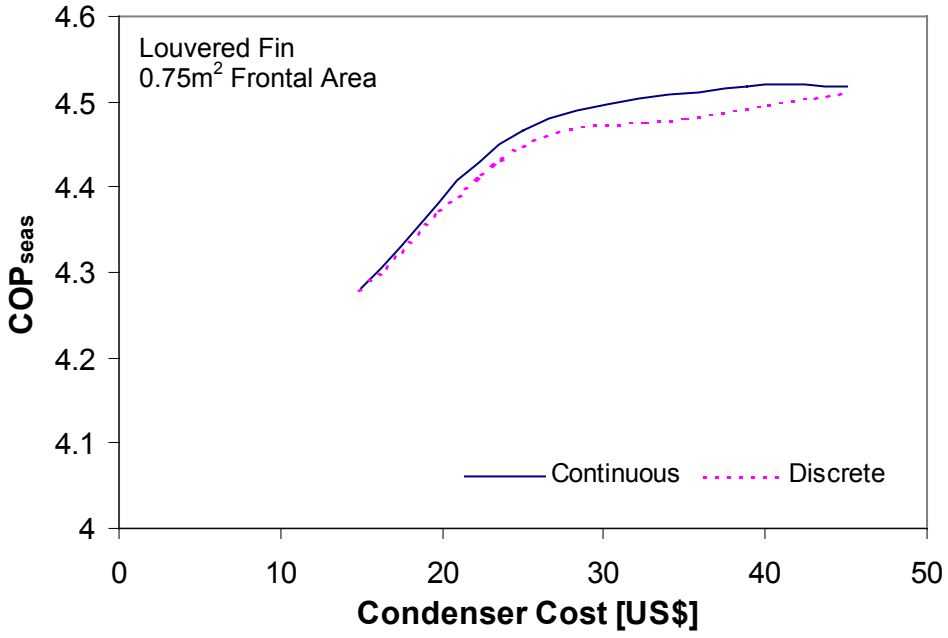

Figure 6-12: Optimum COP_{seas} vs. Condenser Cost

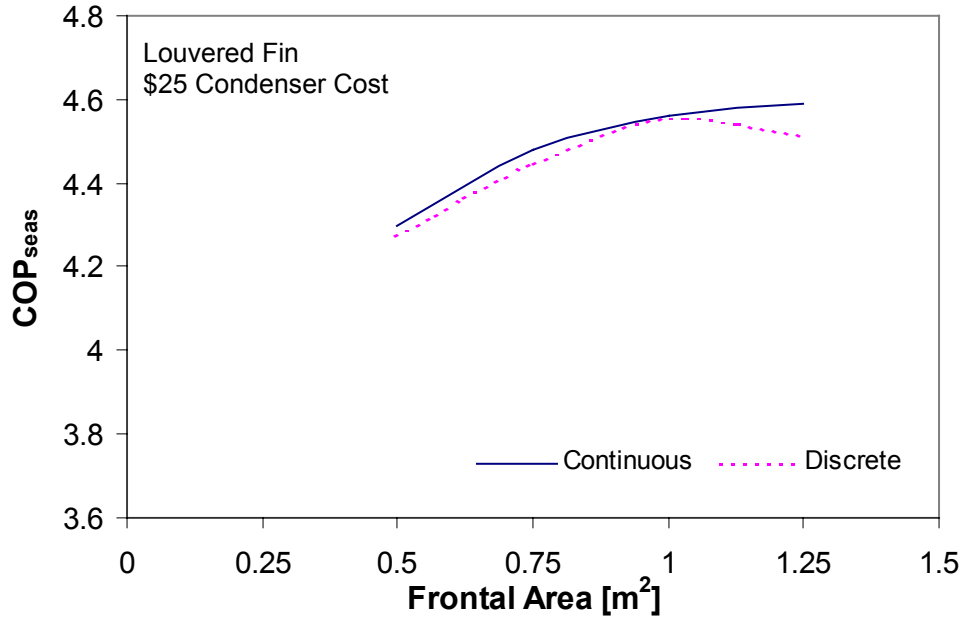

Figure 6-13: Optimum COP_{seas} vs. Condenser Frontal Area

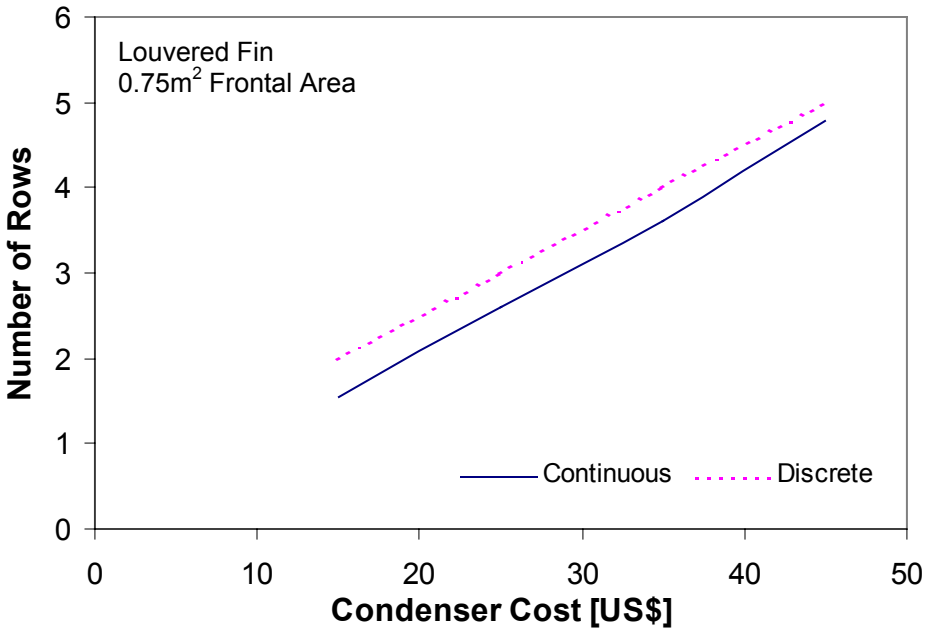

Figure 6-14: Louvered Fins, Optimum Number of Rows vs. Condenser Cost

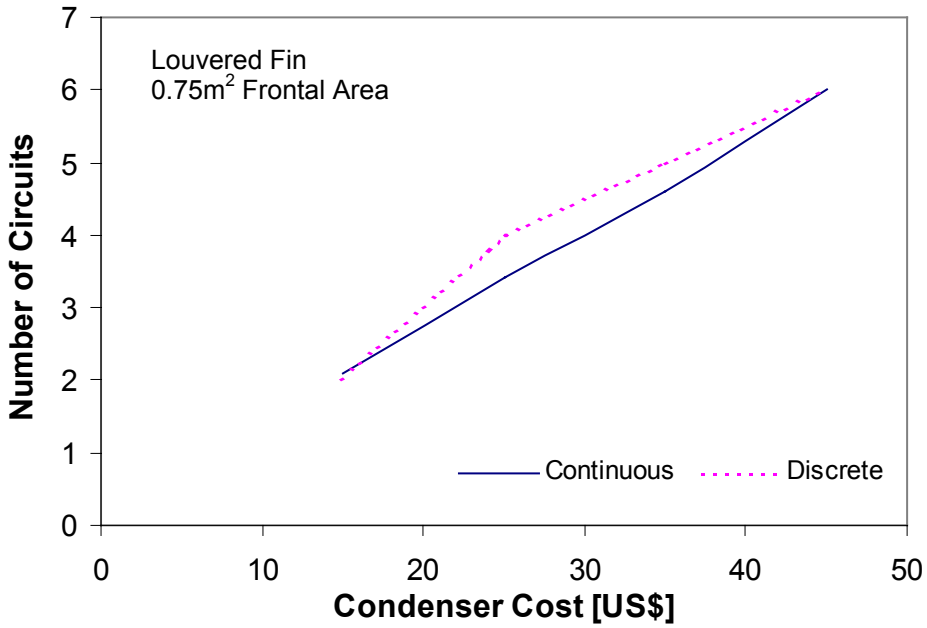

Figure 6-15: Louvered Fins, Optimum Number of Circuits vs. Condenser Cost

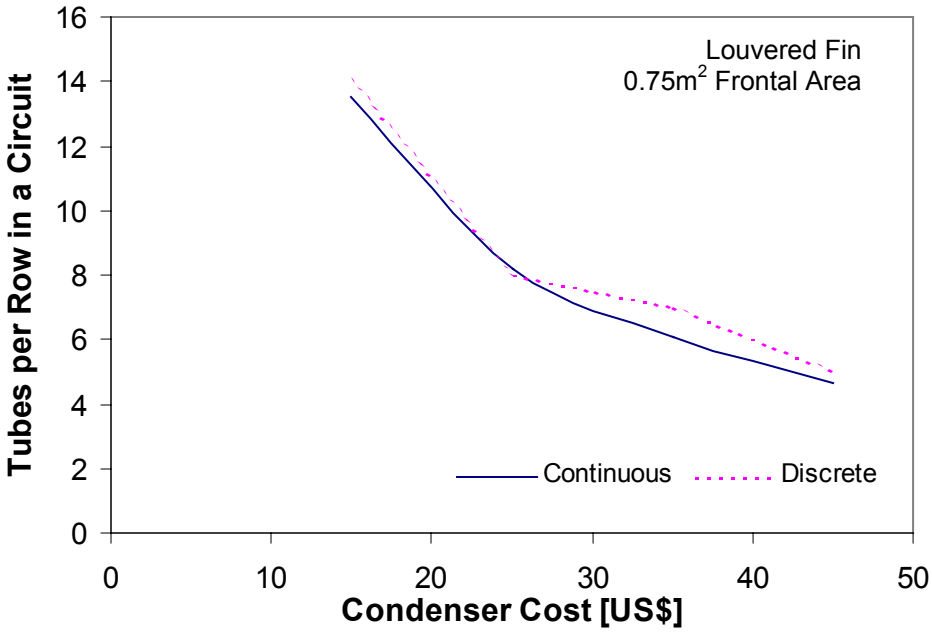

Figure 6-16: Optimum Number of Tubes per Row in a Circuit vs. Condenser Cost

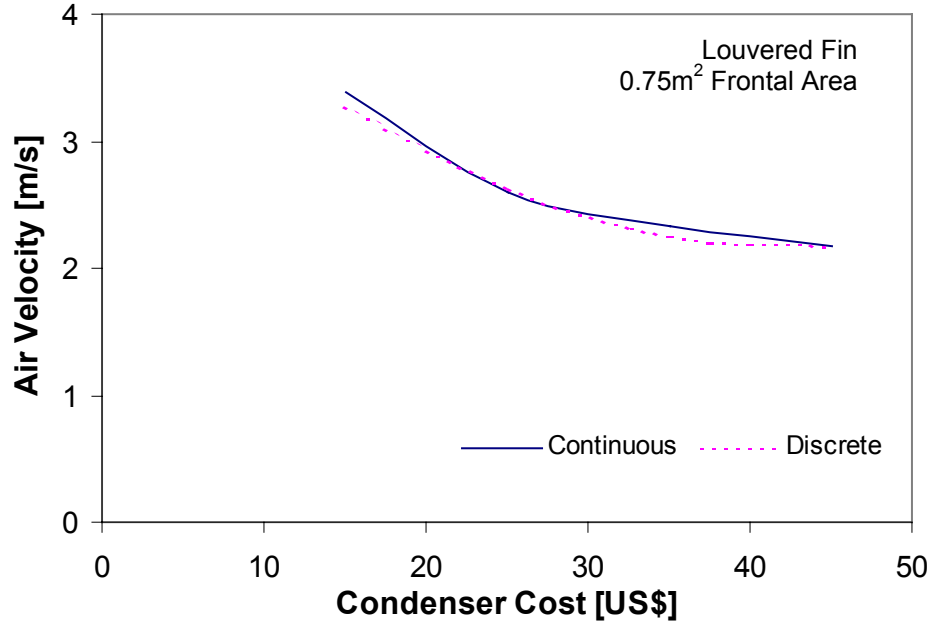

Figure 6-17: Optimum Air Velocity vs. Condenser Cost

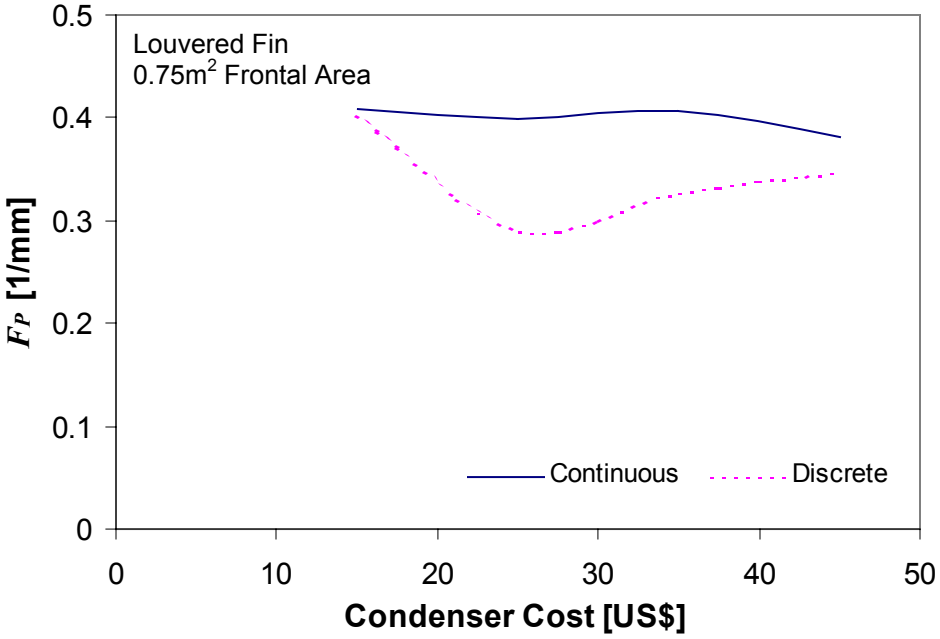

Figure 6-18: Optimum Fin Pitch vs. Condenser Cost

However, the dicretized design tradeoff effects on the fin pitch, shown in Figure 6-18, are obviously quite large. Upon closer inspection, it is noticed that the optimum discrete designs also had a much higher total number of tubes per row (number of tubes per row in a circuit multiplied by the number of circuits) than the optimum continuous louvered-fin designs. With this increase in the number of tubes per row, there was an increase in the amount of copper required by the design. To maintain a fixed cost, therefore, the fin pitch decreased, decreasing the amount of aluminum required by the design.

As mentioned earlier, all of the resulting optimum designs are limited by the experimental range of values used to develop the correlations implemented in the model. Interestingly, for the louvered fins, every single optimum design (continuous and discrete) converged to the minimum louver height (L_h) and the maximum louver pitch

(L_p) as shown in Figure 6-19. Therefore it converged to the situation that creates the least possible amount of turbulence from the louvers. This indicates that arbitrary addition of fin enhancement is not prudent. Additionally, the louvered fin cases (continuous and discrete) tend to converge to the minimum allowed transverse tube spacing (X_t), and the maximum allowed longitudinal tube spacing (X_l), as shown in Figure 6-20. This situation makes the heat exchanger deeper without adding extra rows, but allowing for the insertion of more louvers.

This finding relates back to the parametric trade-offs portrayed in Figure 6-18. With an increasing number of tubes per row, in order to maintain a constant surface area at the maximum frontal area aspect ratio, the vertical (transverse) tube spacing would normally decrease to obtain the same height. However, since the louvered fin optimum designs all converged to the minimum allowable transverse tube spacing, the discrete optimum designs increased in total height while decreasing in width to maintain the same surface area, reducing the aspect ratio from the maximum value. This situation actually produced a slightly higher COP than if the number of tubes per row were conserved and the maximum aspect ratio were fully utilized. This was a very surprising result, but it is expected that even better COP's could be obtained (approaching more closely the hypothetical design limit) if the tube spacing were not restricted to such a small range by the empirical correlations.

Comparisons between the optimum louvered-fin designs and the optimum plain fin designs will be discussed in the next chapter.

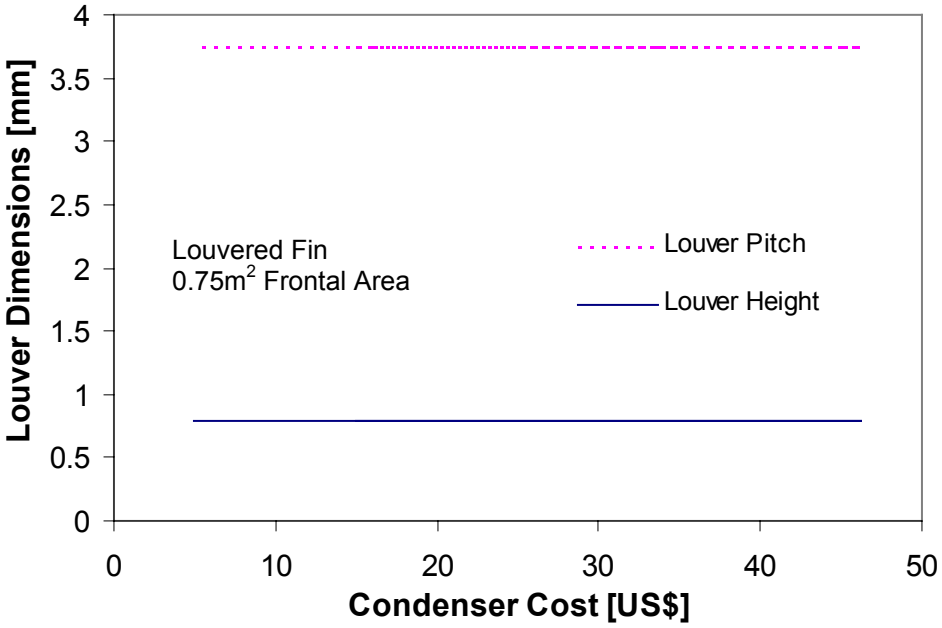

Figure 6-19: Optimum Louver Dimensions vs. Condenser Cost

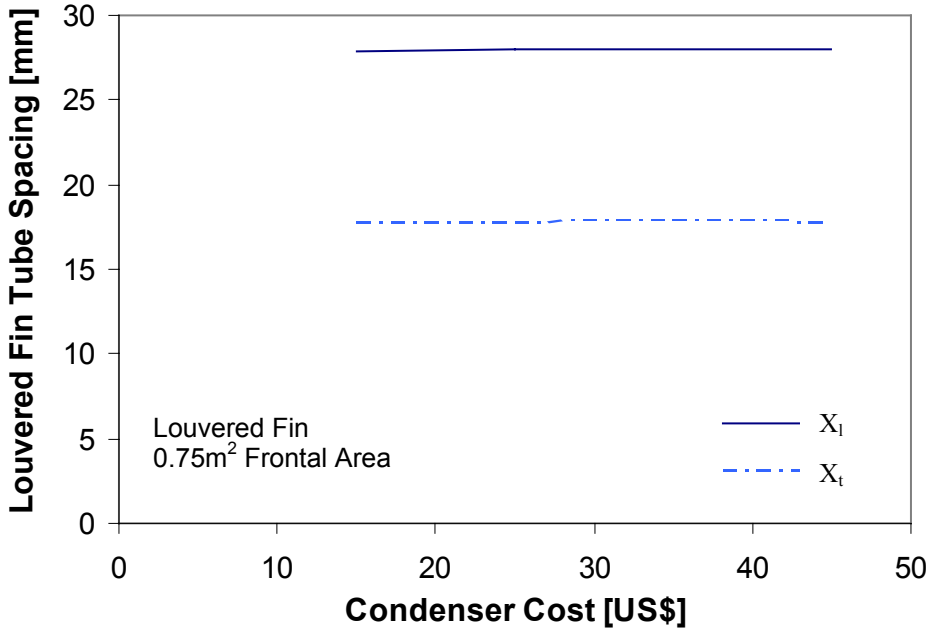

Figure 6-20: Optimum Louvered Fin Tube Spacing Versus Condenser Cost for a Fixed Frontal Area of 0.75m^2

VI-D: Isolated Model

The isolated condenser model using plain fins was also investigated under the conditions described in the first section of this chapter using the simplex optimization search scheme to obtain optimum condenser designs. For each case, there is a fixed frontal area and a fixed cost. The resulting optimum designs for the isolated condenser model are shown in Table 6-7. For the COP calculations (shown in *italics* in Table 6-7), the optimum design determined by the isolated condenser optimization was then entered into the system EES model to determine the system COP for that design. The design trends for the isolated condenser designs were very similar to the plain fin designs found from optimizing via a system model figure of merit. Comparisons between the results from the system model and the isolated model for plain fins will be discussed in detail in the next chapter.

Table 6-7: Optimum Plain Fin Designs from Isolated Model

Cost [US$]	**Frontal Area** [m^2]	V_{ac} [m/s]	# **tpr**	F_p [mm^{-1}]	# **circ**	X_t [mm]	X_l [mm]	**Width** [m]	# **rows**	COP_{seas}
15	0.75	2.65	22.58	0.708	2.39	22.16	13.06	1.499	2	*3.964*
25		2.34	20.69	0.579	3.15	24.19	19.30	1.499	3	*4.185*
35		2.17	20.15	0.467	3.78	24.97	25.76	1.490	4	*4.271*
45		2.03	18.88	0.464	4.30	26.50	27.93	1.499	5	*4.311*
25	0.5	2.62	17.50	0.511	2.98	23.45	25.51	1.219	4	*3.984*
	0.75	2.34	20.69	0.579	3.15	24.19	19.30	1.499	3	*4.185*
	1	1.91	24.62	0.708	3.46	23.51	12.70	1.728	2.6	*4.286*
	1.25	1.72	28.17	0.709	3.58	23.04	13.26	1.926	2	*4.385*

CHAPTER VII

DISCUSSION

VII-A: Plain vs. Louvered

Now that some basic design trends have been established for plain and louvered finned-tube condensers under various cost and frontal area constraints, the stage is set to compare optimum plain-fin designs with optimum louvered-fin designs, both determined by maximizing the system COP_{seas}. Only continuous optimum designs are plotted since they portray more clearly general trends.

Figure 7-1 shows the optimum designs for varying frontal areas at a cost of $25 for plain fins and louvered fins as well as a non-optimized louver design, which will be explained below. It can be seen that in every case shown, the optimized louver fin case shows a 3.8% to 6.2% increase in system performance over the corresponding optimized plain fin.

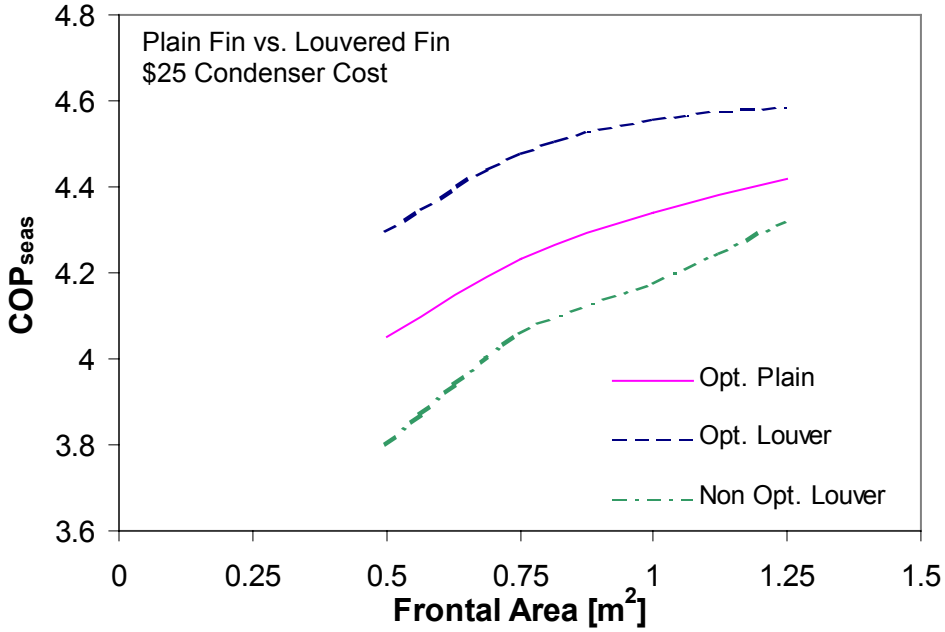

Figure 7-1: COP_{seas} vs. Frontal Area

However, caution should be taken since this analysis compares optimum plain fin designs with optimum louvered designs. This means that taking an optimum plain design and applying louvers to it without re-optimizing the design will not necessarily improve the performance, as shown by the design series "Non Opt. Louver" in Figure 7-1. This heat exchanger design is based on the plain fin optimum design with louvers added (and no other design changes) using mid range values of louver pitch and height (L_h=0.975mm, L_p=2.3mm) based on the experimental data range used to develop Wang's (1999b) correlations. From this figure, it can be seen that there can be a significant decrease in performance of 2.2% to 6.1%, which is of the same order as the possible benefits from the addition of louvers. Therefore, while louvers can give a dramatic increase in performance with no additional cost in many situations, condenser designs

employing louvers must be optimized to ensure the maximum, or any, amount of benefit from the enhancement.

Figure 7-2 shows COP plotted versus condenser material cost for optimum louvered and plain fin designs with a fixed frontal area of 0.75m^2. Each point is an optimum design based on the fixed constraints of heat exchanger material cost and frontal area. Therefore the comparisons between plain and louvered fins are not simply the same heat exchanger design with louvered versus plain fins, but instead they are each different designs determined by optimization for each situation.

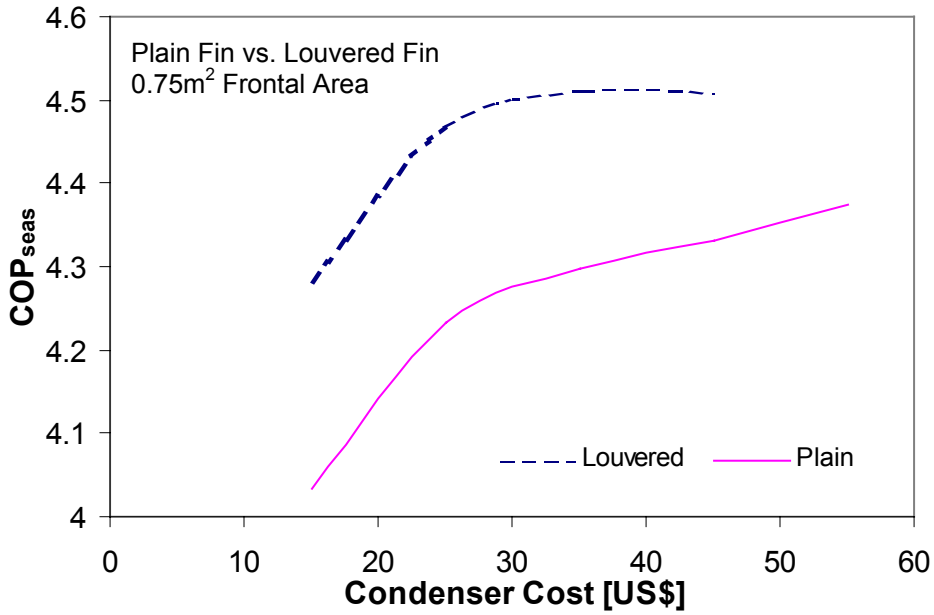

Figure 7-2: Optimum COP_{seas} vs. Condenser Cost

From Fig. 7-2 it can be seen that the optimum louver fin designs have a higher efficiency by 4.1% at $45 fixed cost and up to 6.15% at $15 fixed cost. Also, for the same COP of 4.3, a plain-finned condenser costs $36 while a louver-finned condenser

costs only about $16. Therefore for the same COP, the optimized louver-finned design allows for a 56% reduction in cost compared to the plain fin optimum design.

As can be seen in Fig. 7-2, additional cost increases the COP up to a certain point, after which it levels off. As mentioned in the previous section, the increased frictional pressure drop due to deeper coils at increased costs is initially balanced by decreasing the fin pitch (Figure 7-3) and the air velocity over the condenser (Figure 7-4). After the peak, the fan power effect is greater than the reduced condenser pressure and corresponding compressor power due to the larger condenser overall UA.

It was expected that the louver fin designs would have lower air velocities over the condenser as well as lower fin pitches compared to the optimum plain-fin designs to offset the increase in frictional pressure drop (for a given cost and frontal area) created by the louvers. This general trend can be seen in Figures 7-3 and 7-4.

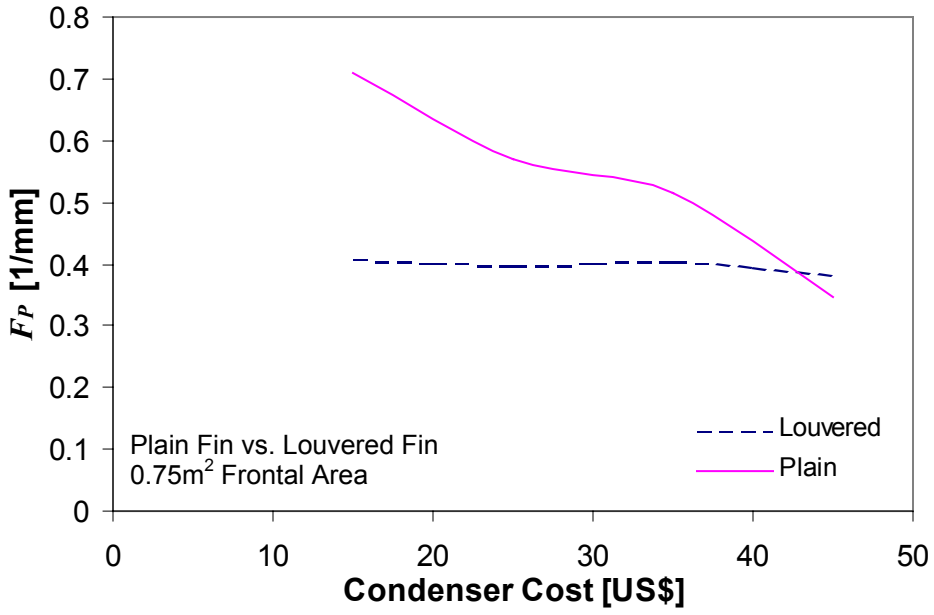

Figure 7-3: Optimum Fin Pitch vs. Condenser Cost

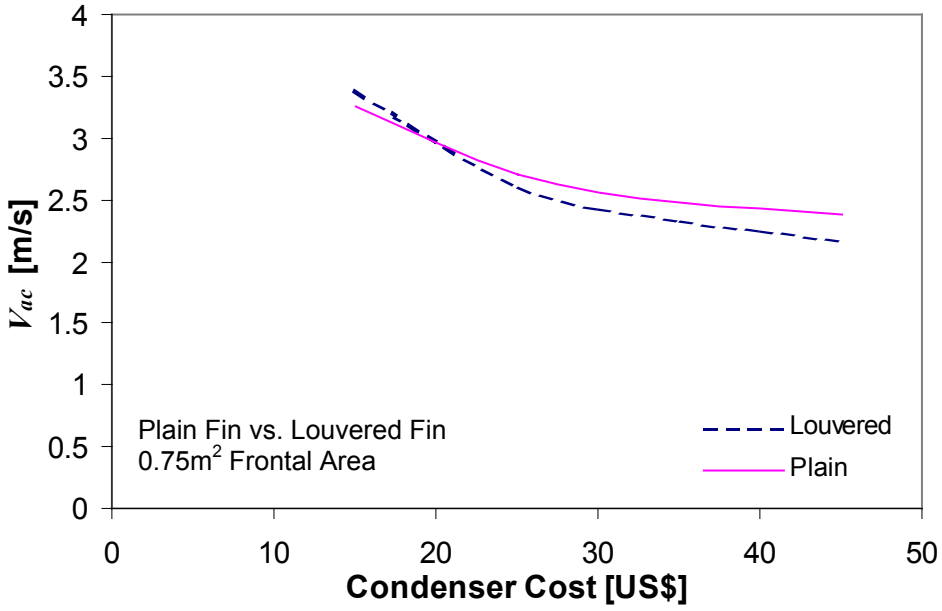

Figure 7-4: Optimum Air Velocity vs. Condenser Cost

As mentioned in the results section, every louvered-fin optimum design converged to the minimum louver height (L_h) and maximum louver pitch (L_p) (Figure 6-19) allowed by the constraints. Additionally, the louvered-fin cases tended towards the maximum allowed longitudinal spacing (X_l) and the minimum transverse tube spacing (X_t). These trends are depicted in Figures 7-5 and 7-6 as compared to the optimum plain fin tube spacings, which increased with increasing cost, allowing for more space between the fins as the coil design became deeper (with increasing cost), reducing the air-side pressure drop.

As shown in Figure 7-7, the optimum number of circuits is slightly higher for the louvered-fins as well as the optimum number of tubes per row (Figure 7-8). This is

because the optimum transverse (or vertical) tube spacing, shown in Figure 7-5 is lower for the louvered-fins, allowing more tubes to fit in the same condenser height.

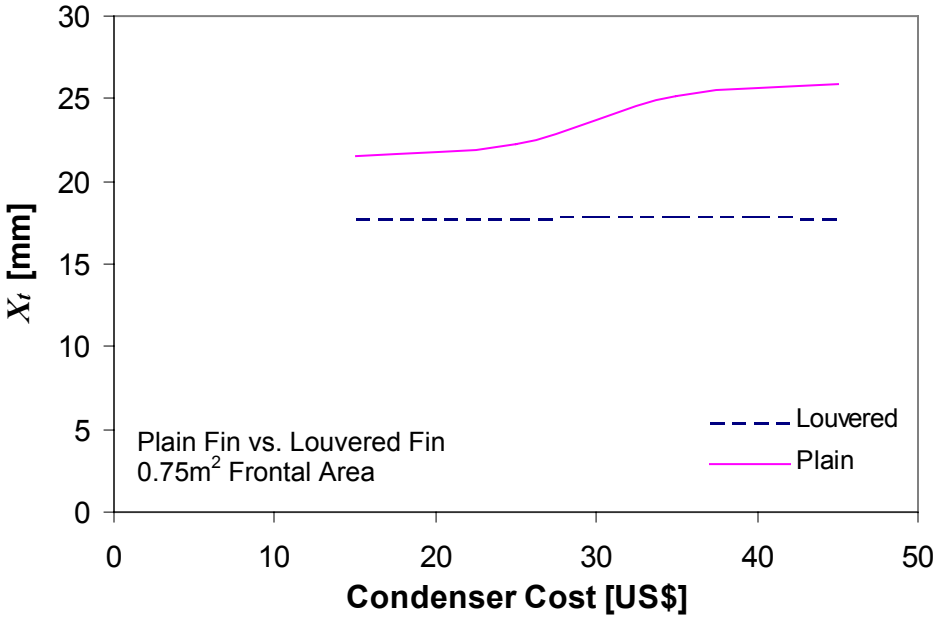

Figure 7-5: Optimum Transverse Tube Spacing vs. Condenser Cost

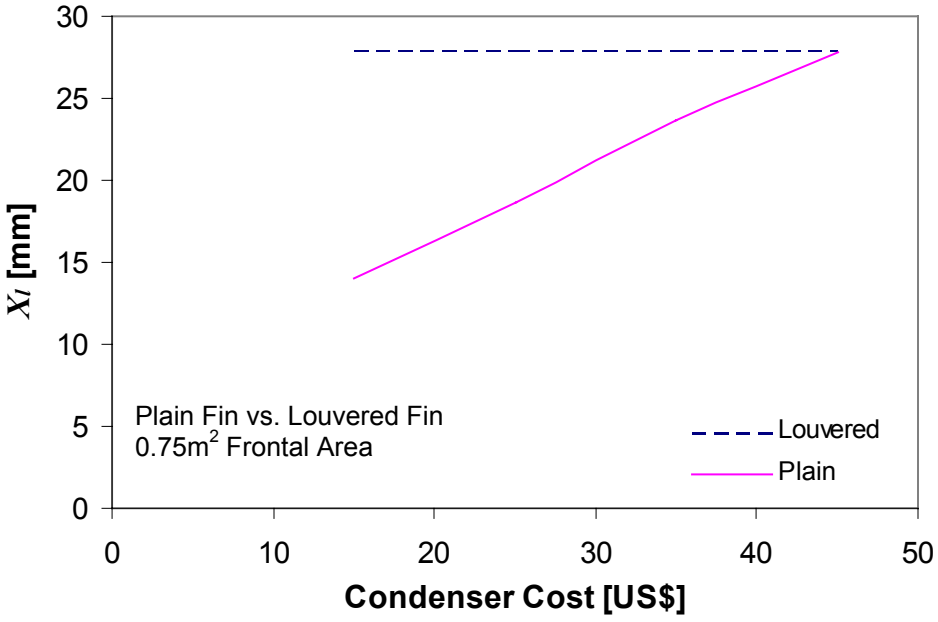

Figure 7-6: Optimum Longitudinal Tube Spacing vs. Condenser Cost

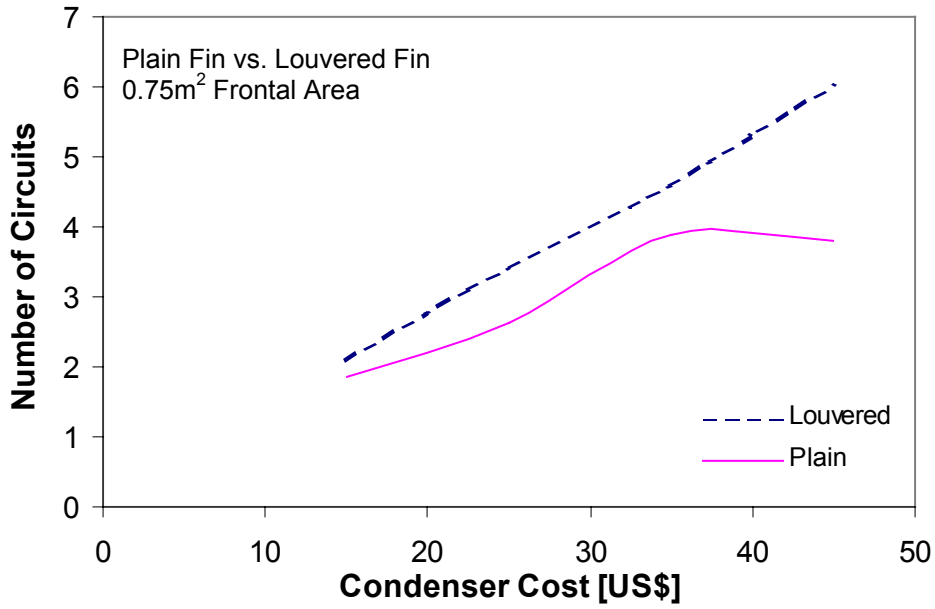

Figure 7-7: Optimum Number of Circuits vs. Condenser Cost

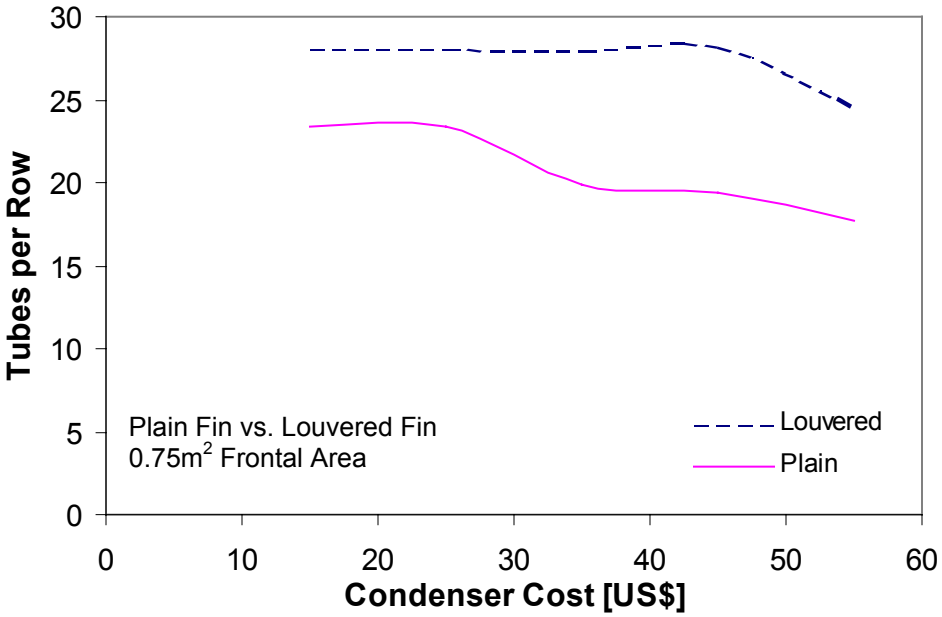

Figure 7-8: Optimum Tubes per Row vs. Condenser Cost

VII-B: Isolated vs. System Model

The resulting optimum designs for the plain fin condenser using the air-conditioning system model (COP figure of merit) and the isolated condenser model (condenser entropy generation minimization figure of merit) are compared in the following figures. Again, comparisons are made using the continuous optimums since the general design trends are clearer than in the discrete optimums.

Figures 7-9 thru 7-12 show the optimum transverse tube spacing, longitudinal tube spacing, fin pitch, and tubes per row respectively vs. varying condenser material cost for a 0.75m^2 frontal area. It can be seen from these figures that the resulting optimum designs from both the system and the isolated model optimizations are quite similar to each other in both trend and value. Additionally the optimum numbers of rows for both cases are identical.

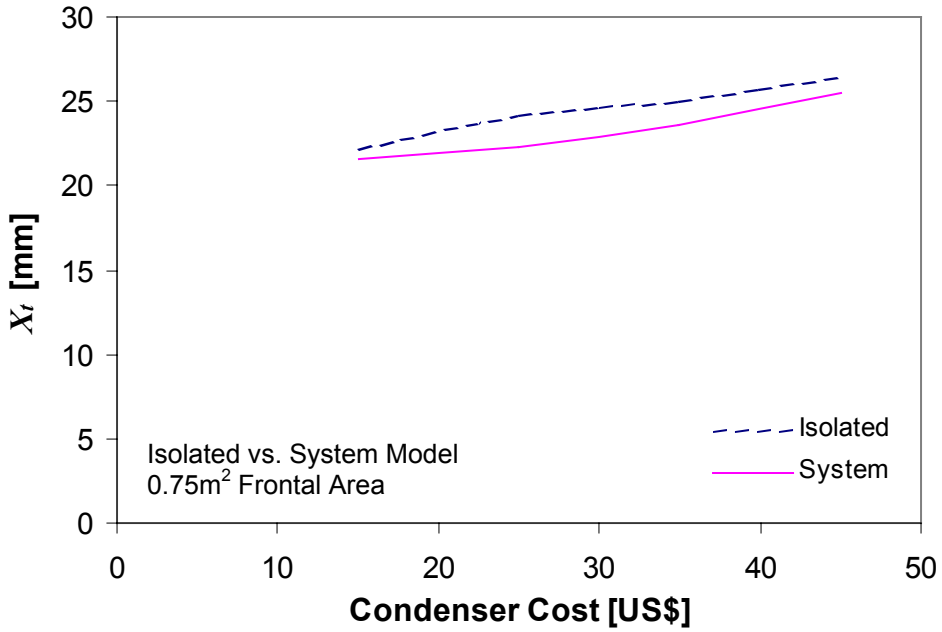

Figure 7-9: Optimum Transverse Tube Spacing vs. Condenser Cost

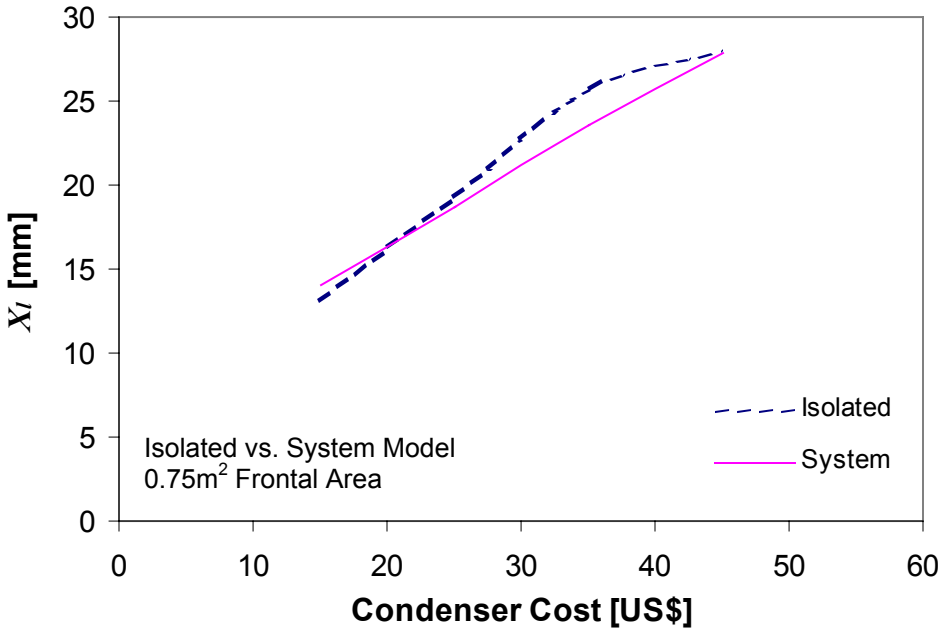

Figure 7-10: Optimum Longitudinal Tube Spacing vs. Condenser Cost

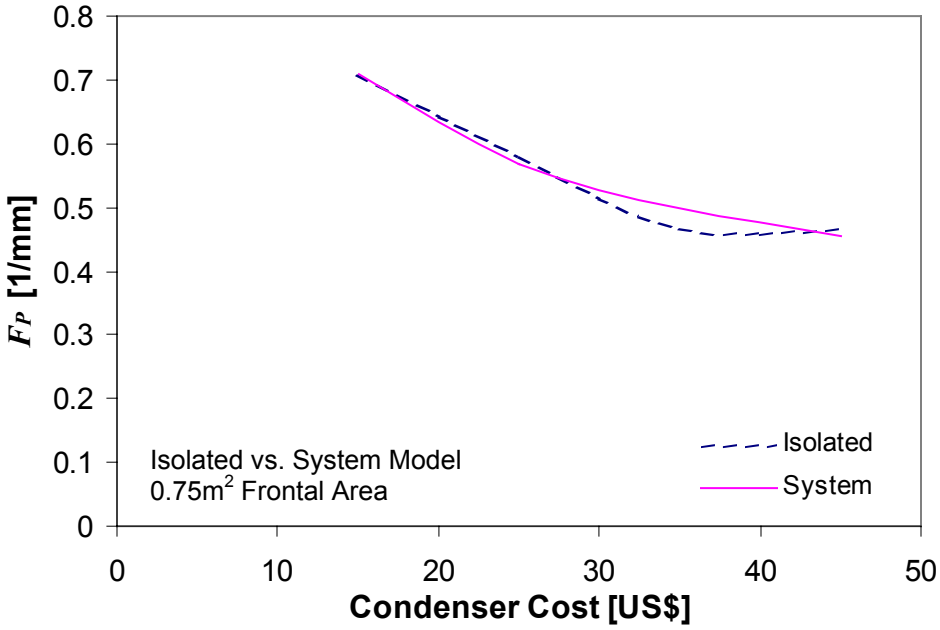

Figure 7-11: Optimum Fin Pitch vs. Condenser Cost

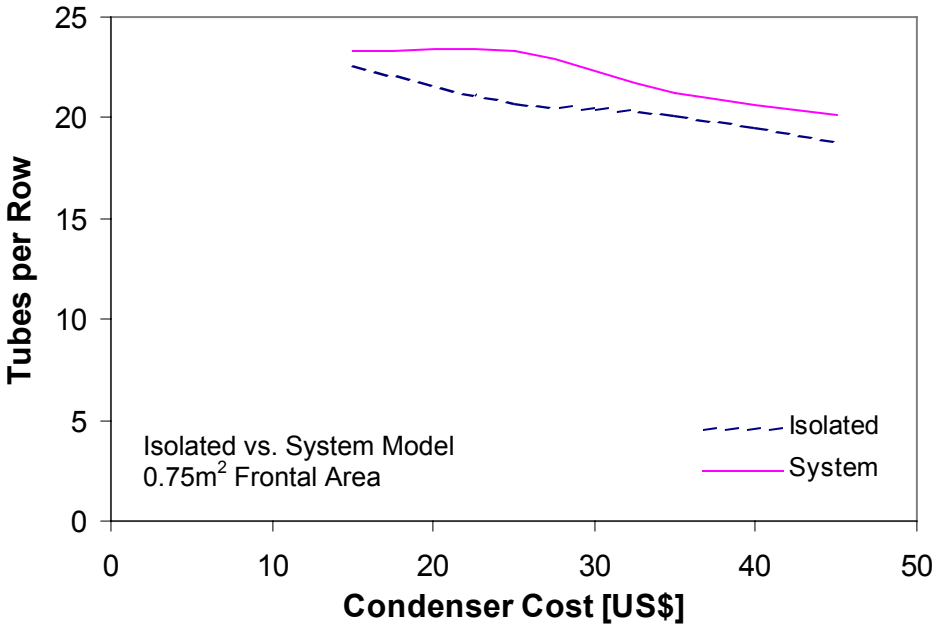

Figure 7-12: Optimum Tubes per Row vs. Condenser Cost

The isolated model optimization search scheme was developed to choose an optimum design based on minimizing the entropy generation in the condenser. The components of this entropy generation are heat transfer through a finite temperature difference and both air and refrigerant pressure drop terms. These temperature and pressure effects compete with each other, *i.e.* as the pressure drop decreases the heat transfer coefficient decreases. Because of this, the optimum design will converge to the case with a minimum of irreversibility due to the trading off of these effects. Therefore, as the isolated optimization scheme reduced the air side velocity (Figure 7-13, for 0.75m^2 frontal area), it reduced both the air and refrigerant-side pressure drops. This is because in order to maintain the constant condenser heat transfer rate, there was a slight increase in the average saturation temperature and pressure in the condenser and a slight increase in the refrigerant side mass flow rate, but this flow rate was split into more (18.2%-

29.3%) parallel circuits (number of circuits), as shown in Figure 7-14, resulting in a lower pressure drop on the refrigerant side compared to the corresponding system optimized design (e.g. at \$25, 0.75m^2: 69.84 kPa vs. 119.1 kPa). The net result of these effects reduced the entropy generation in the condenser, which was the figure of merit for the isolated model.

However, when this isolated optimum design is place in the context of the overall system, the reduction in pressure drop in the condenser creates the need for a larger irreversibility in the expansion valve. Also, the increase in saturation pressure in the condenser (with a fixed ΔT_{SH}) and the increased refrigerant mass flow rate requires a larger compressor power, also creating more irreversibility. The net result of these effects offset the lower entropy generation in the condenser.

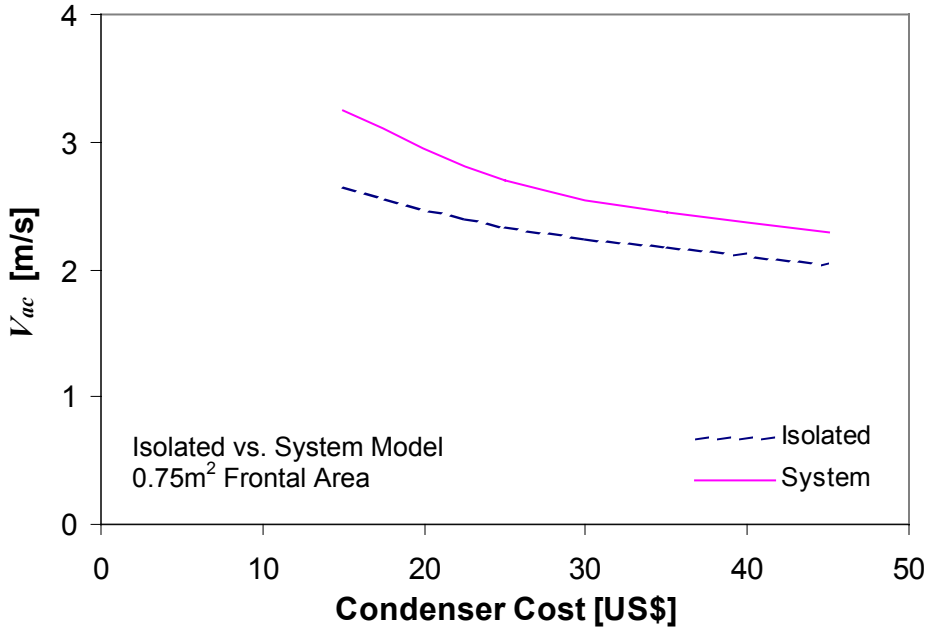

Figure 7-13: Optimum Air Velocity vs. Condenser Cost

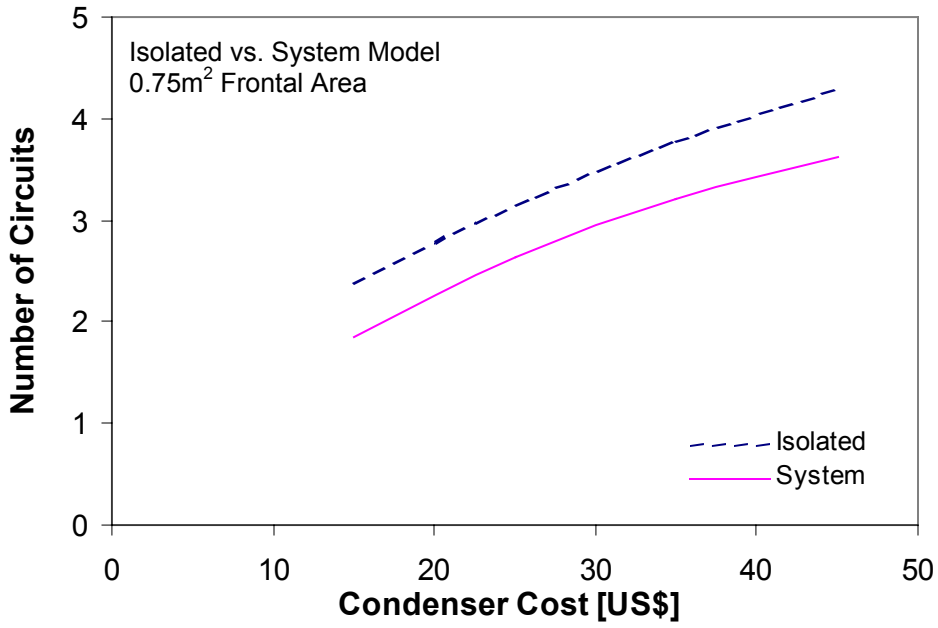

Figure 7-14: Optimum Number Circuits vs. Condenser Cost

The overall effects of these model differences can be seen in Figure 7-15, which shows COP vs. varying condenser material cost for a fixed frontal area of 0.75m^2. It can be seen that the COP's from the system model optimizations are slightly higher than the isolated condenser optimized designs. The variation ranges from 0.62% at \$45 to 1.7% at \$15. So, even though some of the design parameters differed by as much as 29.3% between the two methods, the isolated condenser optimization did produce designs very close in COP to those produced by using an entire system model to optimize the condenser design. The 65% reduction in computation time for the isolated model makes this a very attractive and practical option for the design optimization of finned-tube condenser heat exchangers, with a caution that a prudent choice of constraints must be considered.

Alternatively, at a fixed cost of $25, and varying frontal area the same design trends are seen. The only difference is shown in Figure 7-16 where COP is plotted versus frontal area. Note, as found earlier, that the COP will always increase with increasing frontal area until there is a single row.

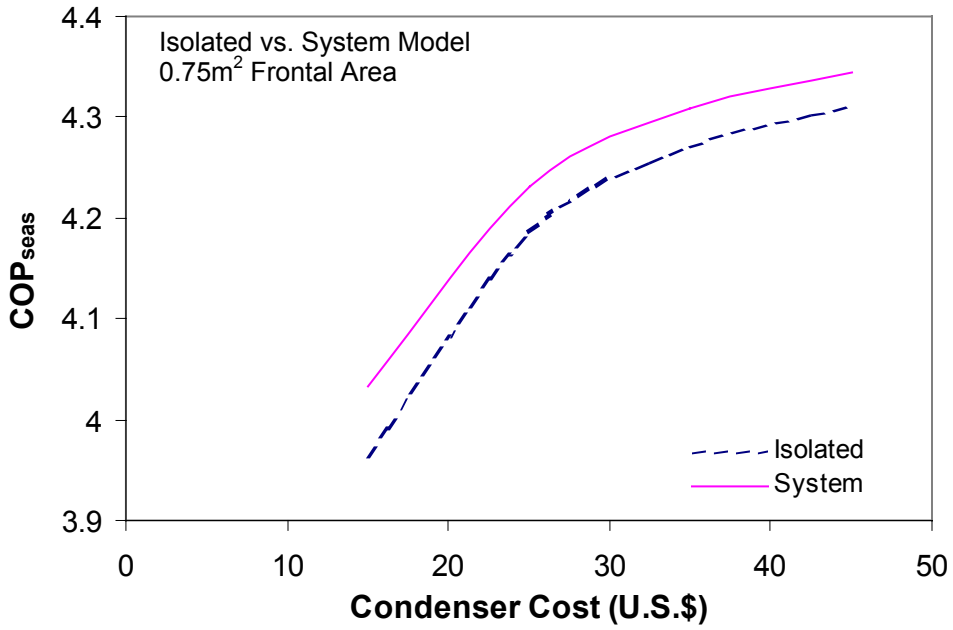

Figure 7-15: Optimum COP_{seas} vs. Condenser Cost

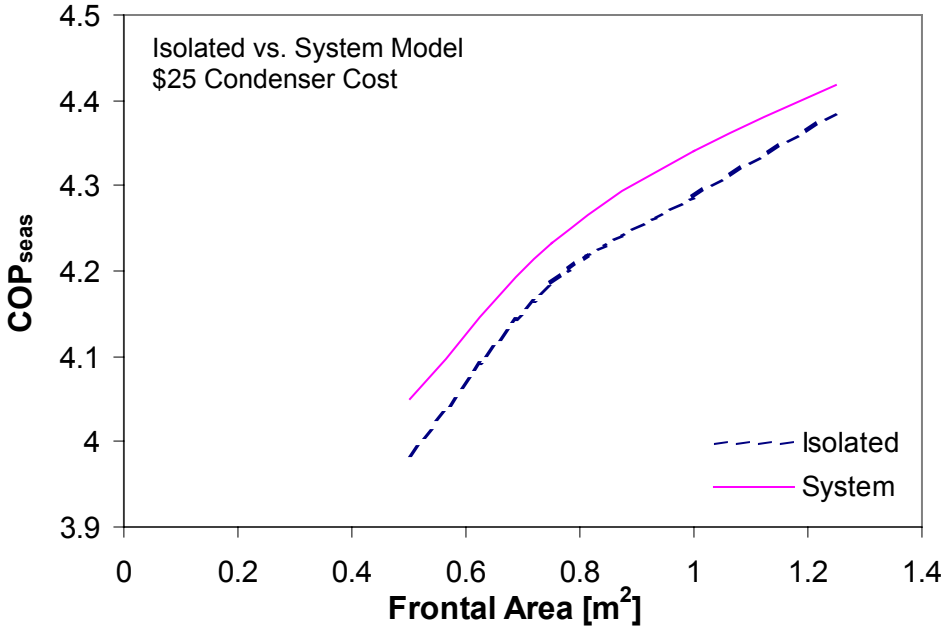

Figure 7-16: Optimum COP_{seas} vs. Frontal Area

CHAPTER VIII

CONCLUSIONS AND RECOMMENDATIONS

VIII-A: Conclusions

The purpose of this study was to develop an optimization tool and design guidelines for finned-tube condenser heat exchangers while investigating effects of fin enhancements on system performance as well as investigating the use of an isolated component based fitness function to reduce computation time and model complexity.

The model and optimization scheme presented in this study were used to optimize 12 design parameters of a plain finned-tube condenser heat exchanger for an 8.8kW (2.5-ton) residential air conditioning system. The results gave some insight into the parametric effects of different designs. It was found that as frontal area is increased at a fixed cost, the optimum design converged to the case of a single row. While as the condenser material cost is increased at fixed frontal area, the corresponding increase in air-side pressure drop due to a deeper coil is balanced by a decrease in air-velocity and fin pitch while the optimum transverse and longitudinal tube spacings increase as well. This increase in tube spacing, at a fixed frontal area, decreases the optimum number of tubes per row with increased cost, while the number of circuits increases (decreasing the number of tubes per row in a circuit) to decrease the refrigerant-side pressure drop for deeper coils. The changes in these parameters with increased cost offset the effects of

having a deeper coil up to a certain point, after which the fan power effect is greater than the reduced condenser pressure and corresponding compressor power due to the larger condenser overall *UA*.

While louvered fins have been used for years by the residential air conditioning industry in finned-tube condenser heat exchangers to produce more compact systems with the same cooling capacity, no systematic studies are available in the public literature investigating the effect of these louvers on system performance using consistent constraints. As seen from the figures, the addition of louvers to the fins of a finned-tube condenser can indeed increase the system performance with fixed cost but optimization of the design is required to achieve the maximum enhanced fin benefits and to avoid possible degradation in performance. It was found that the optimum louver fin designs increase the performance by 4.1% at $45 fixed cost and up to 6.15% at $15 fixed cost. However, when louvers with typical pitch and height are added to an optimized plain fin design without re-optimization, there can be a significant decrease in performance of 2.2% to 6.1% for the cases shown. Also, to achieve a target COP of 4.3, a plain-finned condenser with a material cost of $36 is required while the same COP can be achieved with a louver-finned condenser with material costs of only $16. Therefore, at this condition, for the same COP the optimized louver-finned design allows for a 56% reduction in condenser material cost. This example is applicable to designing a minimum cost system to meet DOE minimum efficiency standards.

Using the detailed system model as a comparison, this study also shows that isolating the condenser component and optimizing it independently by minimizing the entropy generation in the condenser component alone (also known as thermoeconomic

isolation) is a practical way to design the condenser for optimum air-conditioning system efficiency. This task is accomplished by comparing the optimum design determined by maximizing the entire system's COP, with the optimum design determined by minimizing the entropy generation in the isolated condenser component, with consistent constraints used for the two methods. It was found that the most important aspect required for a successful isolated model is a proper set of constraints. In the current study, the condenser heat transfer rate, condenser exit subcool, and the condenser entering superheat were chosen as fixed parameters. These parameters were chosen because they vary little in the system model with changing condenser designs and they do not require detailed system information in order to specify them within reasonable accuracy.

The resulting optimum designs from the isolated model produced a COP within 0.62% to 1.7% of the designs found by optimizing the COP using an entire system model, despite the fact that some of the design parameters showed significant differences in their optimum values (as much as 29.3% different). With a 65% reduction in computation time using the isolated model, this proves to be a very practical and effective method for designing finned-tube condenser heat exchangers. Caution, however, should be taken when using thermoeconomic isolation in choosing the appropriate design aspects to fix in order to complete the model, for the model will work with multiple combinations of parameters but will lack in accuracy with improper choices.

VIII-B: Recommendations

Since the optimum designs led to the expectation that values beyond the current limits of the parameter bounds (established by the experimental data used to develop the correlations used in this study) may improve performance, it is recommended that future works aim to expand the range of empirical correlations for the air side performance. While fin efficiency correlations appropriate for enhanced fins are also needed.

Additionally, it is recommended that the effects of non-uniform air-velocity over the condenser be included in the model since the typical packaging of condensing units place the compressor adjacent to the condenser coil, partially obstructing the airflow.

REFERENCES

Alefeld, G. 1990. What are thermodynamic losses and how to measure them? A Future for Energy, Proceedings of the World Energy Symposium, Italy, May 1990.

Alefeld, G. 1989a. What are "Losses" in Thermodynamic Systems? Heat Recovery Systems and CHP. Editor: D.A. Reay, Pergamon Press.

Alefeld, G. 1989b. The COP of Thermal Power Stations Derived from the Second Law. ASME Meeting, San Francisco, Dec. 1989.

Alefeld, G. 1987a. Efficiency of Compressor Heat Pumps and Refrigerators Derived from the Second Law of Thermodynamics. Int. J. Refrigeration. Vol.10, pp. 331-341.

Alefeld, G. 1987b. What Needs to Be Known about Working Fluids to Calculate Coefficients of Performance. -and- What Needs to Be Known about Fluid Pairs to Determine Heat Ratios for Absorber Heat Pumps and Heat Transformers. Proc. IEA Heat Pump Conference, Orlando, FL, April 28-30, 195-208 and 376-387. Editor: K. Zimmerman, Oak Ridge National Lab.

ARI, 1989. Air-conditioning and Refrigeration Standard 210/240-89, p. 3, section 5.1.

Aspelund, K.A. 2001. Optimization of Plate-Fin-and-Tube Condenser Performance and Design for Refrigerant R-410A Air-Conditioner, M.S. Thesis, Georgia Institute of Technology.

AAON, 2001. AAON Heating and Air-Conditioning Products web site, http://www.aaon.com/

Bejan, A. 1996. Entropy Generation Minimization, The Method of Thermodynamic Optimization of Finite-Size Systems and Finite-Time Processes. CRC Press, New York.

Bejan, A. 1996. Advanced engineering thermodynamics. Wiley, New York.

Bejan, A. 1984. Second-Law Aspects of Heat Transfer Engineering. In T. N. Veziroglu, A. E. Bergles, eds., Multi-Phase Flow and Heat Transfer III. Part A: Fundamentals, Elsevier Science Publ., Amsterdam, The Netherlands, pp. 1-22

Bejan, A. 1984. Second law analysis: The method for maximizing thermodynamic efficiency in thermal systems. ASME-NSF Workshop on Research Goals and Priorities in Thermal Systems, Ft. Lauderdale, FL, April 25-27, publ. in W. O. Winer et al. Research Needs in Thermal Systems, ASME, NY 1986.

Bejan, A. 1982. Entropy Generation Through Heat and Fluid Flow. Wiley, New York.

Bejan, A. 1982. Second-Law Analysis in Heat Transfer and Thermal Design. Advances in Heat Transfer, vol. 15, pp. 1-58.

Bejan, A. and Pfister, P.A. 1980. Evaluation and heat transfer augmentation techniques based on their impact on entropy generation. Letters in heat and mass transfer, Vol. 7, pp. 97-106.

Bejan, A. 1980. Second law analysis in heat transfer. Energy, vol. 5, no. 8-9, pp. 721-732, 1980.

Bejan, A. 1978. General criterion for rating heat-exchanger performance. Int. J. Heat and Mass Transfer, vol. 21, p. 655.

Bejan, A. 1977. The concept of irreversibility in heat exchanger design: Counterflow heat exchanger for gas-to-gas applications. Trans. ASME, J. Heat Transfer, vol. 99, p. 374.

Bensafi, A., Borg, S., and Parent, D. 1997. CYRANO: A computational model for the detailed design of plate-fin-and-tube heat exchangers using pure and mixed refrigerants, Int. J. Refrigeration, Vol. 20, No. 3, pp. 218-228.

Bergles, A.E., Blumenkrantz, A.R. and Taborek, J. 1974. Performance Evaluation Criteria for Enhanced Heat Transfer Surfaces. 4th International Heat Transfer Conference, Vol. 2, pp. 239-243.

Breber, G., Palen, J., and Taborek, J. 1980. Prediction of horizontal tube-side condensation of pure components using flow regime criteria. J. of Heat Transfer vol. 102: 471-476.

Canteloube, A. 1968. "Finned Heat Exchanger." U.S. Patent 3380518.

Cavallini, A.; Censi, G.; Del Col, D. ; Doretti, L. ; Longo, G.A. and Rossetto, L. 2002. In tube condensation of halogenated refrigerants. ASHRAE Transactions, Vol. 108, No. 1, #4507.

Cavallini, A.; Censi, G.; Del Col, D. ; Doretti, L. ; Longo, G.A. ; Rossetto, L. 2001. Experimental investigation on condensation heat transfer and pressure drop of new HFC refrigerants (R134a, R125, R32, R410A, R236ea) in a horizontal smooth tube. Int. J. of Refrigeration, Vol. 24, pp. 73-87.

Cavallini, A. 2002. Condensation Heat Transfer and Energy Efficiency of Working Fluids in Mechanical Refrigeration. Bulletin of the IIR, Vol. 82, no. 6, pp. 4-21.

Chang, Y.-J., Hsu, K.-C., Lin, Y.-T., and Wang, C.-C. 2000. A generalized friction correlation for louver fin geometry. Int. J. of Heat and Mass Transfer, Vol. 43, pp. 2237-2243.

Chen, J. J. J. and Spedding, P. L., 1981. An Extension of the Lockhart-Martinelli Theory of 2-Phase Pressure Drop and Holdup, Int. J. Multiphase Flow, vol. 7, no. 6, pp. 659-675.

Chi, K.-Y., Wang, C.-C., Chang, Y.-J., and Chang, Y.-P. 1998. A comparison of compact plate fin-and-tube heat exchangers. ASHRAE Transactions, #TO-98-3-3.

Chisolm, D., 1983. Two-Phase flow in Pipelines and Heat Exchangers, Longman Inc., New York.

Colebrook, C. F., 1938. "Turbulent Flow in Pipes, with Particular Reference to the Transition between the Smooth and rough Pipe Laws," J. Inst. Civ. Eng. Lond., Vol. 11, pp. 133-156.

Collier, J.G. and Thome, J.R. 1996. Convective Boiling and Condensation. Clarendon Press; New York.

Copeland, 2002. https://www.customer-copeland-corp.com Online product information on Scroll-type Compressor ZP32K3E-TFD, 30,500 BTU/hr.

Corberan, J.M. and Melon, M.G. 1998. Modeling of plate finned tube evaporators and condensers working with R134a, Int. J. Refrigeration, Vol. 21, No. 4, pp. 273-284.

Dipprey, D.F. and Sabersky, R.H. 1963. Heat and momentum transfer in smooth and rough tubes at various Prandtl numbers. Int. J. Heat and Mass Transfer, Vol. 6, pp. 329-353.

Dobson, M.K., and Chato, J.C. 1998. Condensation in smooth horizontal tubes. J. Heat Transfer, Vol. 120:193-213.

Du, Y-J and Wang, C-C. 2000. An experimental study of the airside performance of the superslit fin-and tube heat exchangers. Int. J. of Heat and Mass Transfer, Vol. 43, pp. 4475-4482.

EPA, 2001. United States Environmental Protection Agency: Ozone Depletion Home Page, http://www.epa.gov/ozone/.

ESDU, 1991. Effectiveness-NTU Relationships for the Design and Performance Evaluation of Two-Stream Heat Exchangers. Engineering Science Data Unit

86018 with Amendment A, July 1991, pp.92-107, ESDU International plc, London.

Friedel, L. 1979. Improved friction pressure drop correlations for horizontal and vertical two-phase pipe flow. Europ. Two-phase Flow Group Meeting, Ispra, Paper E2.

Goldberg, D. 1989. Genetic Algorithms in Search, Optimization, and Machine Learning, Addison-Wesley Pub. Co, Reading Mass.

Gray, D.L. and Webb, R.L. 1986. Heat transfer and friction correlations for plate finned-tube heat exchangers having plain fins. Proceedings of 8th Heat transfer Conference, 1986, pp. 2745-2750.

Gunter, A.Y. 1969. "Plate Fins." U.S. Patent 3438433.

Haupt, R.L and Haupt, S. E. 1998. Practical Genetic Algorithms. John Wiley & Sons; New York.

Hesselgreaves, J.E. 2000. Rationalisation of second law analysis of heat exchangers. Int. J. Heat and Mass Transfer, Vol. 43, pp. 4189-4204.

Hiller, Carl. Improving Heat Pump Performance Via Compressor Capacity Control: Analysis and Test. PhD Thesis. Massachusetts Institute of Technology, 1976, p. 370-387.

Hiller, C. C. and Glicksman, L. R., 1976. Improving Heat Pump Performance via Compressor Capacity Control-Analysis and Test, Report No. 24525-96, Heat Transfer Laboratory, Massachusetts Institute of Technology.

Holland, J. (1975). Adaptation In Natural and Artificial Systems. The University of Michigan Press, Ann Arbor.

Hong, K.T. and Webb, R.L., 1996, Calculation of fin efficiency for wet and dry fins, HVAC&R Research, vol.2, no.1: pp.27-41.

Incropera, F. P. and DeWitt, D. P., 1996. Fundamentals of Heat and Mass Transfer, 4th Edition, John Wiley & Sons, New York.

Jiang, H., Aute, V., and Radermacher, R. 2002. A user friendly simulation and optimization tool for design of coils, Ninth International Refrigeration and Air Conditioning Conference at Purdue, Paper # R5-1.

Kang, H.C. and Webb, R.L. 1998. Performance comparison of enhanced fin geometries used in fin-and-tube heat exchangers. Heat Transfer 1998, Proceedings of the 11th IHTC, Vol. 6, pp. 273-278.

Kays, W. M. and London, A. L. 1964, Compact Heat Exchangers, 2nd Edition, McGraw-Hill; New York, 1964.

Kays, W. M. and London, A. L. 1984, Compact Heat Exchangers, 3rd Edition, McGraw-Hill; New York, 1984.

Kim, N.-H., Yun, J.-H., and Webb, R.L. 1997. Heat transfer and friction correlations for wavy plate fin-and-tube heat exchangers. Transactions of ASME, Vol. 119, pp. 560-567.

Klein, S.A. and Alvarado, F.L. 2003. Engineering Equation Solver, F-Chart Software, Professional Version 6.763.

Klein, S. A. and Reindl, D. T., 1997. The Relationship of Optimum Heat Exchanger Allocation and Minimum Entropy Generation for Refrigeration Cycles, Proceedings of the ASME Advanced Energy Systems Division, Vol. 37, pp. 87-94.

Lagarias, J. C., Reeds, J. A., Wright, M. H. and Wright, P. E., 1998. Convergence properties of the Nelder-Mead Simplex method in low dimensions, SIAM J. Optim., Vol. 9, No. 1, pp. 112-147.

Lin, W.W. and Lee, D.J. 1998. Second law analysis on a pin-fin array under cross flow. Int. J. of Heat and Mass Transfer, Vol. 40, No. 8, pp. 1937-1945.

Lockhart, R. W. and Martinelli, R. C., 1949. A Proposed Correlation of Data For Isothermal Two-Phase, Two-Component Flow In Pipes, Chem. Eng. Progr., Vol. 45, No. 1, pp. 39-48.

London Metals Exchange, October 2003. http://www.lme.co.uk/

McClintock, F.A., 1951, The Design of Heat Exchangers for Minimum Irreversibility, Paper No. 51-A-108, presented at the 1951 ASME Annual Meeting.

McQuiston, F. C. and Parker, J. P.,1994. Heating Ventilating and Air-Conditioning-Analysis and Design, John Wiley & Sons, New York.

McAQuiston, F.C. 1978. Correlation of heat, mass, and momentum transport coefficients for plate-fin-tube heat transfer surfaces with staggered tubes. ASHRAE Transactions, Vol. 84, No. 1, pp. 294-309.

Moran, M.J. and Shapiro, H.N. 2000. Fundamentals of Engineering Thermodynamics, 4th ed. John Wiley & Sons; New York.

Muñoz, J.R. and von Spakovsky, M.R. 2003. Decomposition in Energy System Synthesis/Design Optimization for Stationary and Aerospace Applications. Journal of Aircraft, Vol. 40, No.1 Jan-Feb.

Nelder, J. A. and Mead, R., 1965. A Simplex Method for Function Minimization, Computer J., **7**: 308-313.

Nikuradse, J. 1950. Laws on flow in rough pipes. NACA TM 1292.

Numerical Recipes in C. 2003. http://www.library.cornell.edu/nr/bookcpdf.html

Perrotin, T. and Clodic, D. Fin efficiency calculation in enhanced fin-and-tube heat exchangers in dry conditions. Proceedings of the 21st Internation Congress of Refrigeration, Paper # ICR0026, August 2003.

Rabas, T.J., and Arman, B. 2000. Effect of the exit condition on the performance of in-tube condensers. Heat Transfer Engineering, Vol. 21:4-14.

Reklaitis, G. V., Ravindran, A., Ragsdell, K. M., 1983. Engineering Optimization, Methods and Applications, John Wiley and Sons.

Rich, D. G. 1973. The Effect of Fin Spacing on the Heat Transfer and Friction Performance of Multi-Row, Smooth Plate Fin-and-Tube Heat Exchangers, ASHRAE Transactions, Vol. 79, No. 2, pp. 137-145.

Richardson, D., Jiang, H., Lindsay, D., and Radermacher, R. 2002. Optimization of vapor compression systems via simulation, Ninth International Refrigeration and Air Conditioning Conference at Purdue, Paper # R1-3.

Saboya, F.E.M. and da Costa, C.E.S.M. 1999. Minimum irreversibility criteria for heat exchanger configurations. J. of Energy Resources Technology, Vol. 121, pp. 241-246.

Sadler, E.M. Design Analysis of a Finned-Tube Condenser for a Residential Air-Conditioner Using R-22, M.S. Thesis, Georgia Institute of Technology, April 2000.

San, J.-Y. and Jan, C.-L. 2000. Second-law analysis of a wet crossflow heat exchanger. Energy, Vol. 25, pp. 939-955.

Sardesai, R.G., Owen, R.G., and Pulling, D.J. 1981. Flow regimes for condensation of a vapour inside a horizontal tube. Chemical Engineering Science, Vol. 36: 1173-1180.

Schenone, C., Tagliafico, L., and Tanda, G. 1991. Second Law Analysis for Offset Strip-Fin Heat Exchangers. Heat Transfer Engineering, Vol. 12, no. 1, pp. 19-27.

Schmidt, T. E. 1945. La Production Calorifique des Surfaces Munies d'ailettes, Annexe Du bulletin De L'Institut International Du Froid, Annexe G-5.

Sekulić, D.P. 1986. Entropy generation in a heat exchanger. Heat Transfer Engineering, Vol. 7, Nos. 1-2, pp. 83-88.

Sekulić, T.E. and Herman, C.V. 1986. One approach to irreversibility minimization in compact crossflow heat exchanger design. Int. Comm. Heat Mass Transfer, Vol. 13, pp. 23-32.

Shah, R.K. 1978. Compact Heat Exchanger Surface Selection Methods. Heat Transfer 1978, Proceedings of the 6th Int. Heat Transfer Conference, Vol. 4, pp. 193-199.

Shah, M. M., 1979. A General Correlation For Heat Transfer During Film Condensation Inside Pipes. Heat and Mass Transfer, Vol. 22, pp. 547-556.

Shah, R.K. & Sekulić, T.E. 2003. Fundamentals of Heat Exchanger Design. John Wiley & Sons; Hoboken, N.J. Chapters 10 and 11.

Stewart, S.W. and Shelton, S.V. 2003. Design study comparison of plain finned versus louvered finned-tube condenser heat exchangers, Proc. ASME Summer Heat Transfer Conference, July 20-23, Las Vegas, NV.

Tandon, T.N., Varma, H.K., and Gupta, C.P. 1982. A new flow regime map for condensation inside horizontal and near horozpntal tubes, ASME J. Heat Transfer, Vol. 104: 763-768.

Tandon, T.N., Varma, H.K., and Gupta, C.P. 1985. Prediction of flow patterns during condensation of binary mixtures in a horizontal tube, ASME J. Heat Transfer, Vol. 107: 424-430.

Tapia, C.F. and Moran, M.J. 1986. Computer-Aided Design and Optimization of Heat Exchangers. ASME AES, Vol. 2, No.1: 93-103.

Tayal, M., Fu, Y. and Diwekar, U. 1999. Optimal design of heat exchanger: A genetic algorithm framework, Ind. Chem. Res., Vol. 38, pp. 456-467.

Threlkeld, J. R., 1970. Thermal Environmental Engineering, 2nd Edition, Prentice Hall International, New York, pp.55.

Tong, L.S. 1965. BoilingHeat Transfer and Two-Phase Flow, John Wiley & Sons; New York, Chapter 5 (Taken from Hiller, p. 370-375).

Tribus, M. and Evans, R.B. 1962. A Contribution to the Theory of Thermoeconomics. UCLA Engineering Department Report No. 62-36.

Vardhan, A. and Dhar, P.L. 1998. A new procedure for performance prediction of air conditioning coils, Int. J. Refrigeration, Vol. 21, No.1, pp. 77-83.

von Spakovsky, M.R. and Evans, R.B. 1988. The optimal design and performance of components in thermal systems. Second-Law Analysis on Heat/Mass Transfer and Energy Conversion, ASME HTD-Vol. 97.

Wallis, G.B., Crowley, C.J., and Hagi, Y. 1977. Conditions for a pipe to run full when discharging liquid into a space filled with gas. ASME J. Fluids Eng. Vol. 99: 405-413.

Wang, C.-C., Lee, W.-S., and Sheu, W.-J. 2001a. A comparative study of compact enhanced fin-and-tube heat exchangers. Int. J. of Heat and Mass Transfer, Vol. 44, pp. 3565-3573.

Wang, C.-C., Lee, W.-S., and Sheu, W.-J. 2001b. Airside performance of staggered tube bundle having shallow tube rows. Chem. Eng. Comm., Vol. 187, pp. 129-147.

Wang, C.-C. 2000. Recent progress on the air-side performance of fin-and tube heat exchangers. Int. J. of Heat Exchangers, Vol. 1, pp. 49-76.

Wang, C.-C. and Chi, K.-Y. 2000a. Heat transfer and friction characteristics of plain fin-and-tube heat exchangers, part I: new experimental data. Int. J. of Heat and Mass Transfer, Vol. 43, pp. 2681-2691.

Wang, C.-C., Chi, K.-Y., and Chang, C.-J. 2000b. Heat transfer and friction characteristics of plain fin-and-tube heat exchangers, part II: Correltaion. Int. J. of Heat and Mass Transfer, Vol. 43, pp. 2693-2700.

Wang, C.-C., Webb, R.L., and Chi, K.-Y. 2000c. "Data reduction for air-side performance of fin-and-tube heat exchangers." Experimental Thermal and Fluid Science, Vol. 21, pp. 218-226.

Wang, C-C, Tao, W-H, Chang, C-J. 1999a. "An investigation of the airside performance of the slit fin-and-tube heat exchangers." Int. J. of Refrigeration, Vol. 22, pp. 595-603.

Wang, C.C., Lee, C.-J., Chang, C.-T., and Lin, S.-P. 1999b. "Heat transfer and friction correlation for compact louvered fin-and-tube heat exchangers." Int. J. of Heat and Mass Transfer, Vol. 42, pp. 1945-1956.

Wang, C.-C., Lee, C.-J., Chang, C.-T, and Chang, Y.-J. 1999c. Some aspects of plate fin-and tube heat exchangers: with and without louvers. Enhanced Heat Transfer, Vol. 6, pp. 357-368.

Wang, C.-C., Tsai, Y.-M., and Lu, D.-C. 1998. Comprehensive study of convex-louver and wavy fin-and-tube heat exchangers. J. of Thermophysics and Heat Transfer, Vol. 12, No.3, July-September 1998, pp. 423-430.

Wang, C.-C., Chang, Y.-J., Hsieh, Y.-C., and Lin, Y.-T. 1996. Sensible heat and friction characteristics of plate fin-and-tube heat exchangers having plane fins. Int. J. of Refrigeration, Vol. 19, No. 4, pp. 223-230.

Webb, R.L. 1994. Principles of Enhanced Heat Transfer, John Wiley & Sons, New York.

Wenzel, T. P., Koomey, J. G., Rosenquist, J. G., Sanchez, M., and Hanford, J. W. 1997. Energy data sourcebook for the U.S. residential sector, Lawrence Berkeley National Laboratory, LBL-40297.

Witte, L.C. and Shamsundar, N. 1983. A thermodynamic efficiency concept for heat exchange devices. J. of Eng. Power, Vol. 105, pp. 199-203.

Wright, M. F., "Plate-Fin-and-Tube Condenser performance and Design for Refrigerant R-410a Air-Conditioner", M.S. Thesis, Georgia Institute of Technology, 5/2000.

Yun, J-Y and Lee, K-S. 2000. Influence of design parameters on the heat transfer and flow friction characteristics of the heat exchanger with slit fins. Int. J. of Heat and Mass Transfer, Vol. 43, pp. 2529-2539.

Zeller, M. and Grewe, M. A Generalized Approximation Equation for the Efficiency of Fins on Circular and Elliptic Tubes, Warme und Stoffubertragung-Thermo and Fluid Dynamics. Vol. 29, No. 6, pp. 379-382, June 1994.

Zukauskas, A. and Ulinskas, R., 1998. Banks of Plain and Finned Tubes, Heat Exchanger Design Handbook, G. F. Hewitt Edition, Begell House, Inc., New York, pp. 2.24-1 – 2.24-17.

VITA

Susan Stewart, daughter of Brian and Dawn White and sister of Lisa White, was born Susan Jennifer White in State College, Pennsylvania, on May 3rd, 1977. She graduated from State College Area High School in 1995 and then began her undergraduate studies at Penn State University, majoring in Meteorology before switching to Mechanical Engineering after her freshman year. Susan then received her B.S. degree in May 1999.

In August 1999, Susan began graduate studies at the Georgia Institute of Technology. She received a Master of Science degree in Mechanical Engineering in December 2001. Susan's M.S. thesis involved the design and optimization of the bubble pump component used in single pressure absorption refrigeration cycles. Funding for Susan's graduate work at Georgia Tech was provided by GE, NSF, ASHRAE, ASME, and ARCS.

Susan married John Andrew (Drew) Stewart on July 7th, 2001. In her spare time, she enjoys home improvement projects, traveling, and reading.